

Classical Molecular Dynamics Simulation of Fluorophilic and Lipophilic Molecules in a Membrane Environment

DISSERTATION

zur Erlangung des Doktorgrades der Naturwissenschaften
(Dr. rer. nat.)

der
Naturwissenschaftlichen Fakultät II
Chemie, Physik und Mathematik

der Martin-Luther-Universität
Halle-Wittenberg

vorgelegt von

Herrn Ghulam Saddiq

geb. am 09.01.1980 in Bannu, Pakistan

Gutachter:

1. Prof. Dr. Daniel Sebastiani
2. Prof. Dr. Wolfgang Paul
3. Prof. Dr. Michael Vogel

der Verteidigung: 10. March 2017

Classical Molecular Dynamics Simulation of Fluorophilic and Lipophilic Molecules in a Membrane Environment

Abstract

This thesis deals with the prediction of the spatial distribution and diffusive dynamics of functionalized perfluorinated alkane molecules within a phospholipid bilayer by means of large-scale atomistic molecular dynamics simulations. Perfluorinated molecules exhibit a special type of philicity (fluorophilicity) which is neither with hydrophilic nor with lipophilic characteristics. This special feature makes perfluorinated molecules an interesting agent for insertion into lipid bilayers, because their particular behavior might be used to tune the properties of the membrane.

In this thesis, the focus is put on the simulation of the spatial and dynamical properties of relatively small molecules (from hexane to decane) which are partially or perfluorinated or genuine (not fluorinated). A particular spotlight is put on the effect of adding a further functionality (an acidic and an alcoholic end-group) on the properties of the alkanes within the phospholipid membrane. The membrane itself is represented by a dipalmitoylphosphatidylcholine bilayer (DPPC) under periodic boundary conditions which is fully solvated in liquid water.

The aim of this project is to elucidate the complex interplay of the lipophilic core and the hydrophilic polar head groups of the lipid bilayer with the functionalized fluorophilic alkane molecules. Besides genuine structural and dynamical properties, also the aggregation tendency as function of chain length and functionalization is of high relevance within this project. Several of the quantities simulated here can be measured experimentally in collaborating groups. The available experimental data is fully consistent with the predicted structural and dynamical properties of the perflu-

orinated alkanes. More specifically, the following trends are observed in the molecular dynamics simulations; During their interactions, the short chain fluorophilic molecules took longer time to penetrate into the leaflet of the bilayer, while the longer chain molecules showed faster penetration with a reduction in their translational and rotational movement. In contrast to shorter chain perfluorinated molecules, a clustering phenomenon were observed in longer chain perfluorinated molecules. The clustering effects appeared at a distance of approximately 5 Å from each other. The formation of clusters in the fluorinated acid molecules was also observed, but not so dominant as in F10 and FTOH molecules. This confirms the better miscibility of perfluorinated acid with the lipid bilayer membrane as compared to perfluorinated alkanes and fluorinated alcohol molecules. Dynamical observations such as an increase of the order parameters and gauche-trans conformations, related to the alkyl chains of the lipid bilayer were also computed. The order parameters of the lipid alkyl chains in the presence of longer chain molecules such as (F10 , FTOH, and PFODA) were increased strongly as compared to shorter chain molecules such as F6 and F8. In case of F10 and FTOH molecules, all-trans conformations in lipid alkyl chains were increased by 19%, while in the case of a fluorinated acid (PFODA) this increase was 16%. On the basis of informations obtained from the density profiles, tilt angle of the alkyl chain of DPPC molecules and significant reduction of Area/Lipid, one can observe, that the perfluorinated decane (F10) and fluorinated alcohol (FTOH) molecules are incorporated into the lipid bilayer leaflet and cause a tilting transition of the lipid.

Keywords: Dipalmitoylphosphatidylcholine, Fluorinated compounds, Fluorotelomer alcohol, Phase transition, Diffusion, Miscibility, Fluorophilicity, onfigurations.

Contents

Title Page	i
Abstract	ii
Table of Contents	iv
List of Figures	vii
List of Tables	xii
Acknowledgments	xiii
Dedication	xv
1 Introduction	1
1.1 Biomembranes	1
1.1.1 Membrane Models	4
1.1.2 Lipid Bilayer	4
1.2 Fluorophilic and Lipophilic Molecules	6
2 Molecular Dynamics Simulation - Fundamentals and Methods	9
2.1 Fundamentals of Molecular Dynamics	9
2.1.1 Newton's Equation of Motion	10
2.1.2 Lagrangian Equation of Motion	11
2.1.3 Hamiltonian Equation of Motion	12
2.2 Integrating the Classical Equations of Motion	13
2.2.1 The Verlet Algorithm	13
2.2.2 The Velocity Verlet Algorithm	14
2.2.3 The Shake and Rattle Algorithms	15
2.3 Computational Details	16
2.4 Simulating Temperature and Pressure	17
2.5 Fundamentals of Force Fields	19
2.6 Parameters for Fluorocarbons	22
2.7 Experimentally Observable Physical Quantities	22
2.7.1 Area per Lipid	22
2.7.2 Mean Square Displacement	23
2.7.3 Center of Mass Distribution	23

2.7.4	Vector Autocorrelation	24
2.7.5	Flexibility of the Additive Molecules	24
2.7.6	Tilt Angle with Respect to Normal of the Bilayer Surface	24
2.7.7	Clustering Phenomena of the Additive Molecules	25
2.7.8	Lipid Orientation	25
2.7.9	Fluctuations in the Bilayer Thickness over Time	26
3	Perfluorinated n-Alkanes with a Membrane Bilayer	27
3.1	System Setup	27
3.1.1	Initial Configuration	27
3.1.2	Embedding Protocol	29
3.2	Convergence of the Molecular Dynamics (MD) Simulations	31
3.3	Behavior of the Additive Molecules	36
3.3.1	Density Profiles	36
3.3.2	Rotational Dynamics of the Additive Molecules	37
3.3.3	Flexibility of the Additive Molecules	39
3.3.4	Tilt Angle of the Additive Molecules in the Membrane Environment	41
3.3.5	Clustering Phenomena of the Additive Molecules	42
3.4	Response of the DPPC Bilayer System	44
3.4.1	Area per Lipid	44
3.4.2	Gauche-Trans Conformations of the DPPC Alkyl Chains	46
3.4.3	Lipid Orientation	49
3.4.4	Tilt Angle of the Alkyl Chain of DPPC Molecules	51
3.4.5	Fluctuations in the Bilayer Thickness over Time	53
3.4.6	Final Configuration of the F10 Molecules and Lipid Molecules	54
4	Fluorinated Alcohol with a Membrane Bilayer	56
4.1	Convergence of the Molecular Dynamics Simulations	57
4.2	Density Profile	59
4.3	Clustering Phenomena of the Additive Molecules	61
4.4	Area per Lipid	62
4.5	Gauche-Trans Conformations of the DPPC Alkyl Chains	64
4.6	Tilt Angle of the Alkyl Chains of DPPC Molecules	65
4.7	Tilt Angle of the Additive Molecules in the Membrane Environment	66
4.8	Lipid Orientation	67
4.9	Fluctuations in the Bilayer Thickness over Time	69
4.10	Final Configuration of FTOH Molecules and DPPC Molecules	70
5	Perfluorinated Acids with a Membrane Bilayer	72
5.1	Convergence of the Molecular Dynamics Simulation	73
5.2	Density Profile	74

5.3	Clustering Phenomena of the Additive Molecules	75
5.4	Gauche-Trans Conformations of the DPPC Alkyl Chains	76
5.5	Fluctuations in the Bilayer Thickness over Time	77
5.6	Lipid Orientation	78
5.7	Final Configuration of PFOA Molecules and Lipid Molecules	79
6	Summary	81
7	Appendix A	84
7.1	List of Symbols and Abbreviations	84
8	Appendix B	87
8.1	Data Related to the Parametrization Process of Fluorocarbons	87
8.1.1	Total Energy Function of CHARMM Force Field, its Model Interactions and Parameters	87
8.1.2	Optimization Procedure for Bonded Parameters and Charges	88
8.1.3	Optimization of van der Waals Parameters	88
8.1.4	Atom Types used for Parametrization	89
8.1.5	Bonded Parameters	90
8.1.6	Charges	92
8.1.7	Dihedral Angles	93
	Bibliography	95
9	Curriculum Vitae	103
10	DECLARATION	106

List of Figures

1.1	Simplified fluid-mosaic model of biomembranes.	3
1.2	T-P phase diagram of DPPC bilayers in excess water. Besides the Gel1, Gel2 and Gel3 phase, an additional crystalline gel phase can be induced in the low-temperature regime after prolonged cooling, which is not shown here.	3
1.3	Cross-section view of the structures that can be formed by phospholipids in aqueous solutions.	5
3.1	Initial configuration of 12 perfluorinated alkane molecules arranged in the x-y plane, and 72 molecules of DPPC molecules surrounded by 2189 water molecules.	29
3.2	Initial configuration of 12 perfluorinated molecules embedded into 72 molecules of DPPC surrounded by 2189 water molecules.	31
3.3	Area/Lipid versus time for DPPC bilayer in the presence of fluorophilic and lipophilic organic molecules (F6, F8, H10, H5F5, and F10) are presented in two categories (a) F6, F8, F10 and (b) F10, H5F5, H10.	33
3.4	Mean square displacement (MSD) of (a) perfluoro n-alkanes molecules (F6, F8, and F10) and (b) the decane derivatives of varying fluorine content (H10, H5F5, and F10) inside the DPPC environment.	35
3.5	(a) Area/Lipid versus time for DPPC membrane in the presence of F6 and (b) MSD for F6 molecules, during the last 200 ns out of 470 ns.	35
3.6	Center of mass (CM) distribution profiles of additive molecules (a) F6, F8, F10 and (b) F10, H5F5, H10 in the DPPC bilayer environment during the last 20 ns out of the total simulation time.	37
3.7	Vector (vect) auto-correlation for (a) F6, F8, F10 and (b) H10, H5F5, F10 molecules in the DPPC environment, explaining their rotational dynamics. The decaying process of the autocorrelation function indicates that the motion of the F10 molecules is hindered significantly in the DPPC environment.	39

3.8	The population density of dihedral angles, illustrating the flexibility of (a) hydrogenated decanes (H10) and (b) fluorinated decanes (F10) in the DPPC environment. Every line shows a histogram of one dihedral angle, listed from the dihedral angle of the first four carbon atoms starting from one end's carbon up to the another end's carbon of additive molecule.	40
3.9	Tilt angle of the additive molecules (a) F6, F8, F10 and (b) H10, H5F5, F10, showing probability of their orientation within DPPC bilayer.	42
3.10	Two-dimensional radial pair distribution function, explaining the clustering phenomena of the additive molecules (a) F6, F8, F10 and (b) H10, H5F5, F10 in the DPPC environment.	44
3.11	The Area/Lipid, shifting from higher value to lower value for the DPPC bilayer in the presence of additive molecules (F6, F8, H10, H5F5 and F10). The horizontal axis represents the total magnitude of Area/Lipid while the vertical axis represents the probability of the area being occupied. A shift in F6 and F10 molecules is significant while for F8 and H5F5 molecules it is under process.	46
3.12	Bar plot representation of average Area/Lipid in the presence of F6, F8, H10, H5F5 and H10 molecules.	46
3.13	Population (Pop) density of dihedral angles illustrating the alkyl chains flexibility of the pure DPPC bilayer alkyl chain in comparison to alkyl chain in the presence of F10 molecules. Every line shows the histogram of the dihedral angle population listed from the dihedral angle of the first four carbon atoms near the head group region (bottom) upto the outer end's carbon (top) of the lipid alkyl chain.	48
3.14	Population (Pop) density of dihedral angles illustrating the alkyl chains flexibility of the pure DPPC bilayer alkyl chain in comparison to alkyl chain in the presence of H10 molecules. Every line shows the histogram of the dihedral angle population listed from the dihedral angle of the first four carbon atoms near the head group region (bottom) upto the outer end's carbon (top) of the lipid alkyl chain.	48
3.15	The average amount of all-trans conformations in DPPC alkyl chains in the pure lipid system (gray) and the effect induce by hydrogenated decanes (H10) and fluorinated decanes (F10) (black).	49
3.16	Order parameter magnitude $ S_{CH} $ versus carbon index number for the alkyl chain-1 and alkyl chain-2 of DPPC bilayer. Comparing the pure DPPC alkyl chain order parameters (Triangle) with the order parameters of alkyl chain in the presence of F6 molecules (Solid circle).	50
3.17	Order parameter magnitude $ S_{CH} $ versus carbon index number for the alkyl chain-1 and alkyl chain-2 of DPPC bilayer. Comparing the pure DPPC alkyl chain order parameters (Triangle) with the order parameters of alkyl chain in the presence of F8 molecules (Solid circle).	51

3.18	Order parameter magnitude $ S_{CH} $ versus carbon index number for the alkyl chain-1 and alkyl chain-2 of DPPC bilayer. Comparing the pure DPPC alkyl chain order parameters (Triangle) with the order parameters of alkyl chain in the presence of F10 molecules (Solid circle). . .	51
3.19	Tilt angle of the alkyl chain of DPPC molecules with regard to normal of the bilayer surface. (a) pure DPPC bilayer and (b) DPPC bilayer in the presence of F10 molecules.	52
3.20	Fluctuations in the DPPC bilayer thickness over time in the presence of (a) F6, F8, F10 and (b) H10, H5F5, F10 molecules.	54
3.21	Final configuration of the system representing a fully hydrated DPPC bilayer with F10 molecules after total simulation time for two different concentration (a) 6:1 and (b) 3:1	55
4.1	(a) Area/Lipid of DPPC bilayer in the presence of FTOH molecules at different concentration and different temperatures. (b) MSD of the FTOH molecules in the DPPC environment.	58
4.2	Center of mass (CM) distribution profile of FTOH molecules and DPPC bilayer at different concentrations and different temperatures during the last 20 ns out of the total simulations time.	60
4.3	Two-dimensional radial pair distribution function, explaining the clustering phenomena of the FTOH molecules in the DPPC environment. Clustering effects are observed for these molecules in both types of system (4:1 and 6:1) and at temperatures 323 K.	62
4.4	The shift in the Area/Lipid from a higher value to lower value of the DPPC bilayer. The horizontal axis represents the total magnitude of Area/Lipid while the vertical axis represents the probability of the area being found.	63
4.5	Population (Pop) density of dihedral angles illustrating the alkyl chains flexibility of the pure DPPC bilayer alkyl chain in comparison to alkyl chain in the presence of FTOH molecules. Every line shows the histogram of the dihedral angle population listed from the dihedral angle of the first four carbon atoms near the head group region (bottom) of the alkyl chain upto the outer end's carbon (top) of the alkyl chain. . .	65
4.6	Tilt angle of the alkyl chains of DPPC molecules with regard to normal of the bilayer surface. (a) pure DPPC bilayer and (b) DPPC bilayer in the presence of FTOH molecules. The solid line is for alkyl chain-1 and dashed line is for alkyl chain-2 of lipids.	66
4.7	Tilt angle of the additive molecules within the DPPC bilayer. The tilt angle is with regard to normal of the bilayer surface, which coincides with the z-direction of the coordinate system.	67

4.8	Order parameter magnitude $ S_{CH} $ versus carbon index number for alkyl chains of DPPC bilayer simulated at 333 K in the presence of FTOH molecules (Solid circle), and pure DPPC bilayer (Triangle).	68
4.9	Order parameter magnitude $ S_{CH} $ versus carbon index number for alkyl chains of DPPC bilayer simulated at 323 K in the presence of FTOH molecules (Solid circle), and pure DPPC bilayer (Triangle).	69
4.10	Fluctuations in the DPPC bilayer thickness over time in the presence of FTOH molecules during the total simulations time.	70
4.11	Final configuration of the system presenting the DPPC bilayer with penetrated FTOH molecules, at the end of the total simulation time.	71
5.1	(a) Area/Lipid of DPPC bilayer in the presence of PFODA molecules. (b) MSD of the PFODA molecules in the DPPC environment.	74
5.2	Center of mass (CM) distribution profile of a pure DPPC (magenta) and PFODA molecules in the DPPC environment (green) during the last 20 ns out of the total simulation time. Zero represents the center of bilayer plane on x-axis.	75
5.3	Two-dimensional radial pair distribution function explaining the clustering phenomena of PFODA molecules in the DPPC environment.	76
5.4	Population (Pop) density of dihedral angles illustrating the alkyl chains flexibility of the (a) pure DPPC bilayer and (b) DPPC bilayer in the presence of PFODA molecules. Every line shows the histogram of the dihedral angle population listed from the dihedral angle of the first four carbon atoms near the head group region (bottom) of the DPPC molecules to the outer end's carbon (top) of alkyl chain.	77
5.5	Fluctuations in the DPPC bilayer thickness over time in the presence of PFODA molecules during total simulation trajectory.	78
5.6	Order parameters magnitude $ S_{CH} $ versus carbon index numbers for alkyl chain-1 and alkyl chain-2 of DPPC bilayer in the presence of PFODA molecules (Solid circle) and pure DPPC bilayer (Triangle).	79
5.7	Final configuration of bilayer membrane with PFODA molecules at the end of total simulation trajectory.	80
8.1	Model interactions and parameter usage for the total energy function of the CHARMM force field.	87
8.2	Parametrization schema for the CHARMM force field as applied for preparation of fluorocarbons parameters.	89
8.3	Atom types used for parametrization as an notation to one of the sample compounds. FCF ₂ , FCF ₃ , CCF ₂ and CCF ₃ are the newly introduced atom types.	90

-
- 8.4 Top: Interaction energy (MD) normalized by the MP2/6-31G(d) results (■) and interaction distances normalized the same way (●) over the FCF₂ net charge for f₂ together with the ideal target value (/). The CCF₂ net charge has been set such that the overall CF₂ group is neutral. It is clearly visible that there is no optimum that fits both the interaction energies and the interaction distances. Bottom: Given the weighting in Eq. 8.2, the deviation from the target values depending on the charges of FCF₂ and FCF₃ has been rasterized. The optimal value is highlighted (○). 93

List of Tables

8.1	Introduced atom types with their CHARMM-style label	90
8.2	Bond lengths b_0 in Angstroms and force constants K_b in kcal/mol/Å ²	91
8.3	Angles θ_0 in degrees and force constants K_θ in kcal/mol/rad ² . (All Urey-Bradley terms are set to zero).	91
8.4	Lennard-Jones parameter ε in kcal/mol and R_{min} in Angstroms along with charges in e. For charge in e, a correction (ε' and R'_{min}) for 1,4 atoms is suggested by CGenFF.	92
8.5	Dihedrals and their offset δ in degrees, force constants K_χ in kilocalories per mol and multiplicity η	94

Acknowledgments

All praises to Almighty Allah, the most merciful and beneficent, who is Omnipotent, Omnipresent and the source of all knowledge and wisdom. I also pay my respect to Hazrat Muhammad (P.B.U.H) and his faithful companions, who are forever a true torch of guidance for humanity as a whole.

Completing this doctoral work has been a wonderful and often overwhelming experience. It is hard to know whether it has been grappling with the physics and chemistry itself which has been the real learning experience, or grappling with how to write a paper, give a coherent talk, work in a group, code intelligibly, stay up until the birds start singing, and... stay, um... focused.

I have been very privileged to have undoubtedly the most intuitive, smart and supportive advisor anyone could ask for, namely Prof. Dr. Daniel Sebastiani. Ever since I learned from him what an avoided crossing was (animated in full colour, naturally), I have been stimulated and excited by his constant flow of good ideas. Daniel has an ability to cut through reams of quantum chemistry and physics with a single visual explanation that I will always admire, and I have learned a great deal of quantum chemistry and physics from him. He has fostered certainly the most open, friendly, collaborative and least competitive research group in the theory wing of this institute. He has also known when (and how) to give me a little push in the forward direction when I needed it.

I would like to express my profound gratitude to my supervisor Prof. Dr. Wolfgang Paul for his useful suggestions and encouragement throughout this research work. I want to express my deep appreciation to him for his supervision and for accepting me into his group.

I am indebted to Prof. Dr. Jorg Kressler and Prof. Dr. Alfred Blume for continuous guidance about the interactions of fluorinated molecules with phospholipids and for other scientific discussions.

Daniel's other students and post-docs, comprise a superb research group. The ability to bounce ideas off so many excellent minds has been priceless. My most intense collaboration has been with Tobias Watermann, whose clarity, persistence, ability to create new models, and ability to write a new publication, has taught me a lot. Christian Dressler has similarly influenced me, and I think I can safely say that everyone in the group has benefited from his generosity and collaboration. In my first years in the Daniel group, I swapped many thoughts on numerical methods, while Guido Falk von Rudorff prevented me from getting too scarred by the new realm of quantum chemistry, classical molecular dynamic simulation. Our group's secretary Tilo Wiczorek is surely the kindest, coolest and most witty person, I gone many time gossiping with. He has also helped me out many time during administrations panics. However, nothing will be complete if I don't mention the name of my friends who made my stay at Germany so joyful. From the world of physics as well quantum chemistry, Dr. Hossam Elgabarty, Dr. Martin Brehm, Felix Hoffmann, Gul Bekcioglu-Neff, Gabriel Kabbe, Arne Scherrer, Sascha Jaehnigen, Svetlana Pylaeva, Somayeh Khazaei, M. Haris Samiullah, Paul Ahlert, Laura Scarbath-Evers, and Christopher Peschel are those people with whom I have shared a camaraderie which is unparalleled.

Last but not the least, I am very much thankful to my unforgettable, affectionate and sympathetic parents, brothers, sisters, daughters, sons and wife for their endless cooperation, prayers, and passions for my brilliant future.

*Dedicated to my parents,
and my all family members.*

Chapter 1

Introduction

1.1 Biomembranes

Investigations into the functionality of membranes have evolved over time since the discovery of the fluid mosaic model [1]. A simple representation of the fluid mosaic model is shown in Figure 1.1, extracted from wikipedia. Biological membranes are composed of various types of molecules. They consist of a variety of proteins and a bilayer of lipid molecules. The position of the proteins is not fixed. They may be bound, embedded or located somewhere in the periphery [2]. Nowadays, it is generally accepted that proteins are responsible for the transport of most drugs, metabolites, active components and ingredients through cell membranes. The fate of a molecule situated in the extracellular fluid is determined by its chemical structure and the corresponding functional groups on the membrane surface.

The choice of phospholipids as a constituent in model membranes is important in describing the partitioning in a real biological system. A prominent phospholipid is

the DPPC bilayer, for which a phase transition at 41 °C has been reported [3]. For DPPC bilayers in excess water, a T-P phase diagram is shown in Figure 1.2 explaining the different phase regime [4]. DPPC is one of the constituents of the pulmonary surfactant found in lung alveoli [5]. DPPC bilayers are well characterized [6, 7], and are often used as models of the outer membrane cell leaflet. A characteristic feature of the DPPC is the gel-liquid crystalline phase transition, which occurs at a temperature T_m (melting temperature) that is dependent on the bilayer properties and solution conditions [8]. In the gel phase ($< T_m$), the lipid chains are tightly packed with strong van der Waals interactions. The chains exist in restricted lateral and rotational motion, with perpendicular alignment to the head group plane (trans conformation) and parallel alignment to each other [9, 10]. Above T_m , in the liquid crystalline phase, the bilayer is characterized by a less organized arrangement with a trans-gauche conformation of the hydrocarbon chains, increased lateral expansion, and rotational motion. The phase transition involves the melting of hydrocarbon tails which is dependent on the cohesion of the hydrocarbon chains. The gel phase is rigid with high microviscosity, which decreases with increasing temperature, and a transition to the more fluid liquid crystalline state eventually occurs. Typically, for a well-ordered bilayer, the change from gel to fluid phase is a quick transition, occurring over a very narrow temperature range. This is due to conformational restrictions of the ordered chains and excluded volume interactions between the terminal methyl groups in the bilayer [10]. As a result of these packing constraints, the chains in the bilayer became disordered by a cooperative event. Studies have demonstrated significant improvement in liposome stability with the incorporation of fluorinated chains.

Vesicles formed from partially fluorinated DPPC lipids displayed a 50-fold higher stability than pure DPPC liposomes, with additional resistance to heat sterilization [11].

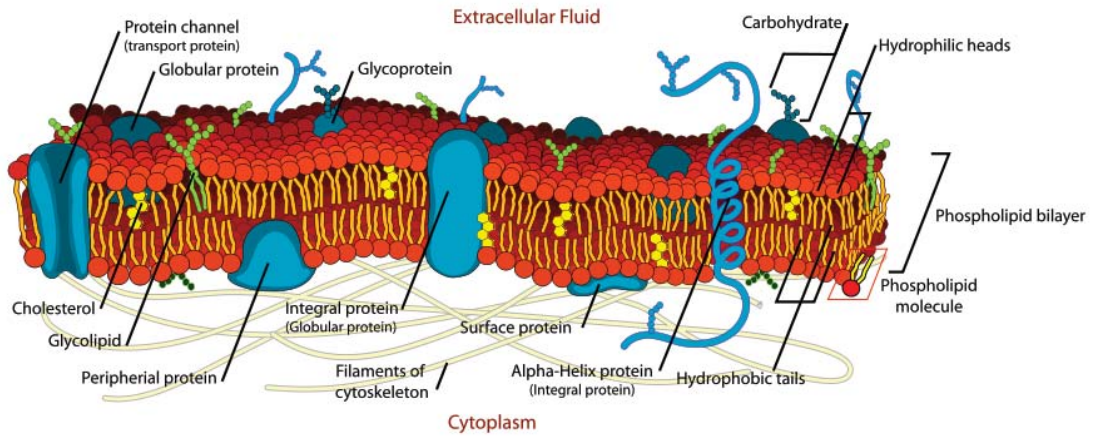


Figure 1.1: Simplified fluid-mosaic model of biomembranes.

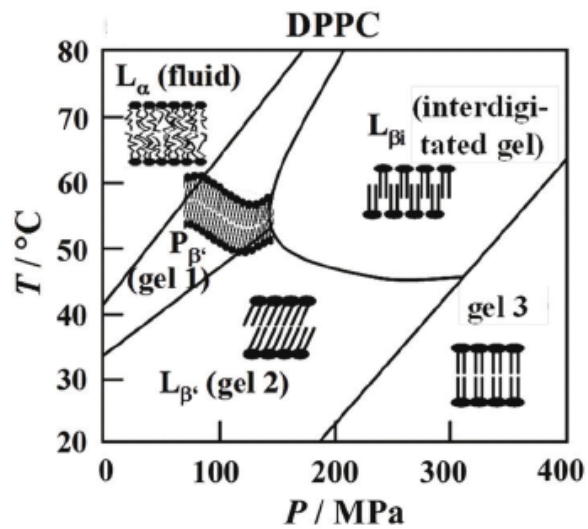


Figure 1.2: T-P phase diagram of DPPC bilayers in excess water. Besides the Gel1, Gel2 and Gel3 phase, an additional crystalline gel phase can be induced in the low-temperature regime after prolonged cooling, which is not shown here.

1.1.1 Membrane Models

The membrane systems of cells are of a composite character in nature [12]. The study of their interactions with substances such as fluorocarbons, drugs, and other small molecules is of significant biological importance. However, much simpler membrane models are utilized for reasons relating to computational effort. The most common models are lipid monolayers and bilayer liposomes [13]. In this theoretical study, the lipid bilayer will be investigated.

1.1.2 Lipid Bilayer

Phospholipid bilayers have been studied extensively as model systems for biological membranes. It is well known that lipid molecules aggregate in aqueous solution by forming spherical vesicles comprised of lipid bilayers. These vesicles, commonly known as liposomes, vary in size generally between $0.025 \mu\text{m}$ and $2.5 \mu\text{m}$ [14]. The smaller unilamellar vesicles consist of a single bilayer, whereas the multilamellar vesicles contain more than one lipid bilayer. Their generalized appearances are shown in Figure 1.3 (adapted from wikipedia) in the form of vesicles, micelle and bilayer sheet. In aqueous solution, the lipid molecules display a variety of lyotropic phases, comprising the micellar, lamellar and hexagonal state [15]. In most cases, lamellar phases consist of bilayers and exhibit thermotropic polymorphism depending upon the lipid structure [16]. The manifestation of phases is also dependent on the degree of hydration, the pressure, and the environmental conditions [16]. Under physiologically relevant conditions with regard to temperature and hydration, these bilayers exist in a fluid state that is characterized by a high degree of disorder and is very difficult to

structurally characterize using standard techniques such as X-ray diffraction. Molecular dynamics simulations have emerged to play a crucial role in understanding the structure and dynamics of these lipid bilayers. Simplified systems are usually used for computational studies with varying concepts of membrane model investigations [13]. In this project, a series of molecular dynamics simulations has been carried out to investigate the interactions of a fully hydrated fluid state DPPC bilayer with fluorophilic and lipophilic organic molecules in the isothermal-isobaric (NPT) ensemble.

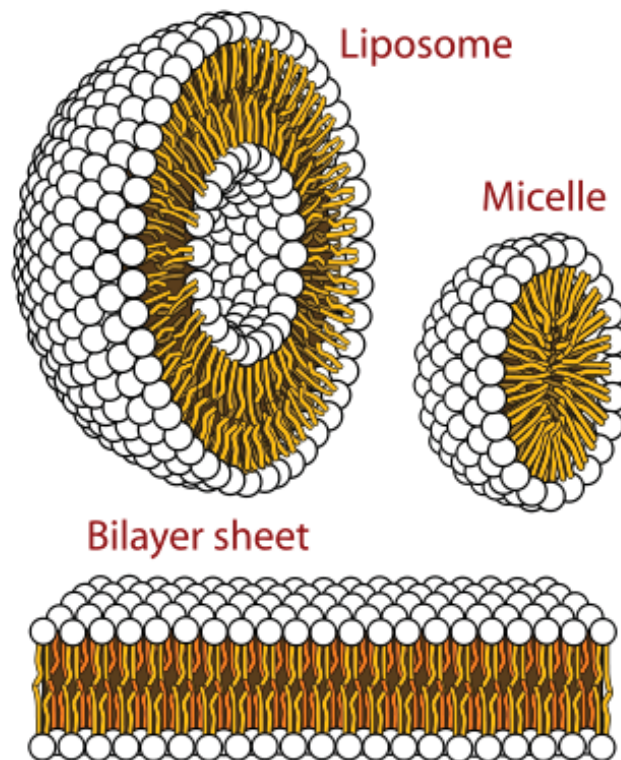


Figure 1.3: Cross-section view of the structures that can be formed by phospholipids in aqueous solutions.

1.2 Fluorophilic and Lipophilic Molecules

The investigation of fluorophilicity on the basis of a genuine structure serves as a foundation for various uses and applications in a range of scientific fields. As a preliminary step on the way to investigating large polyphilic molecules with membranes, the simplest type of fluorophilic and lipophilic additives are investigated, namely perfluoro n-hexane (F6), perfluoro n-octane (F8), perfluoro n-decane (F10), partially fluorinated decane (H5F5) [*5 carbons attached to hydrogens, and 5 carbons attached to fluorine*], normal decane (H10), fluorotelomer alcohol (FTOH), and perfluoro octadecanoic acid (PFODA) molecules. Some of these molecules exhibit both hydrophobicity and lipophobicity, while some are lipophilic. These small molecules investigation with membrane is an elementary building block and fundamental starting point for the investigation of large polyphilic molecules (linear, X-shaped, and T-shaped polyphile) interacting with phospholipid bilayer membranes. Perfluorinated n-alkanes represent a very interesting class of molecules due to their specific and unusual properties. As a result of this nature, they are considerably more hydrophobic than lipids, but they are not lipophilic either, and they have substantial applications in biochemistry. Despite their structural similarity to hydrocarbons, they have high thermal stability and chemical inactivity [17]. Although strong intramolecular forces are ensured by the C-F bond, the weak polarizability of the fluorinated chains results in low intermolecular or van der Waals interactions [18]. Minimal intermolecular interactions, coupled with the bulkiness and rigidity of the C-F chains, lead to higher density, higher melting points, lower surface tension, low refractive indices, lower boiling points and surface spreading of fluorocarbon compounds in comparison with hydrocarbons [19]. Per-

fluorinated compounds (PFCs) have numerous applications for medical purposes as oxygen-carrier fluids [20, 21], in purification or polymerization [20], and as lubricants [22]. PFCs are especially interesting due to their phase separation behavior in hydrocarbon environments [23]. The versatility of their applications can be attributed to the strength of the C-F covalent bond, which results in physicochemical properties that are distinct from traditional hydrocarbon-based systems [24, 25].

Fluorinated amphiphiles are also attractive because of their properties such as combined hydrophobicity and lipophobicity [26], high gas-dissolving capacity, chemical and biological inertness, and high fluidity [26, 27]. The fundamental properties and potential applications of fluorinated amphiphiles have been reviewed in the literature [21, 22]. It is generally perceived that fluorine exerts only a moderate steric influence relative to hydrogen in organic compounds [28], but the electronegativity of fluorine can have significant electronic influences. Amphiphiles with short F-chains ($nF \leq 8$) are considered to be acceptable in clinical applications. In addition, highly fluorinated amphiphiles have multiple applications in materials science [21, 29, 30] as well as in the biomedical field, often involving colloidal systems, stabilized by monomolecular films of fluorinated amphiphiles. They could find applications as blood substitutes [29, 31, 32, 33, 34] and lung surfactant replacements [35, 36, 37, 38]. As examples, fluorinated alcohols such as hexafluoroisopropanol (HFIP) and trifluoroethanol (TFE) are not considered *sensu stricto* as fluorous media [39]. However, the presence of one or more fluoroalkyl groups introduces specific properties to fluorinated alcohols compared with those that are non-fluorinated. They have high ionizing power [40] and an acidic character [41]. They are strong hydrogen bond donors [42] and poor

nucleophiles [43]. The properties of fluorinated alcohols have been exploited in physical organic chemistry [43], in the stabilization of radical cations [44], and for their effect on the conformation of proteins and peptides [45].

Among fluorinated alcohols, fluorotelomer alcohols (FTOHs) play a significant role in studies of atmospheric chemistry. FTOHs are linear fluorinated alcohols with the formula $C_nF_{2n+1}C_2H_4OH$ ($n = 2, 4, 6, \dots$) [46, 47]. An individual molecule is commonly named by the number of fluorocarbons to the number that are hydrocarbon-based. For example, a molecule with 8 fluorinated carbons and 2 hydrogenated carbons with an alcohol group can be represented by 8:2 FTOH. The FTOH molecules have similar physicochemical properties to those of perfluoro-*n*-alkanes. For this reason, the author has focused on fluorinated alcohols, i.e., $C_8F_{17}(C_2H_4)OH$, which have a hydroxyl group of very weak acid in a normal aqueous environment and are not strongly affected by pH. Some properties of this alcohol have already been investigated; however, there are no systematic investigations. We have investigated the properties of fluorinated acids with the aim of improving knowledge of amphiphiles. Long-chain PFCAs ($C_nF_{2n+1}COOH$) where ($n \geq 6$) have been observed in large lakes [48]. PFCAs resist degradation by oxidation and hydrolysis, and have a tendency to accumulate in the human body [49, 50, 51, 52]. Their fundamental properties such as miscibility, philicity, and the phase behavior are still poorly documented; the physicochemical properties of PFCAs have been well characterized, but their interactions with other compounds have not been well investigated. In particular, it has not yet been clarified how the degree of fluorination in a molecule affects its original properties. For this reason, we chose to investigate the interaction of PFODA with a membrane.

Chapter 2

Molecular Dynamics Simulation - Fundamentals and Methods

This chapter introduces a summary of the theoretical framework to carry out a molecular dynamics simulation, with particular emphasis on large scale biomolecular systems. For more detailed information, refer to the numerous excellent book cited in Ref. [53] available on these particular theoretical subjects.

2.1 Fundamentals of Molecular Dynamics

Molecular dynamics is a technique to investigate assemblies of molecules, and explore their microscopic interactions in different environments at the atomistic level. This computational method provides the prediction of the time evolution of a set of interacting particles by solving the classical equations of motions numerically at ambient conditions. Integration of these equations of motions for each particle in the

given system provides a set of configurations of the system, the so-called trajectory. This output describes the positions and velocities of the particles as they evolve with time. One can then extract the averaged values of the structural and dynamical properties from this generated trajectory.

2.1.1 Newton's Equation of Motion

The molecular dynamics simulation method is based on solution of Newton's second law or the classical equations of motion given by

$$\vec{F}_i = m_i \frac{d^2 \vec{r}_i}{dt^2}, \quad (2.1)$$

where \vec{F}_i is the force acting upon the particle i at time t , m_i and $r_i = (x_i, y_i, z_i)$ are the mass, and the position vector of the particle i , respectively. For conservative forces, the exerted force on the particle i can be determined by the gradient of the potential energy U of the system of N interacting particles with respect to the atomic displacements as:

$$\vec{F}_i = -\nabla_{r_i} U(\vec{r}_1, \dots, \vec{r}_N). \quad (2.2)$$

To solve Eq. (2.2), one needs to specify the instantaneous forces acting on the particles in the system and their initial positions and velocities. Due to the complexity (coupling of differential equations) of the many particle problem, these classical equations of motion must be solved numerically. Several methods exist to propagate the positions and velocities with a finite time interval by integrating the equations of motions [54]. The following section will introduce the most common numerical algorithms for integration of the classical equations of motion used in molecular dynamical simulations.

2.1.2 Lagrangian Equation of Motion

Another formalism for describing mechanical systems are the Lagrangian equations of motion. Such a system is completely described by its characteristic Lagrange function $\mathcal{L}(q_i, \dot{q}_i, t)$, where q_i and \dot{q}_i denote the position and velocity of particle i , respectively. In case of an autonomous system (*i. e.*, with time-independent potential function), the Lagrange function does not explicitly depend on the time and can be written as $\mathcal{L}(q_i, \dot{q}_i)$. For a given system, the Lagrange function can be defined by

$$\mathcal{L} = T - V, \quad (2.3)$$

where T stands for the kinetic energy and V for the potential energy of the system. The kinetic energy term usually reads

$$T(\dot{q}) = \frac{m}{2} \dot{q}^2, \quad (2.4)$$

with generalized mass m , whereas the potential energy term is completely system-dependent.

In order to derive the equations of motion from such a Lagrange function, the Euler-Lagrange equation is applied, which reads

$$\frac{d}{dt} \frac{\partial \mathcal{L}}{\partial \dot{q}_i} - \frac{\partial \mathcal{L}}{\partial q_i} = 0 \quad (2.5)$$

for each degree of freedom i under consideration. This means that a set of N such second-order differential equations needs to be solved to obtain the equations of motion for a system with N degrees of freedom.

2.1.3 Hamiltonian Equation of Motion

Based on the Lagrange formalism introduced in the last section, another important formalism for mechanical systems can be derived, which is the Hamilton formalism. Given an autonomous system and its Lagrange function $\mathcal{L}(q_i, \dot{q}_i)$, the Hamilton function $\mathcal{H}(q_i, p_i)$ of the system can be obtained by applying a Legendre transformation

$$\mathcal{H}(q, p) = p\dot{q} - \mathcal{L}(q, \dot{q}) \quad (2.6)$$

with the conjugate momentum defined by $p = \frac{\partial \mathcal{L}}{\partial \dot{q}_i}$.

The Hamilton function still depends on the coordinates q_i , but instead of the velocities \dot{q}_i which appeared in the Lagrange function, it depends on the generalized momenta p_i . By inserting the definition of \mathcal{L} and subsequently applying $p = m\dot{q}$, one obtains

$$\mathcal{H}(q, p) = p\dot{q} - \mathcal{L}(q, \dot{q}) \quad (2.7)$$

$$= p\dot{q} - T + V \quad (2.8)$$

$$= p\dot{q} - \frac{m}{2}\dot{q}^2 + V \quad (2.9)$$

$$= m\dot{q}^2 - \frac{m}{2}\dot{q}^2 + V \quad (2.10)$$

$$= \frac{m}{2}\dot{q}^2 + V \quad (2.11)$$

$$= T + V. \quad (2.12)$$

Therefore, we find that the Hamilton function of the system equals the total energy.

To derive the system's equations of motion from the Hamilton function, the canonical Hamilton equations are applied, which are given by

$$\frac{\partial \mathcal{H}}{\partial p_i} = \dot{q}_i, \quad (2.13)$$

$$\frac{\partial \mathcal{H}}{\partial q_i} = -\dot{p}_i. \quad (2.14)$$

In contrast to the Lagrange formalism, one needs to solve a set of $2N$ first-order differential equations to obtain the equations of motion for a system with N degrees of freedom. As first-order differential equations are easier to solve than second-order differential equations, the Hamilton formalism is very important in many fields of science.

By considering the total time derivative of \mathcal{H} , we find

$$\frac{d\mathcal{H}}{dt} = \frac{\partial\mathcal{H}}{\partial p}\dot{p} + \frac{\partial\mathcal{H}}{\partial q}\dot{q} + \frac{\partial\mathcal{H}}{\partial t} \quad (2.15)$$

$$= \dot{q}\dot{p} - \dot{p}\dot{q} + \frac{\partial\mathcal{H}}{\partial t} \quad (2.16)$$

$$= \frac{\partial\mathcal{H}}{\partial t}. \quad (2.17)$$

Therefore, if \mathcal{H} does not explicitly depend on time (*i.e.*, autonomous system), it directly follows that \mathcal{H} is constant over time, which means that the total energy is conserved. This means that every mechanical system with time-independent Hamilton function is energy-conserving.

2.2 Integrating the Classical Equations of Motion

2.2.1 The Verlet Algorithm

The aim of the numerical integration of the equations of motion is to propagate the positions $\vec{r}_i(t + \Delta t)$ at time $t + \Delta t$ in terms of the initial positions at time t . The Verlet algorithm is one of the most common and simplest of all other integrator algorithms used in molecular dynamical simulations [54], which can be derived from

the Taylor expansions for the positions $\vec{r}_i(t)$; it follows

$$\begin{aligned}\vec{r}_i(t + \Delta t) &\approx \vec{r}_i(t) + \Delta t \vec{v}_i(t) + \frac{1}{2} \Delta t^2 \ddot{\vec{r}}_i(t) \\ &\approx \vec{r}_i(t) + \Delta t \vec{v}_i(t) + \frac{\Delta t^2}{2m_i} \vec{F}_i(t).\end{aligned}\tag{2.18}$$

in Eq. 2.18, the velocity term can be replaced by writing a similar expansion for $\vec{r}_i(t - \Delta t)$ as :

$$\vec{r}_i(t - \Delta t) \approx \vec{r}_i(t) - \Delta t \vec{v}_i(t) + \frac{\Delta t^2}{2m_i} \vec{F}_i(t).\tag{2.19}$$

By adding Eq. 2.18 and Eq. 2.19, the final expression for the positions $\vec{r}_i(t + \Delta t)$ is obtained as:

$$\vec{r}_i(t + \Delta t) \approx 2\vec{r}_i(t) - \vec{r}_i(t - \Delta t) + \frac{\Delta t^2}{2m_i} \vec{F}_i(t).\tag{2.20}$$

With Eq. 2.20, positions and velocities of the particles can be propagated forward in time by a time step Δt . Note that, the Verlet algorithm does not use explicit velocities to determine the positions. The velocities at any time are computed by a centered difference:

$$\vec{v}_i(t) = \frac{\vec{r}_i(t + \Delta t) - \vec{r}_i(t - \Delta t)}{2\Delta t}.\tag{2.21}$$

is interesting to note that by adding Eq. 2.19 and Eq. 2.20 we get rid of all the odd-order terms thus the *local* error in the Verlet algorithm is $\mathcal{O}(\Delta t^4)$, even though it contains no explicit third-order term [55].

2.2.2 The Velocity Verlet Algorithm

An improvement over the Verlet algorithm is introduced by explicit inclusion of the velocities of the particles at each time step, the so-called velocity Verlet algorithm [56]. Therefore, the positions and velocities are propagated on a single time step. These

equations can be written by starting from $\vec{r}_i(t + \Delta t)$ and move by a time step of $-\Delta t$, which reads

$$\vec{r}_i(t) \approx \vec{r}_i(t + \Delta t) - \Delta t \vec{v}_i(t + \Delta t) + \frac{\Delta t^2}{2m_i} \vec{F}_i(t + \Delta t). \quad (2.22)$$

The velocities $\vec{v}_i(t + \Delta t)$ are then generated as

$$\vec{v}_i(t + \Delta t) \approx \vec{v}_i(t) + \frac{\Delta t}{2m_i} \left[\vec{F}_i + \vec{F}_i(t + \Delta t) \right]. \quad (2.23)$$

It should be mentioned here that both the Verlet and the velocity Verlet algorithms are very robust and numerically very stable. More details about the important features of numerous integrators can be found in Ref. [53].

2.2.3 The Shake and Rattle Algorithms

One of the most crucial problem with all numerical integration algorithms is that the time step Δt must be smaller than the fastest modes in the given molecular system. Typically, these modes oscillate on the range of few femtoseconds e.g. bond stretches involving hydrogen atoms. However, this time step size is very short compared to many important reactions happening in large biological systems. For example, folding or conformational changes of proteins occur of the order of nanoseconds to microseconds. In order to reduce the computational effort of simulating such large scale molecular systems, it is necessary to use a time step as large as possible. The most common approach to increase the time step is to apply constraints to the fastest degrees of freedom in the system and to solve the classical equations of motion for the slower degrees of freedom. The SHAKE and RATTLE algorithms are widely used constraint schemes in large scale molecular simulations [57, 58, 59]. The SHAKE

algorithm is mostly used with the Verlet algorithm. Referring to the Eqs. 2.18, 2.19, 2.20, the Verlet algorithm within the presence of constraints is expressed as:

$$\vec{r}_i(t + \Delta t) \approx 2\vec{r}_i(t) - \vec{r}_i(t - \Delta t) + \frac{\Delta t^2}{2m_i}\vec{F}_i(t) + \frac{\Delta t^2}{2m_i}g_S[\vec{r}(t), \vec{v}(t)], \quad (2.24)$$

where g_S includes the forces associated with the constraints. The velocities are then recalculated based on the the coordinates, which are constrained throughout. On the other hand, the RATTLE algorithm is particular to the velocity Verlet algorithm. Again, referring to the Eqs. 2.22, 2.23:

$$\vec{r}_i(t) \approx \vec{r}_i(t + \Delta t) - \Delta t\vec{v}_i(t + \Delta t) + \frac{\Delta t^2}{2m_i}\vec{F}_i(t + \Delta t) + \frac{\Delta t^2}{2m_i}g_{RR}[\vec{r}(t)], \quad (2.25)$$

where g_{RR} is again the force associated with the constraints. The velocities $\vec{v}_i(t + \Delta t)$ are then generated as

$$\vec{v}_i(t + \Delta t) \approx \vec{v}_i(t) + \frac{\Delta t}{2m_i} \left[\vec{F}_i + \vec{F}_i(t + \Delta t) + g_{RR}(t) + g_{VR}(t) \right], \quad (2.26)$$

where g_{RV} is the constrained forces.

2.3 Computational Details

Simulations were performed with newly developed parameters based on the CHARMM force field [17]. The simulation contains a bilayer of 72 DPPC molecules and 2189 water molecules. The lipid bilayer was sandwiched between the layers of water. The total system size was initially $47.4222 \times 47.4222 \times 68.333 \text{ \AA}$, and periodic boundary conditions were used to minimize the artificial boundary effects. In these simulations, the temperature was controlled by weak coupling to a heat bath of 323 K. The pressure was kept at 1.013 bar, while the height of the simulation box was allowed

to vary independently from the lateral directions. The time step was 1.5 fs with all rigid bond lengths constrained using a Verlet algorithm. The cutoff distance for the non-bonded interactions was 15 nm and a switch distance of 12 nm was used. The treatment of electrostatic interactions has the largest impact on the space occupied by the bilayer structure during the simulation [60]. With this effect in mind, we applied the particle mesh Ewald summation to avoid possible artifacts created by cutting the long-range electrostatic interactions. The initial atomic velocities were randomly generated from a Maxwell-Boltzmann distribution at 323 K. Different potential functions have been developed over the last three decades for the water monomer and liquid water [61, 62, 63, 64, 65, 66, 67, 68, 69, 70, 71, 72, 73]. For water, the TIP3P (transferable intermolecular potential 3P) model is used here. The classical geometry minimization and MD simulations have been calculated with NAMD 2.9 [74]. Parts of the analysis were carried out with the help of VMD, its force field toolkit and MD analysis [75, 76, 77, 78].

2.4 Simulating Temperature and Pressure

The integration of Newton's equations of motions of an isolated system generates a dynamics in which the total energy is conserved. In this situation, the total number of particles N , the volume V of the simulation box and the total energy E of the system are constant. This setup is called NVE or microcanonical ensemble [53]. Experiments are often done at constant temperature or constant pressure and not at constant energy of the system. The first situation at constant temperature corresponds to a constant number of particles N , a constant volume V and a constant temperature T .

The NVT ensemble is also called canonical ensemble. With a constant number of particles N at constant pressure P and constant temperature T we obtain the NPT ensemble. Another reason to do simulations at constant pressure is the choice of the volume of the simulation. In the setup of the calculation it is difficult to determine the total density of a system consisting of different phases, because only the densities of the components in the bulk are generally available. An equilibration of the simulation box can help here. We want to simulate the NVT and NPT ensembles to compare our results with experiment. To do this, additional effects need to be added to Newton's equations of motion. In NAMD, the Langevin equation is used to generate the dynamics at constant temperature [74].

$$M\dot{\vec{v}} = \vec{F}(\vec{r}) - \gamma\vec{v} + \sqrt{\frac{2\gamma k_B T}{M}}\vec{R}(t) \quad (2.27)$$

The particle of mass M is at position \vec{r} with velocity \vec{v} . It feels the force $\vec{F}(\vec{r})$. The Langevin equation has two additional terms. The first additional term is a friction term with a friction coefficient γ . The second term is a random variable which follows a Gaussian process. These two terms add noise to the dynamics of the particle, which models the interaction of the particle with the environment. The friction coefficient and the random variable are used to control the temperature of the simulation. To model a changing pressure, NAMD uses the Langevin piston algorithm [72].

$$\dot{\vec{r}} = \vec{p}/M + \frac{1}{3}\frac{\dot{V}}{V}\vec{r} \quad (2.28)$$

$$\dot{\vec{p}} = \vec{F}(r) - \frac{1}{3}\frac{\dot{V}}{V}\vec{p} \quad (2.29)$$

$$\ddot{V} = \frac{1}{W}[P(T) - P_{ext}] - \gamma\dot{V} + R(t) \quad (2.30)$$

The Langevin piston is modeled as an additional degree freedom. The equations of motions of the particles now have additional terms that depend on the volume of the simulation cell and its time derivative.

2.5 Fundamentals of Force Fields

Many of the molecular systems that could be tackled with theoretical methods are unfortunately too large to be considered by quantum mechanical methods. Even if one ignores some of the electrons (e.g. using pseudopotentials or semi-empirical quantum mechanical methods), the length scales and time scales that need to be covered to answer some questions are simply far beyond the computational capabilities of the present-day, or even those of the foreseeable future. Force field methods (also known as molecular mechanics), using simple empirical potential energy functions, calculate the energy of a system as a function of the nuclear positions only, ignoring any explicit consideration of the electrons all together. The energy functions in force fields are based upon a rather simple model of the interactions within molecular systems with energy contributions from the stretching of bonds, the opening and closing of angles and the rotations about single bonds ... etc. The gain of course is substantial regarding the number of atoms that can be simulated, with the trade offs being in the loss of any explicit treatment of the electronic structure, and a heavy dependence on tedious parametrization schemes.

The utility of force fields depends on the validity of two core assumptions that are always implicitly taken for granted. One of these assumptions is the validity of the Born-Oppenheimer approximation, as it would be meaningless to talk at all about po-

tential energy functions of the atomic positions without this approximation. Another assumption is the transferability of the force field parameters, i.e. a set of parameters developed and tested on a relatively small number of cases to be applied to a much wider range of problems. Transferability allows parameters developed from data on small molecules to be used to study much larger molecules such as polymers.

Most of the present-day molecular force fields are composed of a collection of bonded and non-bonded energy terms. The bonded terms associate energy penalties with the deviation of bonds (two-atom terms) and angles (three atom terms) and dihedrals (four atom terms) from some chosen reference or equilibrium values. The exact form of the penalty function (functional form), the atom-specific parameters (equilibrium reference values, steepness of the potential... etc), and the rules to identify the atoms to which the parameters apply (atom types), all collectively define the force field. In addition to the bonded terms, a force field also includes non-bonded terms, which typically include a long-range Coulombic interaction and a shorter-range van der Waals term. The last terms are the most computationally intensive to calculate as they must be calculated for each pair of atoms in the system. Atoms that are topologically connected via one or two bonds are typically excluded from contributing to non-bonded interactions. Force fields differ in the way they exclude or (partially) include non-bonded interactions between atoms separated by three bonds. In this work we use the popular CHARMM force field [79, 80, 81, 82], which has been extensively applied in the literature to model lipid bilayers. For our context, the new CHARMM force field parameters were found to give a nearly quantitative description of the lipophilicity/lipophobicity of perfluorinated chains [17]. The functional form

of the CHARMM force field is given as:

$$\begin{aligned}
 E = & \sum_{bonds} K_b(b - b_0)^2 + \sum_{angles} K_\theta(\theta - \theta_0)^2 \\
 & + \sum_{dihedrals} K_\phi(1 + \cos(n\phi - \delta)) + \sum_{improper} K_\varphi(\varphi - \varphi_0)^2 \\
 & + \sum_{Urey-Bradley} K_u(u - u_0)^2 \\
 & + \sum_{i < j} 4\epsilon \left[\left(\frac{\sigma_{ij}}{r_{ij}} \right)^{12} - \left(\frac{\sigma_{ij}}{r_{ij}} \right)^6 \right] + \sum_{i < j} \frac{q_i q_j}{4\pi\epsilon_0 r}
 \end{aligned} \tag{2.31}$$

The first five terms in the CHARMM energy function are the bonded terms, the expressions iterate only over bonded segments of the overall topology (which is typically kept constant over the whole simulation run). In addition to the generic force field bonded terms that we have previously outlined, the CHARMM force field includes an improper torsional term that is essentially an out-of-plane bending term, and the Urey-Bradley term, which is an additional angle-bending term that works via a 1,3 non-bonded interaction rather than the explicit angle-bending potential. The force field parameters are depicted in Figure (8.1). For non-bonded interactions, the CHARMM force field uses the common Lennard-Jones model [83], and a coulomb term for the charge interactions. The origin of the r^{-6} attractive part of the Lennard-Jones potential is the molecular dipole-dipole interactions, which is indeed the physical origin of intermolecular (van der Waals) attraction. The repulsive part has its origin in the Pauli exclusion principle and it would be better reproduced by an exponential term[84], but for computational convenience it is simply represented as a squared r^{-6} term. The proper handling of long-range electrostatics in biomolecular simulations cannot be overemphasized. These interactions are the most demanding to compute, and a simple truncation would lead to serious artefacts even when using very long

cutoff distances[85]. Due to this reason, efficient numerical implementations, mostly based on the Ewald summation method, are typically employed [86, 87].

2.6 Parameters for Fluorocarbons

In this work there is a particular focus on polyphilic molecules in a membrane environment, specifically, perfluorocarbons. A precursor theoretical project dealt with the CHARMM-compatible parametrization of fluorocarbons[17], using the standard parametrization procedure for the CHARMM force field, thus ensuring compatibility with the other existing CHARMM parameters. In developing those parameters particular emphasis was placed on the careful tuning of the Lennard-Jones parameters, which is of paramount importance given the prominent role of van der Waals interactions within membrane environments. This extension of the CHARMM parameter set toward perfluorinated organic molecules enlarges the applicability of this (already versatile) force field to applications in the structural and dynamical properties of polyphilic organic compounds embedded in lipid membranes. In this work we have adopted those parameters, which are given in detail in Appendix B.

2.7 Experimentally Observable Physical Quantities

2.7.1 Area per Lipid

To understand the effect of the additives on the lateral density of the bilayer structure, the area per lipid of the liquid crystalline phase of DPPC bilayer is calculated from the simulations. The area per lipid is determined by multiplying the x

dimension and y dimension of a unit cell made of the lipid molecules and dividing by the number of lipids present in a single layer without consideration of fluorophilic or lipophilic molecules in the bilayer. To compare with simulations, this quantity can also be determined experimentally by neutron and X-ray scattering analysis.

2.7.2 Mean Square Displacement

Another quantity of interest is the self diffusion of additive molecules inside the membrane environment, which is described by the mean square displacement (MSD) of the molecules. It can be obtained from the simulations by calculating

$$MSD \equiv \langle r^2 \rangle = \langle |[\vec{R}_F(t) - \vec{R}_s(t)] - [\vec{R}_F(0) - \vec{R}_s(0)]|^2 \rangle \quad (2.32)$$

where $\vec{R}_F(t)$ is the center of mass vector of the additive molecules for time t . In order to eliminate system drift during the simulation, it is necessary to subtract the center of mass vector \vec{R}_s . Experimentally, self diffusion can be determined by fluorescence correlation spectroscopy (FCS) analysis in the liquid phase.

2.7.3 Center of Mass Distribution

Based on the simulations, the distribution of the additive molecules within the membrane environments can be investigated by calculating the density profile of the molecules center of mass along the membrane surface normal. These density profiles give insight if a certain additive molecule is more likely to be found on the surface of the membrane or in the interior.

2.7.4 Vector Autocorrelation

Another interesting quantity which gives insight into the dynamics of the simulations is the autocorrelation function of some vector within the molecules, which depicts the vector reorientation dynamics. Generally, it can be obtained by

$$C(t) = \frac{1}{NT} \sum_{i=1}^N \sum_{t=0}^T \frac{\langle V_i(t) \cdot V_i(t + \tau) \rangle}{\langle V_i(t) \cdot V_i(t) \rangle} \quad (2.33)$$

where $V(t)$ is the time-dependent vector and “ \cdot ” denotes the vector dot product and τ is the increasing correlation time. The resulting function ranges from -1 up to 1. If the two vectors are parallel to each other, then the result is one, and if they are either perpendicular or anti-parallel, then it becomes 0 and -1, respectively. Within this thesis, the vector is defined from the carbon atom at one end, to the carbon at the other end of the molecule.

2.7.5 Flexibility of the Additive Molecules

Flexibility of the additive molecules within the simulation can be elucidated, e.g., in terms of dihedral angles. The dihedral angle defined by the first four atoms of the carbon chain of the additive molecules is presented by histogram. The histogram of the mentioned dihedral angle will be discussed. Experimentally the statistics of gauche-trans conformations can be observed by NMR studies.

2.7.6 Tilt Angle with Respect to Normal of the Bilayer Surface

In the simulations, the DPPC bilayer is oriented in such a way that the normal vector of the bilayer surface coincides with one Cartesian axis (z-axis). The alignment

of the additive molecules relative to the normal of the bilayer surface can then be easily calculated by considering a vector within the additive molecules. This vector is defined from the carbon atoms of the additive molecule. Experimentally, NMR technique can be used for to determine fluctuations, particle movement, conformational changes.

2.7.7 Clustering Phenomena of the Additive Molecules

To investigate clustering phenomena from the simulations, the radial pair distribution function $g_{XY}(r)$ is used, which is proportional to the probability of finding molecule Y at a distance r from molecule X . $g_{XY}(r)$ of the additive molecules is evaluated in the membrane environment according to the pairwise distance concept. According to this concept, the corresponding number of molecules around a reference point was estimated. The system was considered as a two-dimensional box. One molecule out of the 12 molecules was considered as a reference point. The distribution function yields the probability density of neighboring molecules at a given distance r around the reference molecule. Experimentally, this quantity can be investigated by, e.g., monitoring depletion in the cluster signal, using a bolometer, or mass spectroscopy as well as IR spectroscopy.

2.7.8 Lipid Orientation

The alkyl chain order parameters are used to explain the lipid packing phenomena. Experimentally, Deuterium (^2H) NMR spectroscopy provides detailed information regarding the structural fluctuations of the lipid bilayer and lipid packing, including both the equilibrium properties and dynamics. It reveals detailed aspects with regard

to the lipid chain packing from which structural parameters can be obtained. During the simulations, the orientation of the phospholipid tail groups is investigated in terms of the consideration of hydrogen order parameters with respect to the position along the alkyl chain. C-H order parameters were calculated by first generating the hydrogen locations for all molecules in each time configuration. Then hydrogen order parameters S_{CH} were computed using the following equation,

$$S_{CH} = \frac{1}{2nm} \sum_{n=1}^n \sum_{m=1}^m \left(\frac{3r_{nm,z}^2}{|r_{nm}|^2} - 1 \right) \quad (2.34)$$

where r_{nm} is the C-H vector at molecule m with a time frame n while the z -axis of the system was parallel to the bilayer normal.

2.7.9 Fluctuations in the Bilayer Thickness over Time

Experimentally the bilayer thickness for liquid crystalline DPPC bilayer can be determined by neutron and X-ray scattering analysis. Computationally, it can be calculated on the basis of the average distance concept. According to this concept, the net average distance is obtained from the position of the phosphorus in the head group region of the upper layer to the phosphorus position in the head group region of the lower layer. The average through all DPPC molecules in the upper and lower layer over time is taken. The average thickness is expressed by

$$\langle R \rangle = \frac{1}{T} \int_0^T \left\| R_z(t) - r_z(t) \right\| dt, \quad (2.35)$$

where $R_z(t)$ and $r_z(t)$ represent the time-dependent z coordinate of the phosphorus atom within upper and lower lipid layer, respectively.

Chapter 3

Perfluorinated n-Alkanes with a Membrane Bilayer

3.1 System Setup

3.1.1 Initial Configuration

Phospholipid bilayers have been studied extensively as a model for biological membranes. Under specific conditions of temperature and hydration, these bilayers exist in a fluid state and exhibit a high degree of disorder that is very difficult to characterize by standard techniques such as X-ray diffraction. For this reason, molecular dynamics simulations have played a very important role in characterizing the structure and dynamics of these lipid bilayers. In this project, a series of molecular dynamics simulations have been carried out to investigate the interaction of a fully hydrated DPPC bilayer with fluorophilic and lipophilic molecules under the isothermal-isobaric (NPT)

ensemble. Our system consists of 72 DPPC molecules, stacked as bilayer, 12 fluorinated molecules and a total of 2189 water molecules, which enveloped the bilayer from both sides. This corresponds roughly to 30 water molecules per lipid, which is within the range found experimentally for the number of water molecules at saturation [18]. In our simulations, we follow the usual convention, i.e., the normal vector to the membrane plane was considered to be along the z -direction of the coordinate system. Equilibrating a membrane bilayer is computationally expensive due to the slow relaxation time of the system. In membrane simulations, the common practice is to start from an already pre-equilibrated membrane patch that is provided by other research groups (usually the developers of the lipid force field parameters). For this work, we obtained the starting pre-equilibrated DPPC bilayer system from Dr. Jefferey B. Klauda, University of Maryland. In addition to the standard CHARMM parameters for DPPC and water, we have introduced new atom types and CHARMM-compatible force-field parameters for our fluorinated molecule [17].

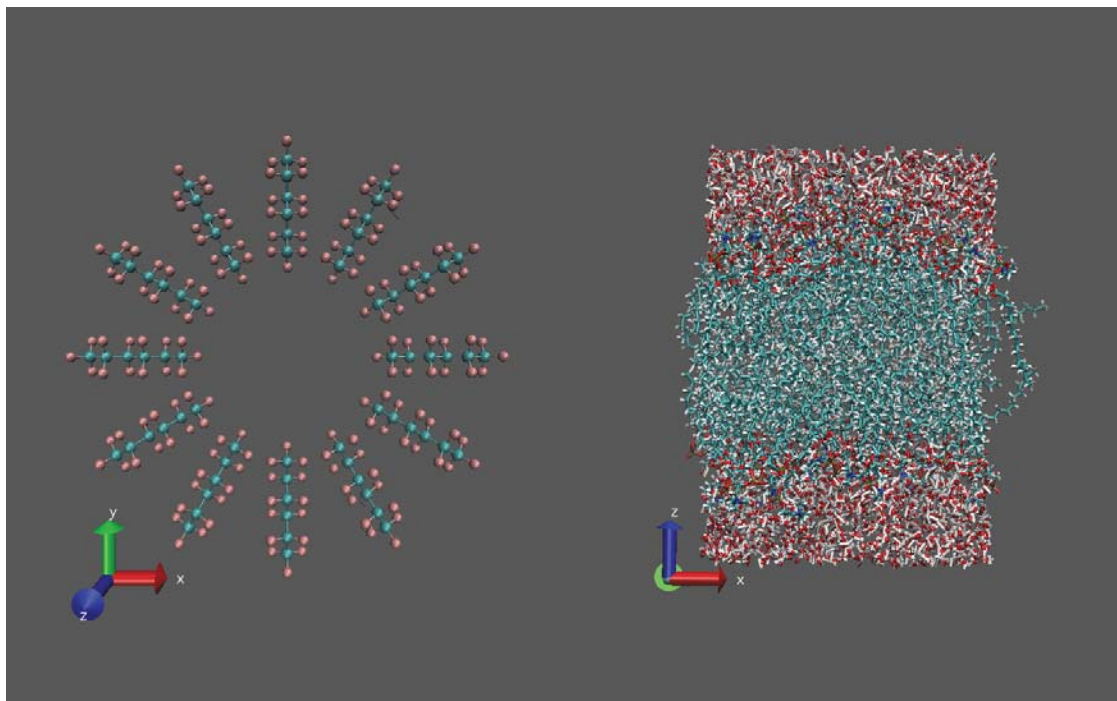


Figure 3.1: Initial configuration of 12 perfluorinated alkane molecules arranged in the x-y plane, and 72 molecules of DPPC molecules surrounded by 2189 water molecules.

3.1.2 Embedding Protocol

Even with a pre-equilibrated membrane bilayer, the simulation of molecules embedded in the membrane environment is not a trivial process. Molecules should be introduced into the membrane environment using a carefully designed simulation protocol. Lipid bilayers are densely packed to such an extent that they cannot accommodate even a small additive molecule without collisions or clashes. One cannot rely on standard computational methods (e.g. energy minimization) to remove these initial clashes as these methods become numerically unstable with the existence of very high forces due to the repulsive behavior of the Lennard-Jones potential. Also, there is a danger that these strong initial repulsive forces can introduce serious artifacts into the

membrane structure that become very difficult to get rid of, considering the very slow relaxation time of the system. Several methods have already been developed to safely embed a molecule in a lipid bilayer [88, 89]. One particular approach often used is to shrink the molecules drastically (i.e., by decreasing the atomic van der Waals radii), to insert these molecules into the membrane, and then gradually bring them back to their original size with continued minimization of energy. This is the approach implemented in the GROMACS tool chain [89]. However, it should be noted that, for long molecules, using this approach during the rescaling of the system back to its initial size introduces some additional problems. For example, the newly introduced long additive molecules can push the lipid molecules out into the aqueous phase during the rescaling of the system. Another technical difficulty with GROMACS tools in general is the difficulty of introducing external force field parameters (e.g., for the additive molecule) as the process is manually laborious and thus error-prone. We found that the program NAMD is more efficient for this purposes. For this reason, we use the Tool Command Language (TCL) interface, the extension of NAMD2. With this tool, a repulsive sphere is slowly grown in the membrane environment during MD simulation, pushing the membrane molecules away. The simulation ensures that any heat generated during the process is dissipated. Once the sphere has grown to a sufficient size to accommodate the additive molecule, this molecule can be embedded without any clashes or collisions as shown in Figure 3.2.

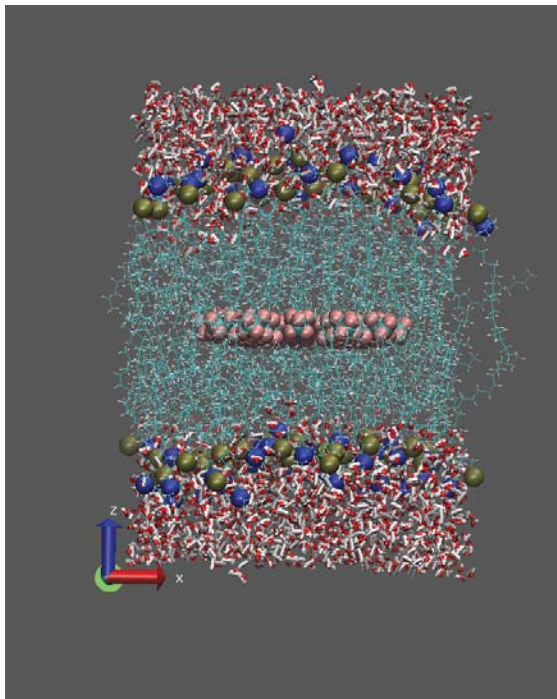


Figure 3.2: Initial configuration of 12 perfluorinated molecules embedded into 72 molecules of DPPC surrounded by 2189 water molecules.

3.2 Convergence of the Molecular Dynamics (MD) Simulations

In lipid bilayer simulations, two commonly employed convergence criteria are the area per lipid (Area/Lipid) and the mean square displacement (MSD). The Area/Lipid for a DPPC bilayer and the MSD with various fluorophilic and lipophilic organic molecules such as perfluoro *n*-hexane (F6), perfluoro *n*-octane (F8), perfluoro *n*-decane (F10), partially fluorinated *n*-decane (H5F5) and *n*-decane (H10) were calculated here. The simulation trajectories for all other molecules with a DPPC bilayer are 300 ns, except for the F6 molecules; in the case of the F6 molecules, the simulation was run up to 470 ns. This was done to check whether the drop in the Area/Lipid

of a DPPC bilayer in the presence of F6 molecules is temporary or permanent. The time evaluation of Area/Lipid and MSD plots are divided into two categories. Figure 3.3(a) describes the Area/Lipid of a DPPC membrane in the presence of F6, F8, and F10 molecules. The Area/Lipid plots fluctuated around a common value in the presence of all three types of molecules up to 35 ns. In the case of F10 molecules, the Area/Lipid value was reduced due to their penetration into the leaflet of the bilayer. At 100 ns, it had reduced by 21% and had a value of 51 \AA^2 , which is in excellent agreement with the value generally obtained in the gel phase of a DPPC membrane. This indicates that the simulation in the presence of F10 molecules reached the equilibrium state and probably converged. The plots for the small molecules i.e., F6 and F8 merged initially, accompanied by microscopic fluctuation around a common value of area, i.e., 61 \AA^2 . Due to their smaller size, these molecules were jumping frequently in and out of the leaflet of the bilayer. After 300 ns, the simulation in the presence of F6 molecules showed similar behavior to that of the simulation for F10 molecules in a DPPC bilayer environment. It can be concluded that the simulation in the presence of F6 molecules probably converged, while the simulation in the case of the F8 molecules did not converge. Figure 3.3(b) shows that the traces of F10, H5F5, and H10 molecules overlapped and one can observe that they fluctuate around a common value of area i.e., 61 \AA^2 up to 35 ns of simulation time. The plot for F10 molecules is already explained in Figure 3.3(a). In the presence of the H5F5 and H10 molecules, the simulation fluctuated around this common value and probably gain an equilibrium state. Also the equilibrium state of this complex system (F10 and DPPC) has been successfully attained using the NPT ensemble. The convergence of

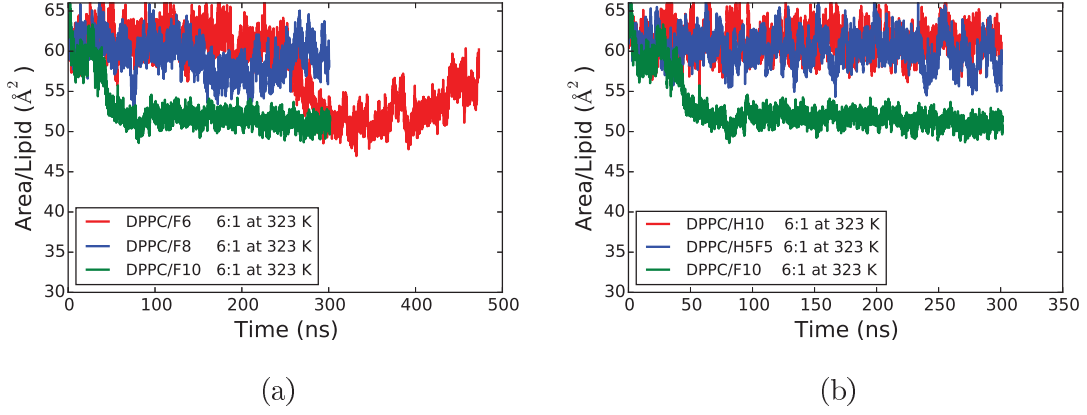


Figure 3.3: Area/Lipid versus time for DPPC bilayer in the presence of fluorophilic and lipophilic organic molecules (F6, F8, H10, H5F5, and F10) are presented in two categories (a) F6, F8, F10 and (b) F10, H5F5, H10.

the simulation can also be explained on the basis of the dynamic properties of the additive (fluorophilic and lipophilic) molecules inside the DPPC environment. One of the most important properties of the additive molecules inside the DPPC membrane is diffusion with the progress of simulation time. Generally, the diffusion is computed on the basis of MSD i.e., $\langle r^2 \rangle$ which is given by

$$MSD \equiv \langle r^2 \rangle = \langle |[\vec{R}_F(t) - \vec{R}_s(t)] - [\vec{R}_F(0) - \vec{R}_s(0)]|^2 \rangle \quad (3.1)$$

where $\vec{R}_F(t)$ is the center of mass vector of the additive molecules for time t . In order to eliminate system drift during the simulation, it is necessary to subtract the center of mass vector \vec{R}_s . To understand the diffusion of any molecule during the simulation, the diffusion coefficient D is calculated according to the following equation

$$\langle r^2 \rangle = 2Dft \quad (3.2)$$

$$D = \frac{\langle r^2 \rangle}{2ft} = \frac{\langle |[\vec{R}_F(t) - \vec{R}_s(t)] - [\vec{R}_F(0) - \vec{R}_s(0)]|^2 \rangle}{2ft} \quad (3.3)$$

In the above equation, t is the time, and f is the degree of freedom of the additive molecules. Along a single axis, the expected value of the displacement is zero, as for any other case an external agent or a non-equilibrium initial position would be needed. However, the period of recurrence may be infinite. Generally, the MSD gives the space accessed by diffusion of the observed molecules. On a two-dimensional membrane surface, this accessed space is considered as an area. Figure 3.4(a) shows diffusion according to equation 3.1 for additive molecules (F6, F8, and F10). It is difficult to fit the variation in the plots to the expected form of the MSD as generally occurred in case of normal diffusion. From visual observation, it can be concluded that the plots for smaller molecules i.e., F6 and F8 overlapped up to 100 ns and both types of molecules have a greater diffusion coefficient than the F10 molecules in the DPPC bilayer. Initially, the movement of F6 molecules was faster, but slowed down at 250 ns, indicating the penetration of these molecules into the leaflet of the bilayer. In the case of F10 molecules, the MSD plot does not show significant fluctuation and gradually increased up to 125 ns. The mobility of the F10 molecules was hindered in the DPPC environment because they penetrate into the leaflet of the bilayer. In Figure 3.4(b), the translational movement of the molecules (F10, H5F5, and H10), which have the same size but different numbers of fluorines attached to the carbons, were compared. The plots of the translational dynamic revealed that the mobility of the F10 molecules was significantly reduced compared the other two types of the molecule (H10, H5F5). At this stage of the simulation, the fluctuations in the MSD plots of H10 and H5F5 molecules were larger compared to the F10 molecules. In general, the simulation in the presence of F10 molecules probably converged. The

simulation with F6 molecules also showed equilibrium state during the last 200 ns. For all the other additive molecules (F8, H5F5, and H10), the simulations fluctuated and maybe reach the same equilibrium state only after two or three times the present computational effort.

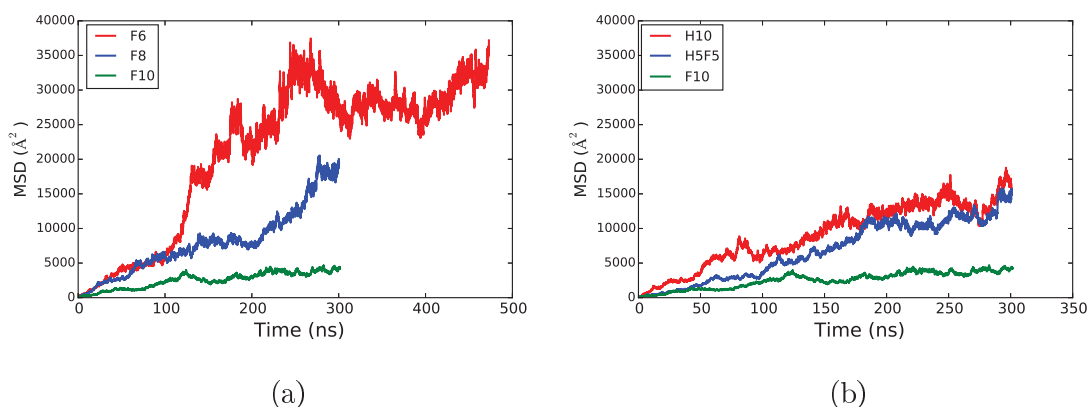


Figure 3.4: Mean square displacement (MSD) of (a) perfluoro *n*-alkanes molecules (F6, F8, and F10) and (b) the decane derivatives of varying fluorine content (H10, H5F5, and F10) inside the DPPC environment.

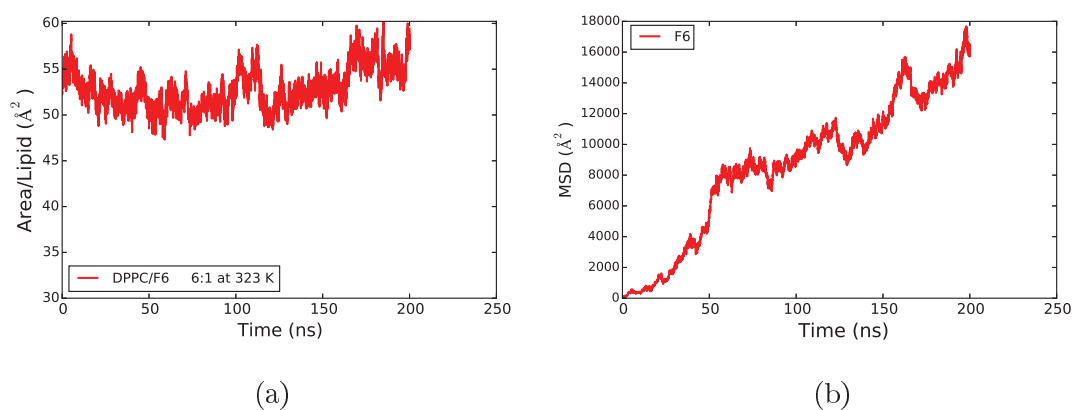


Figure 3.5: (a) Area/Lipid versus time for DPPC membrane in the presence of F6 and (b) MSD for F6 molecules, during the last 200 ns out of 470 ns.

3.3 Behavior of the Additive Molecules

3.3.1 Density Profiles

The center of mass (CM) distribution profiles for additive molecules (F6, F8, F10, H10, and H5F5) were computed during the last 20 ns simulation time in order to analyze the expected density increase in the region, corresponding to the location of these molecules. Zero represents the center of bilayer plane on the x-axis in the density profiles. In Figure 3.6(a), the distribution of the center of mass of the additive molecules (F6, F8, and F10) is compared. It can be observed that the central region of the plot gets broader for the F6 molecules. This shows that only a few molecules started moving toward the leaflet of the bilayer while most of these molecules were still present at the center, i.e., in between the single bilayer leaflet. Also another interesting effect, since F6 molecules is faster than F10 molecules, it could have moved into the layers in the simulation time. As it has more translational entropy than F10 molecules and less energy to gain by moving into the layers, so F6 will not be incorporated. The F8 molecules were partially located in between the single bilayer leaflet and had partially penetrated into the bilayer leaflet. The F10 molecules were completely penetrated into the bilayer leaflet and aligned along the alkyl chain of the DPPC molecules. Similarly, Figure 3.6(b) depicts a comparison between the decane derivatives of varying fluorine content (H10, H5F5, and F10). H10 molecules were found in the center of the bilayer in scattered form as shown by the plot of the center of mass distribution. The H5F5 molecules had partially penetrated into the leaflet of the bilayer. The F10 molecules were fully penetrated into the bilayer leaflet from the

center, where they were initially embedded. From the overall comparison, a remarkable correlation between the center of mass distribution of the additive molecules and the pure DPPC membrane system was observed. In general, the longer the carbon chains with a higher degree of fluorination, the greater will be the tendency to penetrate into the leaflet of the bilayer. The fluidic nature of the DPPC and energy minimization of the additive molecules are responsible for this higher penetration.

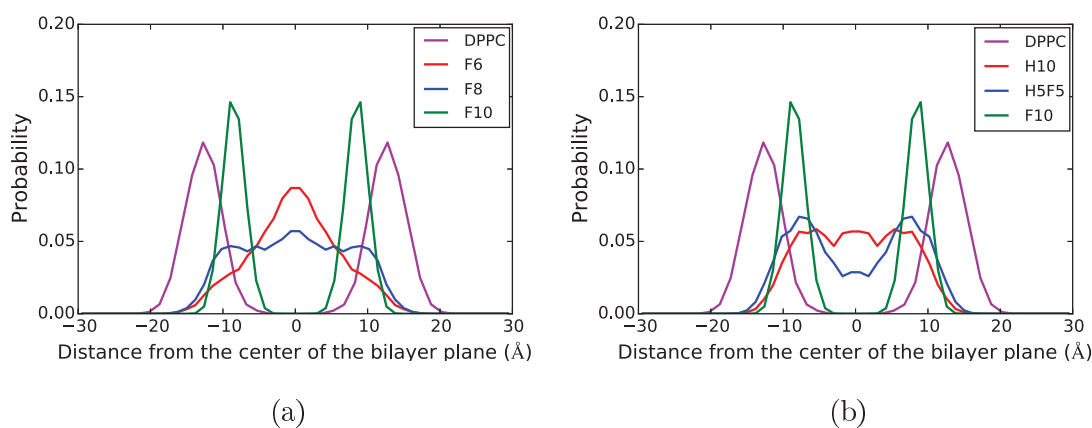


Figure 3.6: Center of mass (CM) distribution profiles of additive molecules (a) F6, F8, F10 and (b) F10, H5F5, H10 in the DPPC bilayer environment during the last 20 ns out of the total simulation time.

3.3.2 Rotational Dynamics of the Additive Molecules

To understand the rotational dynamics of the additive molecules (F6, F8, F10, H5F5, and H10) in the membrane environment, a special vector autocorrelation function was calculated. In our system, each of the above-mentioned additives consists of 12 molecules. Out of these 12 molecules, the velocity of one molecule was taken as a reference vector, while the velocities of all the other molecules were considered as a second vector which was correlated with the reference vector using the dot product.

The result is between 1 and -1, i.e., if the two vectors were parallel to each other, the result is one, and if they are either perpendicular or anti-parallel, the resultant is 0 or -1, respectively. The mathematical description is

$$C(t) = \frac{1}{NT} \sum_{i=1}^N \sum_{t=0}^T \frac{\langle V_i(t) \cdot V_i(t + \tau) \rangle}{\langle V_i(t) \cdot V_i(t) \rangle} \quad (3.4)$$

In Eq. (3.5), $V_i(t)$ and $V_i(t + \tau)$ are the velocity vectors of molecules i in time step t and τ is the increasing correlation time. The rotational movement of the additives i.e., fluorophilic and lipophilic molecules within the DPPC environment was of particular importance, as it offers a connection between experiments and simulations. During the experiment, it is difficult to observe the position of the additive molecules and to determine whether they are actually penetrating the DPPC environment or not. Unfortunately, the probability of observing this type of embedding process is too low in routine simulation studies. In this MD simulation, there was strong evidence that rotational mobility was reduced for penetrating molecules as molecules were likely to be found within the bilayer leaflet. These molecules stabilized themselves inside the bilayer leaflet with a particular orientation with minimum energy. In Figure 3.7(a), the aligned molecules are described using the vector autocorrelation function with respect to a reference molecule for F6, F8 and F10. The F6 molecules showed more wobbling and rotation as compared to F8 and F10 molecules, as indicated by the faster decaying process of the autocorrelation function. This is mainly due to the fact that F6 molecules are in between the single bilayer leaflet at this stage. They have a higher translational entropy as compared to F8 or F10 molecules, which are partially or fully penetrated into the leaflet of the bilayer. Thus the smaller the size, the faster is the rotation and wobbling inside the bilayer. F10 molecules are aligned in parallel

with the alkyl chains of the DPPC molecules. As a result, their rotational movement is impaired. In Figure 3.7(b), various additive molecules of the same chain length, but of different degree of fluorination, are compared. The data shows that the lower the number of fluorines attached to the carbon chains, the stronger is the rotation and wobbling of the molecules.

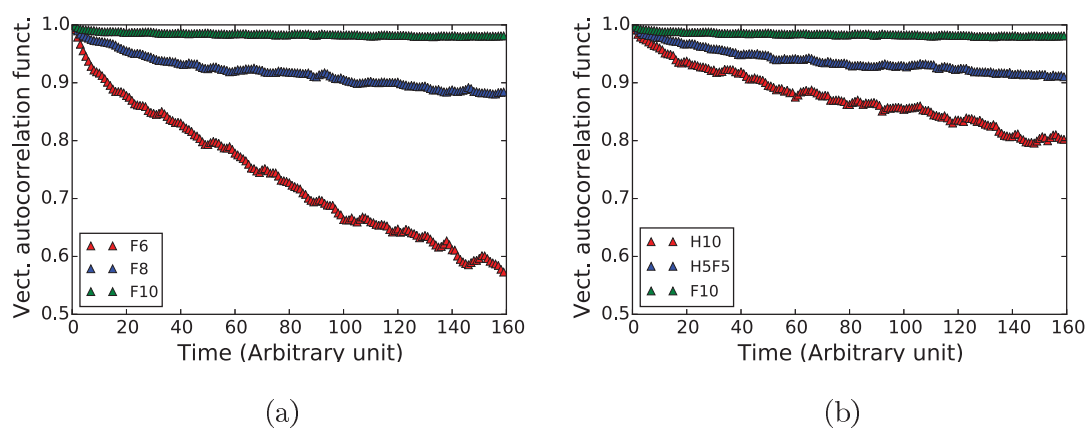


Figure 3.7: Vector (vect) auto-correlation for (a) F6, F8, F10 and (b) H10, H5F5, F10 molecules in the DPPC environment, explaining their rotational dynamics. The decaying process of the autocorrelation function indicates that the motion of the F10 molecules is hindered significantly in the DPPC environment.

3.3.3 Flexibility of the Additive Molecules

An investigation of the nature of additive molecules in the DPPC environment is of great importance as it provides knowledge about the reactive response of the DPPC bilayer to the embedded molecules. The conformational nature of the additive molecules inside the DPPC environment depends not only on their own properties, but also on the locations of these molecules inside the DPPC bilayer. The nature of the additive molecules can be explained with the help of dihedral angles formed by

the chain of carbon atoms of the additive molecule. Figure 3.8 shows a comparison between normal decanes (H10) and perfluorinated decanes (F10). In this histogram, every line shows the dihedral angle of the chain of carbon atoms. This angle is described from the torsional angle of the first four atoms of the carbon chain of the additive molecule. In Figure 3.8(a), the probability of the presence of gauche conformations indicates the flexibility of the H10 molecules. In the case of the F10 molecules, this type of gauche conformation is unlikely as the molecules are like a stiff rod and they are present inside the bilayer leaflet. Secondly, the steric effect is responsible for this behavior.

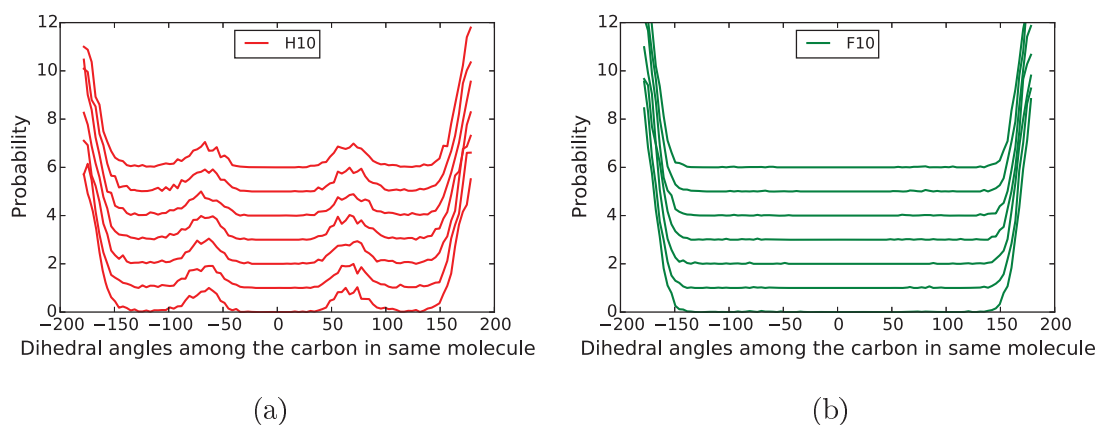


Figure 3.8: The population density of dihedral angles, illustrating the flexibility of (a) hydrogenated decanes (H10) and (b) fluorinated decanes (F10) in the DPPC environment. Every line shows a histogram of one dihedral angle, listed from the dihedral angle of the first four carbon atoms starting from one end's carbon up to the another end's carbon of additive molecule.

3.3.4 Tilt Angle of the Additive Molecules in the Membrane Environment

In order to put the results of the simulation into perspective, it is important to evaluate the accuracy of the process by computing the angle relative to the DPPC bilayer surface. One of the various factors which affect the simulation results is the overall system movement, which is an artifact of the simulation. The kinetic energy of the center of mass motion, which is obtained from the total energy, was negligible during the simulation studies. We are interested in the normal vector of DPPC bilayer surface, as we have to describe the alignment of the additive molecules with the *z*-axis or with the normal vector of the bilayer surface. For convenience, the DPPC is orientated such that the normal vector of its surface is along one Cartesian axis (*z*-axis), instead of considering [90] a plane of the coordinates of all phosphorus atoms in both DPPC layers. In Figure 3.9, the alignment of the additive molecules to the normal of the bilayer surface is calculated by considering a symmetrical vector of the additive molecule. The symmetrical vector starts with carbon at one end of the molecule and goes to another end. Figure 3.9(a) shows the alignment of F6, F8, and F10 molecules. The plots for F6 and F8 molecules do not drop at the boundaries. Although there are some weak signals of drop for F6 molecules, the overall shape of the plot does not indicate the tilted nature. For F10 molecules, sharp drops can be observed on both sides, showing that parallel or anti-parallel alignment with the normal of the bilayer surface becomes very unlikely. This drop covers a range of around 20°, which corresponds to the tilted nature of the alkyl chain of the DPPC membrane (see section 3.4.4). The decane derivatives of varying fluorine content

(H10, H5F5, and F10) are compared in Figure 3.9(b). The traces of H10 and H5F5 molecules show a high probability of parallel or anti-parallel alignment with the *z*-axis. Once again, the curve for the F10 molecules drops sharply by 20° at the boundaries and the curves do not exhibit parallel or anti-parallel alignment along the *z*-axis or normal of the bilayer surface. we can conclude that only the F10 molecules are aligned parallel to the alkyl chains of the DPPC molecules.

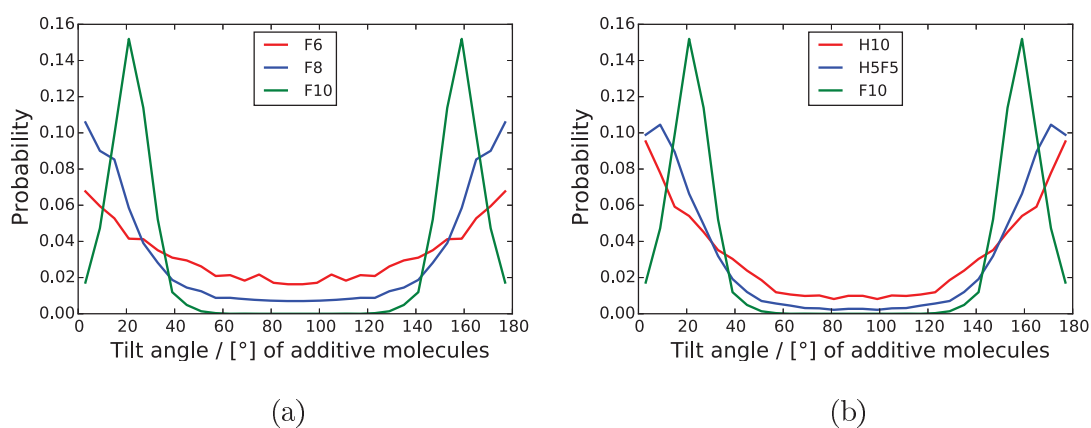


Figure 3.9: Tilt angle of the additive molecules (a) F6, F8, F10 and (b) H10, H5F5, F10, showing probability of their orientation within DPPC bilayer.

3.3.5 Clustering Phenomena of the Additive Molecules

To compute the distribution of the additive molecules in the DPPC environment, the radial pair distribution function $g_{XY}(r)$ is used, which is proportional to the probability of finding molecules *Y* at a distance *r* from molecule *X*.

In our system, $g_{XY}(r)$ of the additive molecules (F6, F8, F10, H5F5, and H10) is calculated according to the pairwise distance concept. According to this concept, the corresponding number of molecules around a reference point was estimated. The

system was considered as a two-dimensional box. One molecule out of the 12 molecules was considered as a reference point. The distribution function yields the probability density of other molecules at a given distance r around the reference molecule. In Figure 3.10(a), the behavior of F6, F8, and F10 molecules is presented. The first higher peak is due to the additive molecules present in the first shell followed by two peaks for F6 and F8 molecules at distances of 5 and 10 Å, respectively. After that, the $g(r)$ value for F6 and F8 molecules is low at higher distances. In the case of the F10 molecules, two small peaks can be observed apart from the same peak at 5 Å. This shows that the additive molecules are scattered at first, and then come closer together, forming clusters. These clustering peaks occurred at a distance of approximately 5 Å from each other. Similarly, Figure 3.10(b) shows the additive molecules of varying fluorine content but same carbon chain length. For H10 molecules, two small peaks are visible at distances of 5 and 10 Å, respectively, while the $g(r)$ values were low at higher distances for these molecules. The H5F5 molecules are clustered and the clustering peaks are visible at distances of 5, 10, 15 and 20 Å, but this effect is not as evident as for the F10 molecules. In general, the F10 molecules are clustered in the DPPC environment. F8 molecules initially show a similar behavior that slowly fades with distance. The F6 molecules exhibit different behavior, showing only a small amount of clustering in the beginning with no regular patterns. In summary, a higher degree of fluorination with longer carbon chains causes a stronger clustering effect.

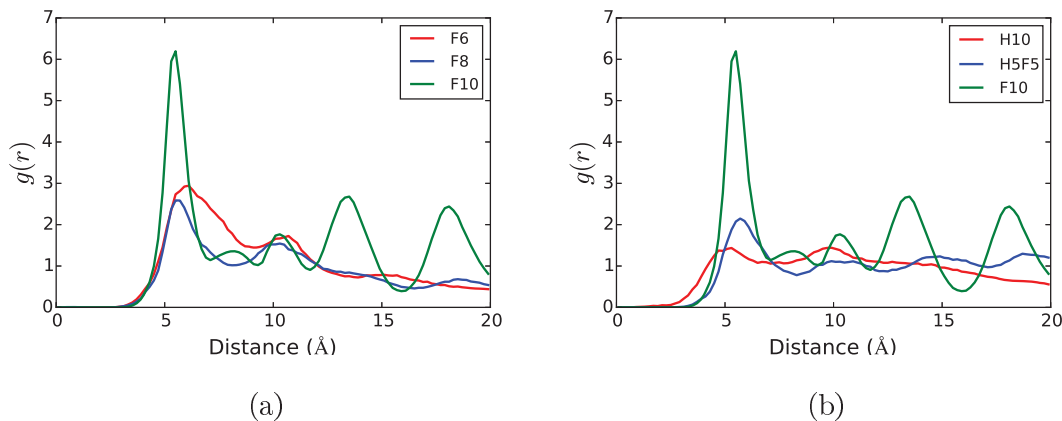


Figure 3.10: Two-dimensional radial pair distribution function, explaining the clustering phenomena of the additive molecules (a) F6, F8, F10 and (b) H10, H5F5, F10 in the DPPC environment.

3.4 Response of the DPPC Bilayer System

3.4.1 Area per Lipid

The area per lipid (Area/Lipid) is calculated simply by taking the x-dimension and y-dimension of the simulation box (unit-cell) and dividing by the number of lipids present in one leaflet, independently of whether there are fluorophilic or lipophilic organic molecules incorporated into the bilayer or not. A comparison of the Area/Lipid for various additive molecules at a temperature of 323K is shown in Figure 3.11. The horizontal axis depicts the average Area/Lipid, while the vertical axis shows the probability of a given area being occupied. In the case of the F6 molecules, the plot describes that the initial Area/Lipid is around 65 \AA^2 . The decrease and shift from the higher to lower value shows that some F6 molecules had penetrated into the leaflet, reducing the area to 51 \AA^2 , while some of the F6 molecules remained elsewhere, allowing more space per lipid. For the F8 molecules, the DPPC system shows some shift

in the Area/Lipid value and the curve is move gradual on the left side. In case of the F10 molecules, significant changes can be observed in the Area/Lipid. The maximum value was 65 \AA^2 , dropping to 51 \AA^2 due to the penetration of additive molecules into the bilayer leaflet. Figure 3.11(b) describes the Area/Lipid for the DPPC system in the presence of F10, H5F5, and H10 molecules. It can be observed that in the presence of H10 molecules there is no such effective change taking place in the Area/Lipid of the DPPC system. In the presence of H5F5 molecules, the area decreased by a small factor and was equal to 60 \AA^2 . The overall effect of the F10 molecules is clearly different than other types of additive molecules (F6, F8, H5F5, and H10). In summary, the higher the number of fluorines attached to the carbon atoms, the greater will be the penetration into the bilayer leaflet, ultimately reducing the Area/Lipid. In Figure 3.12, the average numerical values of Area/Lipid are shown in the form of a bar graph. The horizontal axis indicates the respective additive molecules, while the vertical axis shows the average Area/Lipid. In the presence of F6, F8, F10, H5F5, and H10, the average Area/Lipid for DPPC bilayer is 56 \AA^2 , 59 \AA^2 , 51 \AA^2 , 60 \AA^2 , 61 \AA^2 , respectively.

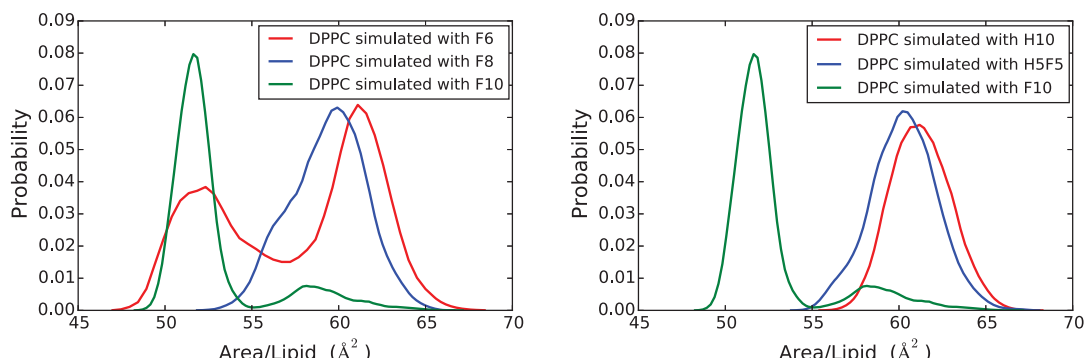


Figure 3.11: The Area/Lipid, shifting from higher value to lower value for the DPPC bilayer in the presence of additive molecules (F6, F8, H10, H5F5 and F10). The horizontal axis represents the total magnitude of Area/Lipid while the vertical axis represents the probability of the area being occupied. A shift in F6 and F10 molecules is significant while for F8 and H5F5 molecules it is under process.

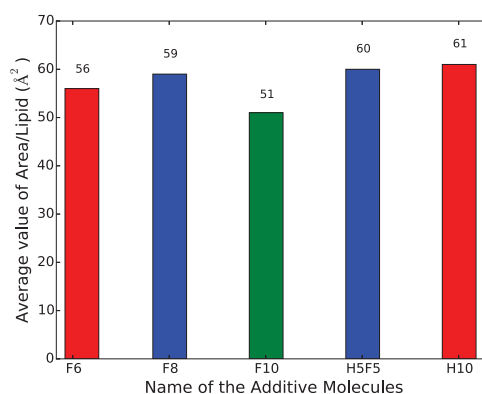


Figure 3.12: Bar plot representation of average Area/Lipid in the presence of F6, F8, H10, H5F5 and H10 molecules.

3.4.2 Gauche-Trans Conformations of the DPPC Alkyl Chains

For the calculation of DPPC alkyl chain flexibility and the gauche-trans conformations of these chains, as indicated by the population density of dihedral angles, the last 20 ns of the total simulation trajectory was used. Each line shows a histogram of the dihedral angle, for which the trajectory was described using the dihedral angle of the first four carbon atoms near the head group region of the DPPC bilayer

molecule to the carbon atom at the outer end of the alkyl chain. In the following, the population density of dihedral angles of alkyl chains in the presence of n-decane (H10) and perfluoro n-decane (F10) are presented in the form of histograms. The dihedral angles of the alkyl chains of the pure DPPC membrane are shown in Figure 3.13(a). The presence of gauche conformations at approximately 70° on either side of the center (zero) along the x-axis was observed, while Figure 3.13(b) shows the histogram of the dihedral angles in the presence of F10 molecules. It is apparent from the histograms that the chances of having a gauche conformation were reduced by approximately 19% and transferred to trans conformations. The observed value for trans conformations of the pure DPPC alkyl chains was 71% as shown in Figure 3.15. The average value of the trans conformations in the alkyl chains rose to 89% upon penetration of the F10 molecules into the bilayer leaflet. On the other hand, the trans conformations for the H10 molecules were reduced by 3%, as shown in Figure 3.14(a and b).

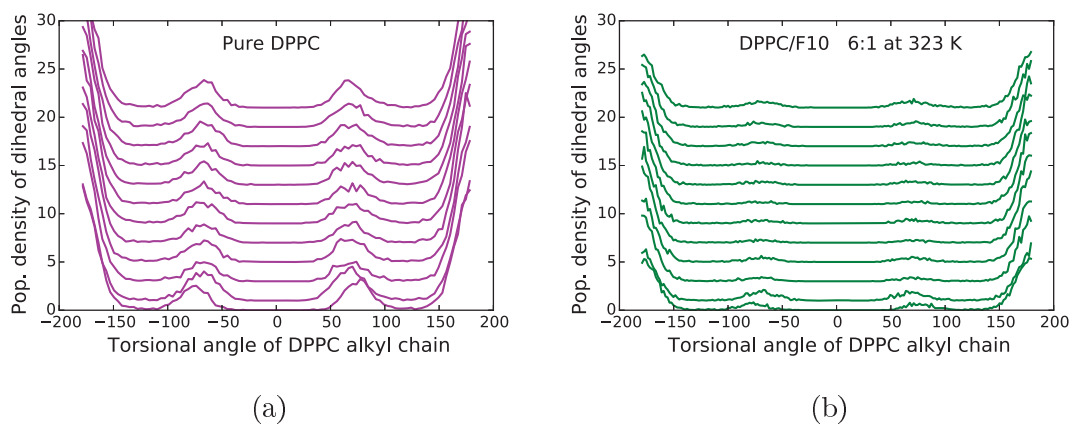


Figure 3.13: Population (Pop) density of dihedral angles illustrating the alkyl chains flexibility of the pure DPPC bilayer alkyl chain in comparison to alkyl chain in the presence of F10 molecules. Every line shows the histogram of the dihedral angle population listed from the dihedral angle of the first four carbon atoms near the head group region (bottom) upto the outer end's carbon (top) of the lipid alkyl chain.

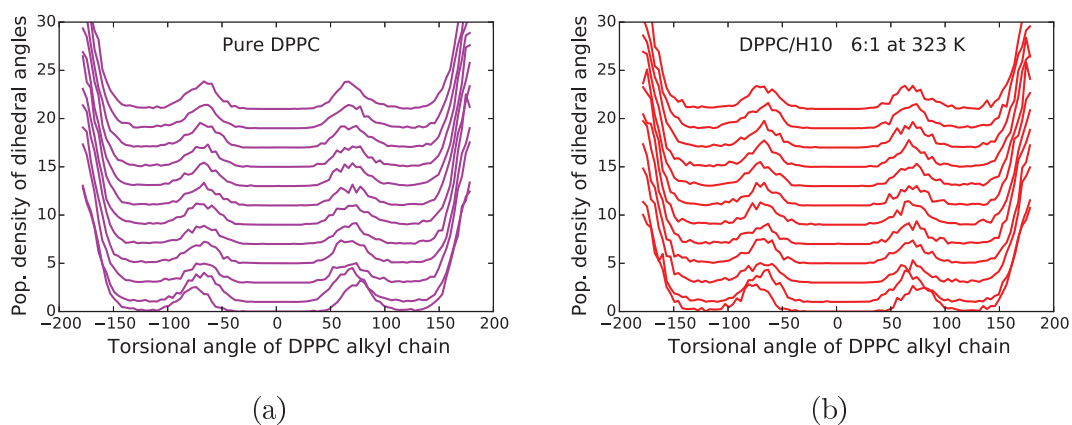


Figure 3.14: Population (Pop) density of dihedral angles illustrating the alkyl chains flexibility of the pure DPPC bilayer alkyl chain in comparison to alkyl chain in the presence of H10 molecules. Every line shows the histogram of the dihedral angle population listed from the dihedral angle of the first four carbon atoms near the head group region (bottom) upto the outer end's carbon (top) of the lipid alkyl chain.

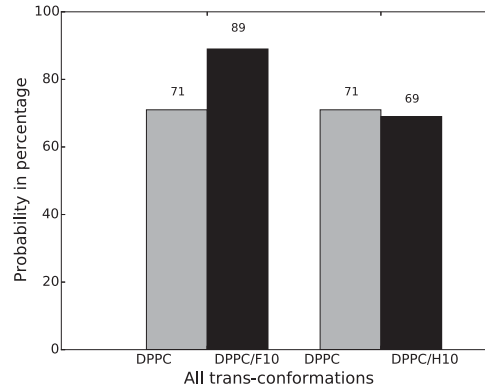


Figure 3.15: The average amount of all-trans conformations in DPPC alkyl chains in the pure lipid system (gray) and the effect induce by hydrogenated decanes (H10) and fluorinated decanes (F10) (black).

3.4.3 Lipid Orientation

The orientation of the phospholipid tail groups was investigated by studying the hydrogen order parameter with respect to position along the alkyl chain. C-H order parameters were calculated by first producing the hydrogen locations for all molecules in each time configuration. The hydrogen order parameters S_{CH} were computed using the following equation,

$$S_{CH} = \frac{1}{2nm} \sum_{n=1}^n \sum_{m=1}^m \left(\frac{3r_{nm,z}^2}{|r_{nm}|^2} - 1 \right) \quad (3.5)$$

where r_{nm} is the C-H vector at molecule m with time frame n while the z -axis of the system was parallel to the bilayer normal. The order parameters for each hydrogen atom are separately computed here, because sometimes the order parameter effect is different for two hydrogens attached to the same carbon atom due to the penetration effect of the additive molecules. Sometimes they are also calculated separately from the experiments as well. Here, C2 represents the carbon atom close to the head group

region in each of the fatty acid chain, and C15 is for the carbon atom in a terminal methyl group. In Figure 3.16(a and b), the incorporation of F6 molecules into the DPPC bilayer appeared to increase the order of C-H bonds related to carbon no. 2 to carbon no. 14 of the DPPC alkyl chain. In the case of F8 molecules, it was increased for carbon no. 3 to carbon no. 14 of the DPPC molecules alkyl chain as shown in Figure 3.17(a and b). In the case of F10 molecules, the increase appears from carbon no. 1 to carbon no. 14. In summary, the order parameters of the lipid alkyl chains are significantly increased in the presence of the F10 molecules, as shown in Figure 3.18(a and b). F10 molecules are expected to be positioned closer to the head group region due to their larger size as compared to F6 and F8 molecules.

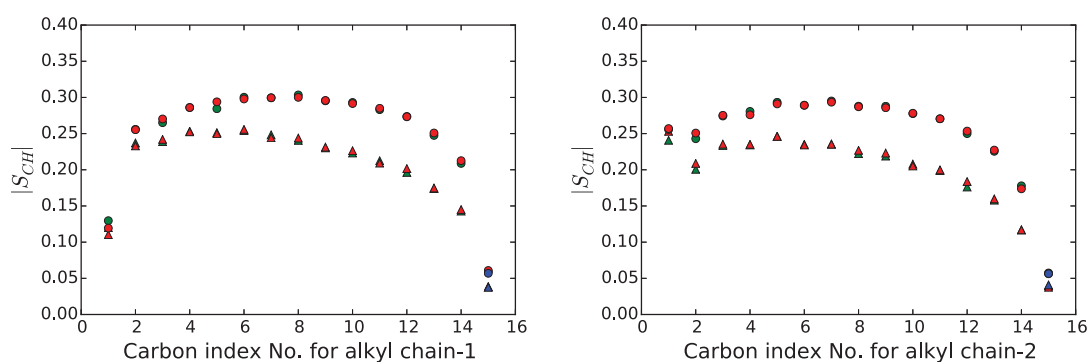


Figure 3.16: Order parameter magnitude $|S_{CH}|$ versus carbon index number for the alkyl chain-1 and alkyl chain-2 of DPPC bilayer. Comparing the pure DPPC alkyl chain order parameters (Triangle) with the order parameters of alkyl chain in the presence of F6 molecules (Solid circle).

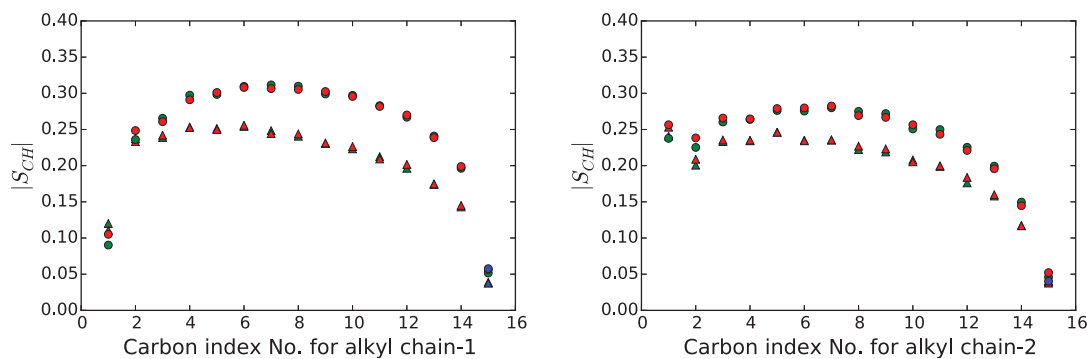


Figure 3.17: Order parameter magnitude $|S_{CH}|$ versus carbon index number for the alkyl chain-1 and alkyl chain-2 of DPPC bilayer. Comparing the pure DPPC alkyl chain order parameters (Triangle) with the order parameters of alkyl chain in the presence of F8 molecules (Solid circle).

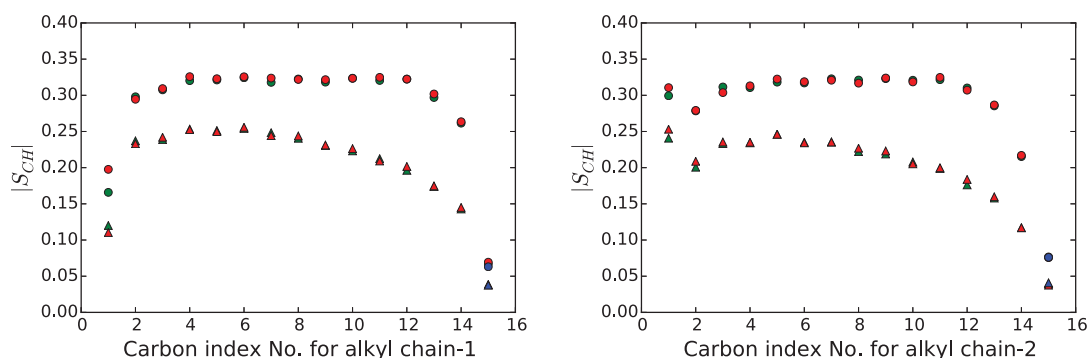


Figure 3.18: Order parameter magnitude $|S_{CH}|$ versus carbon index number for the alkyl chain-1 and alkyl chain-2 of DPPC bilayer. Comparing the pure DPPC alkyl chain order parameters (Triangle) with the order parameters of alkyl chain in the presence of F10 molecules (Solid circle).

3.4.4 Tilt Angle of the Alkyl Chain of DPPC Molecules

Various types of simulations have shown that the F10 molecules have a remarkable effect on the DPPC bilayer structure. Hence, as an example, Figure 3.19(a) presents the angles between the normal to the bilayer surface and the vector formed by the alkyl chain of DPPC membrane in the presence of F10 molecules, along with a comparison with the pure DPPC system. Figure 3.19(a) presents the alignment of alkyl chains

of a pure DPPC with respect to the normal of the bilayer surface. In this case, there is no decrease at the end of the traces, which indicates parallelism or anti-parallelism of the vector formed by the carbons of the alkyl chain. Figure 3.19(b) shows the angle between the alkyl chain and the normal vector of the bilayer surface in the presence of F10 molecules, showing sharp decreases at 20° and 160° . These decreases are due to the low probability of finding perfectly parallel or anti-parallel orientation of the observed alkyl chains vector. This corresponds to the tilted nature of the additive molecules see Figure 3.9(a and b). Comparing Figure 3.19 (a and b) with the additional informations of Figures 3.6 (a and b) and 3.9 (a and b), one can conclude, that the F10 molecules are incorporated into the lipid bilayer leaflet and cause phase transition of the lipid due to the increased density.

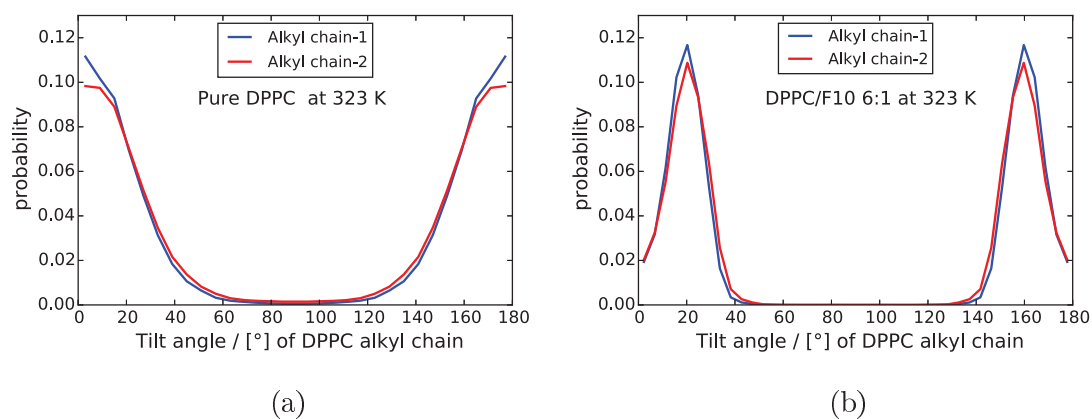


Figure 3.19: Tilt angle of the alkyl chain of DPPC molecules with regard to normal of the bilayer surface. (a) pure DPPC bilayer and (b) DPPC bilayer in the presence of F10 molecules.

3.4.5 Fluctuations in the Bilayer Thickness over Time

The variation in the thickness of a DPPC bilayer is investigated in this section. All simulations were carried out under constant pressure conditions (NPT ensemble), meaning that the size and shape of the simulation box independently adjust the area and thickness of the DPPC bilayer in order to fluctuate. This allows the computation of structural properties such as Area/Lipid. To investigate the effect of the different additive molecules F6, F8, F10, H5F5, and H10 on lipid bilayer thickness, the same bilayer composition was used for all types of additive molecules. Figure 3.20(a) presents the thickness of the bilayer in the presence of F6, F8, and F10 molecules. At the initial stage, the thickness is 39.5 Å. Up to 35 ns it increases by a small factor and fluctuates around a common value. After 35 ns, the thickness of the DPPC bilayer in the presence of the F10 molecules fluctuates around a common value of roughly 46 Å. The fluctuation in the bilayer thickness is larger in the presence of smaller molecules, i.e., F6 and F8. In the case of F6 molecules, the thickness of the bilayer also increases to a maximum of 46 Å. The simulation time was increased to 470 ns in this case. It was confirmed that the bilayer thickness in the case of F6 was temporarily increased but again decreased. Figure 3.20(b) shows the thickness of the bilayer in the presence of fluorophilic and lipophilic organic molecules of various fluorine contents.

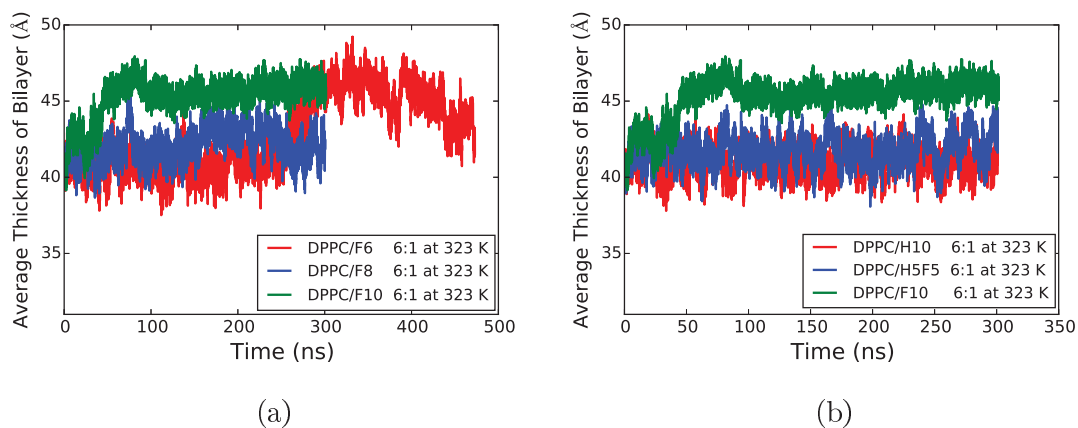


Figure 3.20: Fluctuations in the DPPC bilayer thickness over time in the presence of (a) F6, F8, F10 and (b) H10, H5F5, F10 molecules.

3.4.6 Final Configuration of the F10 Molecules and Lipid Molecules

The combined system of fluorophilic organic molecules and hydrated lipid (DPPC) bilayer is presented in Figure 3.21 after 300 ns of simulation time. In both graphics, the blue and orange spheres are nitrogen and phosphorus, respectively, while on both sides there are layers of water molecules. As regards the lipid molecules, the penetrated perfluorinated molecules are shown. The figure reflects the tilted nature of the lipid molecules, which are tilted by approximately 20° . The tilted nature has already been explained by several properties, i.e., the tilt angle of the alkyl chain of DPPC molecules and the tilt angle of the additives inside the DPPC environment. Also the clustering of the F10 molecules are clearly observable in this snapshots.

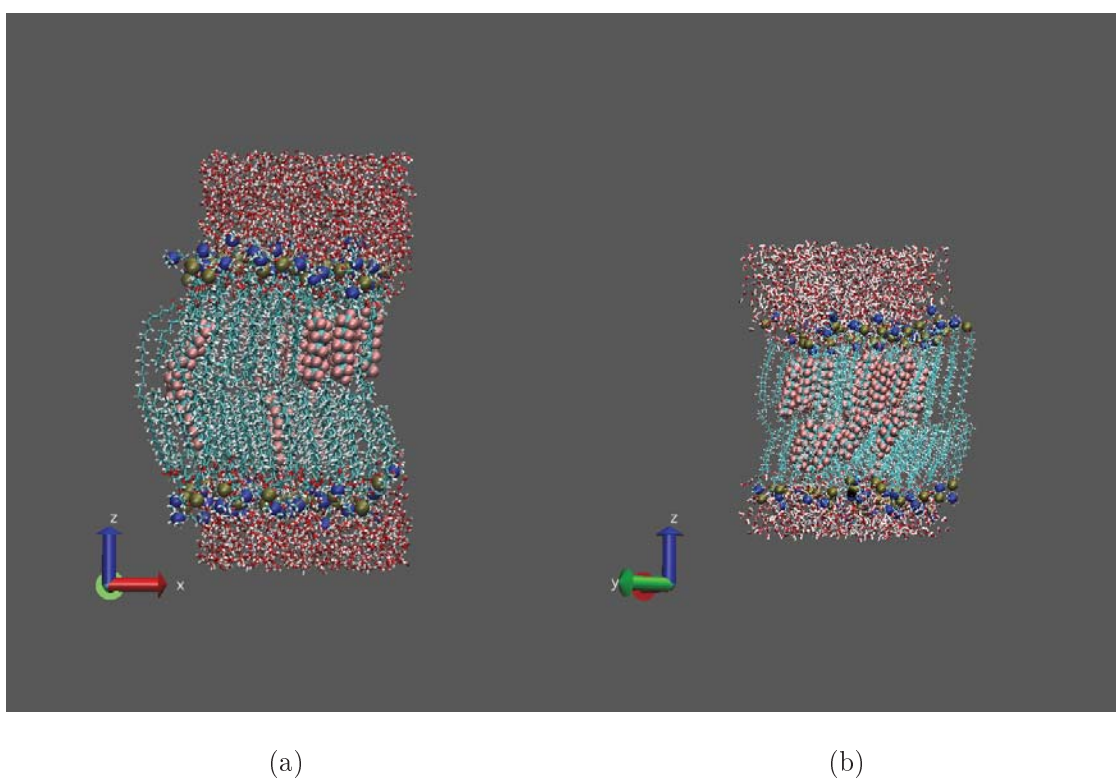


Figure 3.21: Final configuration of the system representing a fully hydrated DPPC bilayer with F10 molecules after total simulation time for two different concentration (a) 6:1 and (b) 3:1

Chapter 4

Fluorinated Alcohol with a Membrane Bilayer

In this chapter, fluorinated alcohol (FTOH) molecules incorporated into the DPPC bilayer are investigated using the same computational approach as that discussed in section 2.3. There are 12 FTOH molecules, which were arranged in the x-y plane in the same manner as in the case of perfluoro n-alkanes. 72 molecules of the DPPC were arranged in a bilayer structure, surrounded by a total of 2189 water molecules on both sides of the bilayer. Both FTOH and DPPC molecules have the same type of initial configuration as discussed in section 3.1.1. The FTOH molecules were embedded into the DPPC system using the extension of “NAMD2” software with its Tool Command Language (TCL) interface. The same methodology was used for the embedding process, as explained in section 3.1.2.

4.1 Convergence of the Molecular Dynamics Simulations

Convergence of a simulation is the basic requirement for obtaining reliable results about the system being investigated in computational studies. The convergence of the MD simulation of a system consisting of FTOH molecules and a DPPC bilayer can be evaluated based on the area per lipid (Area/Lipid) and mean square displacement (MSD). In Figure 4.1(a), the overall fluctuations in the traces of the projected Area/Lipid are small and the equilibrium value of the DPPC bilayer can be estimated in the presence of FTOH molecules. At the beginning, the Area/Lipid is high, with a value of approximately 65 \AA^2 for all types of simulated combinations. The green trace represents the DPPC bilayer in the presence of FTOH molecules at a temperature of 333 K. This trace fluctuates, but the Area/Lipid does not reduce significantly. At 150 ns, it decreases for short interval, followed by another decrease at 200 ns, which indicates the penetration of the FTOH molecules into the leaflet of the DPPC bilayer. As a result, the Area/Lipid of the bilayer was reduced. The blue and red traces (two different concentrations, 4:1 and 6:1) of the simulated system are shown in the same figure. The Area/Lipid in the case of the blue trace decreases sharply as compared to the red trace. After 50 ns, the two simulated systems (indicated by the blue and red traces) reach an equilibrium state accompanied by small fluctuations, and the Area/Lipid is reduced by 20% and has a value of 50 \AA^2 . In general, a significant decrease was found in the Area/Lipid in all three types of traces for the DPPC bilayer in the presence of FTOH molecules. The average Area/Lipid was found to be

higher at 333 K as compared to 323 K during the overall simulation. The decrease in the Area/Lipid at 333 K took slightly more time due to the more fluidic nature of the DPPC system. Thus, an equilibrium state for this complex system (FTOH and DPPC) was successfully attained. The translational movement of the FTOH

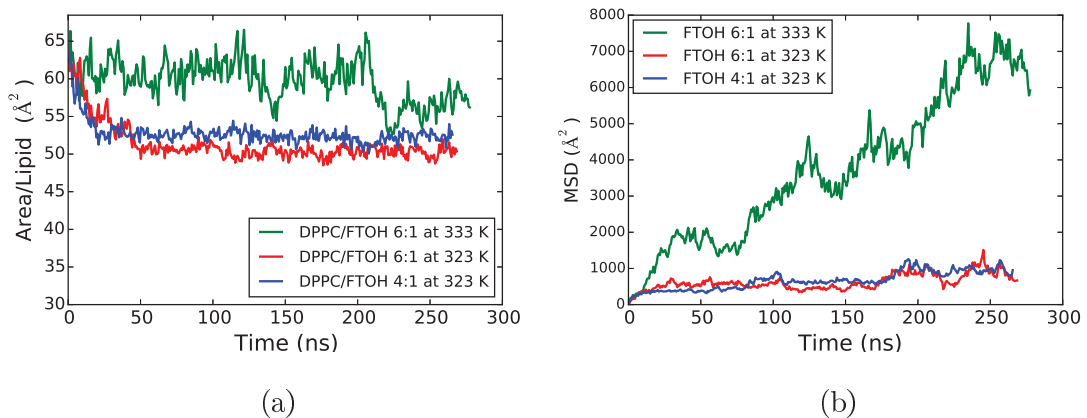


Figure 4.1: (a) Area/Lipid of DPPC bilayer in the presence of FTOH molecules at different concentration and different temperatures. (b) MSD of the FTOH molecules in the DPPC environment.

molecules inside the membrane environment is of great importance, because this reflects the idea about the fluorophilicity. The simulation of the same type of FTOH molecules at two different concentrations and at two different temperatures on the basis of MSD is compared. MSD, i.e., $\langle r^2 \rangle$ is used for understanding diffusion with the progress of simulation time. The same methodology and equations 3.1, 3.2, 3.3, were used for MSD, as explained in section 3.2.

Figure 4.1(b) shows the diffusion according to equation 3.1 for FTOH molecules having concentrations of 4:1 and 6:1 at 323 K, while FTOH molecules are also compared at temperatures of 333 K and 323 K for a concentration of 6:1 in the same figure. Comparing the MSD plots for the system of two different concentrations, it can be

observed that the FTOH molecules are rapidly diffused up to 10 ns. After that, the mobility of these molecules was significantly reduced, although their level of diffusion remains at the same rate with minor fluctuations. The MSD trace at the higher temperature reflects the very fast diffusion of alcohol molecules as compared to the lower temperature. From visual observation of the MSD traces, it appears that the simulation of this system is probably fluctuating at an equilibrium state. In summary, it can be observed from the blue and red traces that the FTOH molecules mobility is hindered significantly, which confirms the frozen nature of the DPPC bilayer. On the other hand, the green trace in the MSD plot shows that diffusion is faster at the higher temperature of the FTOH molecules as compared to the lower temperature. In this case, the bilayer system confirms the liquid phase.

4.2 Density Profile

The distribution profile was computed in order to describe the distribution of the fluorotelomer alcohol (FTOH) molecules within the membrane environment and to investigate the expected density increase in the region corresponding to the FTOH locations. In Figure 4.2, the zero along the x-axis shows the center of the bilayer plane. This figure explains the comparative position of the FTOH molecules at concentrations of 4:1 and 6:1 at 323 K, and the same molecules are also compared at temperatures of 333 K and 323 K for the 6:1 concentration in the same figure with a pure DPPC membrane. There is good correlation and correspondence between the center of mass distribution profiles of the pure membrane system and the FTOH molecules. It can be observed from Figure 4.2 that the molecules that are initially

embedded at the center of the bilayer have penetrated into the bilayer leaflet and are aligned parallel to the alkyl chain. On both sides of the zero position, the plot for the 4:1 ratio is a little bit exposed and broadened from the inner sides at the bottom. This is due to the higher concentration of the FTOH molecules in the case of the 4:1 ratio. The simulation run at a higher temperature (333 K) is described by the green curve, which shows that the molecules had penetrated into the leaflet of the bilayer but still had a probability of remaining at various positions in the bilayer, as shown by the small peaks. The penetration of the molecules from the center of the bilayer into the leaflet is quite fast, which is due to the more fluidic nature of the DPPC molecules and the polar interactions between the FTOH molecules and the head group region of the DPPC molecules. The FTOH molecules also have a tendency to minimize their energy to bring themselves to the more stable state. At this stage of the simulation, the FTOH molecules are stabilized inside the leaflet of the bilayer. It is possible that these molecules could change their position in the bilayer after a very long time for stability reasons.

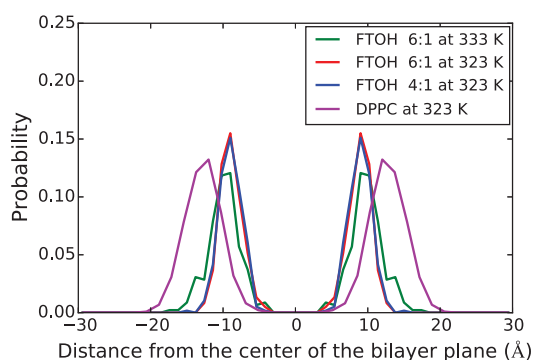


Figure 4.2: Center of mass (CM) distribution profile of FTOH molecules and DPPC bilayer at different concentrations and different temperatures during the last 20 ns out of the total simulations time.

4.3 Clustering Phenomena of the Additive Molecules

Inside the membrane environment, the distribution of the fluorotelomer alcohol (FTOH) molecules plays an important role with regard to fluorophilicity. The radial pair distribution function $g_{XY}(r)$ was used for this purpose.

$g_{XY}(r)$ for FTOH molecules was evaluated according to the pairwise distance concept. Using this approach, the corresponding number of FTOH molecules around a reference point was estimated. The system was considered to be a two-dimensional box. The first molecule was considered as a reference point, and the position of the other molecules in the DPPC bilayer environment was evaluated based on this reference point. In Figure 4.3, for the two different concentrations of FTOH molecules, the higher peaks represent the molecules in the first shell and also indicate the phase separation between the molecules and the DPPC membrane. The peaks in the plots for both concentrations do not exhibit regular forms and do not have the same amplitude, because the number of FTOH molecules is different at different positions. Two molecules may come together at some locations, while more than two molecules may exhibit a clustering effect at other locations. It is observed that the FTOH molecules are clustered for both concentrations i.e., 4:1 and 6:1. The later higher peak for the 6:1 concentration indicates the phase separation between FTOH and the DPPC membrane. In the same figure, the two-dimensional radial distribution plots for the FTOH molecules at the two different temperatures of 323 K and 333 K were also compared. At 333 K, the DPPC bilayer shows a more fluidic nature as compared to 323 K. Due to this behavior, the distribution of the FTOH molecules in the DPPC environment takes place in a better way, and the clustering effect of the FTOH molecules was not

very evident. It can be concluded that the fluorinated alcohol (FTOH) molecules exhibit a clustering effect in the DPPC environment at low temperature. As part of these clustering phenomena, peaks appeared at distances of approximately 5 Å.

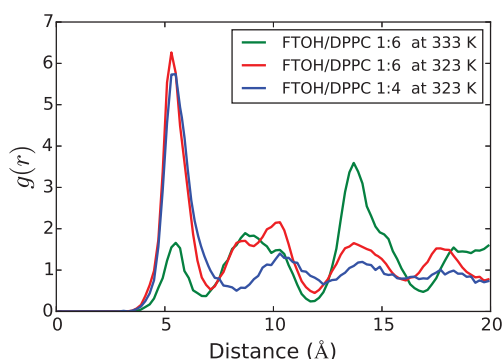


Figure 4.3: Two-dimensional radial pair distribution function, explaining the clustering phenomena of the FTOH molecules in the DPPC environment. Clustering effects are observed for these molecules in both types of system (4:1 and 6:1) and at temperatures 323 K.

4.4 Area per Lipid

The calculation of area per lipid (Area/Lipid) directly relates the simulation with experiments and provides evidence about the phase transition of the lipid (DPPC) bilayer. The reduction in Area/Lipid and the increase in the order parameters confirm that the investigated DPPC fluid phase system is transforming to a gel phase. The Area/Lipid value is calculated here by simply taking the x-dimension and y-dimension of the simulation box (unit-cell) and dividing by the number of lipids present in one leaflet, irrespective of the incorporation of FTOH molecules into the bilayer leaflet. The Area/Lipid for two different concentrations and two different temperatures of the same system is compared in Figure 4.4. The horizontal axis represents the total

magnitude of Area/Lipid, while the vertical axis represents the probability of the area being found. The histogram reflects that the Area/Lipid for all the simulated systems was higher and correlated well with the Area/Lipid of a pure DPPC bilayer. The Area/Lipid for both concentrations at 323 K shifted from a higher value to a lower value during the penetration of FTOH molecules into the bilayer, as is also shown in the same figure. Overall, a significant reduction was observed in Area/Lipid (the values were 51 \AA^2 and 52 \AA^2) for the concentrations 6:1 and 4:1, respectively) due to the penetration of FTOH molecules into the bilayer leaflet. It can be noted that the plot of Area/Lipid was slightly broadened and a shoulder was visible to the left at the higher temperature (333 K). At the same higher temperature, the FTOH molecules penetrated into the leaflet of bilayer, but it took a longer time to squeeze the area compared to the lower temperature (see section 4.1). Because of the fluidic nature at the higher temperature, greater potential is required to shift the system to a phase transition, i.e., from fluid to gel state.

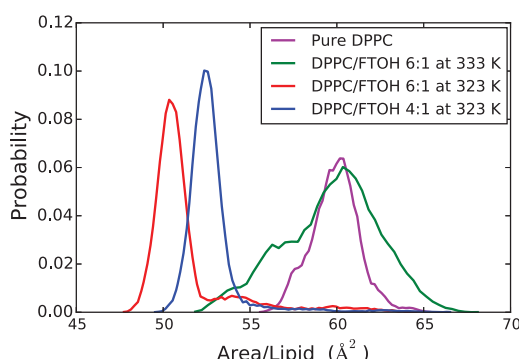


Figure 4.4: The shift in the Area/Lipid from a higher value to lower value of the DPPC bilayer. The horizontal axis represents the total magnitude of Area/Lipid while the vertical axis represents the probability of the area being found.

4.5 Gauche-Trans Conformations of the DPPC Alkyl Chains

For the system being investigated, the gauche and trans conformations of the DPPC alkyl chains can be estimated during the last 10 ns of the overall simulation trajectory. The FTOH molecules embedded initially at the center of the DPPC bilayer have now penetrated into the bilayer leaflet during the simulation. The effect caused on the alkyl chains by these penetrating molecules can be analyzed from the dihedral angles of the alkyl chains. In Figure 4.5(a and b), every line shows a dihedral angle, for which the trajectory was listed from the dihedral angle of the first four carbon atoms near the head group region of the DPPC bilayer molecule and the carbon atom at the outer end of the alkyl chain. The same figures present histograms for the torsional angles of alkyl chains for pure DPPC and in the presence of FTOH molecules. From both figures, the presence of both gauche and trans conformations was observed. The dihedral angles of the DPPC alkyl chain revealed that the gauche and trans conformation structures were changed due to the incorporation of FTOH molecules. On the basis of an overall comparison, it can be concluded that the probability of gauche conformations was reduced, while the probability of trans conformations was increased by 19%.

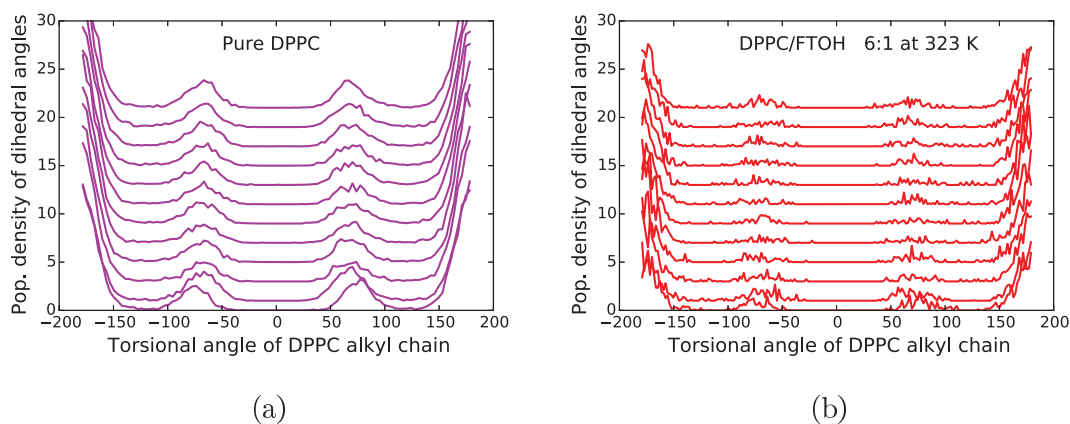


Figure 4.5: Population (Pop) density of dihedral angles illustrating the alkyl chains flexibility of the pure DPPC bilayer alkyl chain in comparison to alkyl chain in the presence of FTOH molecules. Every line shows the histogram of the dihedral angle population listed from the dihedral angle of the first four carbon atoms near the head group region (bottom) of the alkyl chain upto the outer end's carbon (top) of the alkyl chain.

4.6 Tilt Angle of the Alkyl Chains of DPPC Molecules

The tilt angle of the alkyl chains in the presence of FTOH molecules at different concentrations and different temperatures were compared with a pure DPPC bilayer system. Figure 4.6(a) presents the alignment of alkyl chains of pure DPPC with respect to the normal of the bilayer surface. It is clear that there is no decrease at the end of the traces, which indicates parallelism or anti-parallelism of the vector formed by the alkyl chains with respect to the normal of the bilayer surface. Figure 4.6(b) shows the angle between the alkyl chains and the normal of the bilayer surface in the presence of FTOH molecules. For concentrations of 4:1 and 6:1, sharp decreases were observed at 25° , 155° and at 20° , 160° , respectively. For the concentration of 6:1, the only signs of the decrease appeared at the end of the trace on both sides at the higher temperature. This corresponds to the tilted nature of the alkyl chains of a

DPPC membrane (see section 4.7).

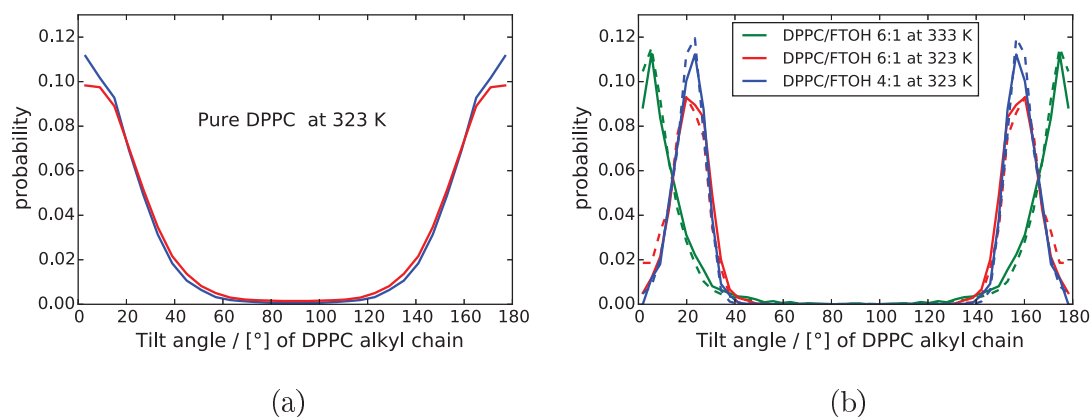


Figure 4.6: Tilt angle of the alkyl chains of DPPC molecules with regard to normal of the bilayer surface. (a) pure DPPC bilayer and (b) DPPC bilayer in the presence of FTOH molecules. The solid line is for alkyl chain-1 and dashed line is for alkyl chain-2 of lipids.

4.7 Tilt Angle of the Additive Molecules in the Membrane Environment

The alignment of the FTOH molecules to the normal of the bilayer surface was calculated by considering a symmetrical vector of these molecules. The symmetrical vector started from one carbon atom of the molecule and pointed to the carbon atom at the opposite end. Figure 4.7 shows the alignment of the FTOH molecules with respect to the normal of the bilayer surface for different concentrations i.e., 4:1 and 6:1 and for the system at a higher temperature. The two sharp decreases at the boundaries of the traces correspond to two different concentrations. These decreases cover a range of around 20° . The trace related to the higher temperature presents

a weak sign of tilted nature of the additive molecules. All these decreases show that the parallel or anti-parallel alignment of the FTOH molecules with the normal of the bilayer surface has vanished at these points and these molecules are now tilted. Comparing Figure 4.6(a and b) and Figure 4.7, one can conclude that incorporation of FTOH molecules into the bilayer, which occur significantly at 323 K, introduce a tilting transition of the lipids.

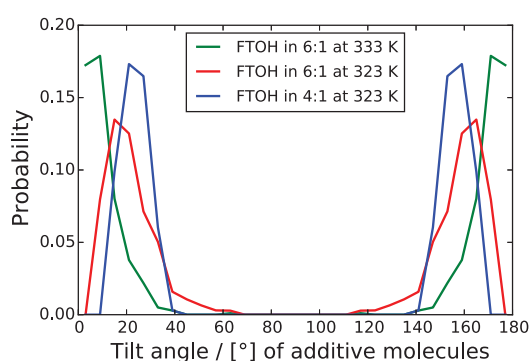


Figure 4.7: Tilt angle of the additive molecules within the DPPC bilayer. The tilt angle is with regard to normal of the bilayer surface, which coincides with the z-direction of the coordinate system.

4.8 Lipid Orientation

One of the basic purposes of investigating orientation is to calculate the order parameters of the alkyl chain of the lipids. On the basis of this property, a basic understanding of the phase transition of the lipid system can be established. The FTOH molecules penetrated into the bilayer leaflet during the simulation. It is expected that the C-H bonds of the phospholipid tails were also affected during the penetration of these molecules. The computational approach and mathematical equation as that discussed in section 3.4.3 was taken here for calculation order parameters.

The magnitude of the S_{CH} order parameters versus the carbon index number is presented in Figures 4.8 and 4.9. Here, C2 represents the carbon atom close to the head group region in each of the fatty acid chain, and C15 is for the carbon atom in a terminal methyl group. In Figure 4.8(a and b), the order parameters of alkyl chains are compared for a pure DPPC system and DPPC in the presence of FTOH molecules at a temperature of 333 K. The comparison showed that the order parameters increased for carbons from C2 to C13. In Figures 4.9(a and b), the order parameters for alkyl chains are presented in the presence of FTOH molecules at 323 K. A significant increase was observed in the order parameters of alkyl chain carbons from C2 to C14. A significant increase in the order parameters was observed at 323 K as compared to 333 K. In summary, the increase in the order parameters shows that an already existing fluid phase of lipid has transformed to the gel phase.

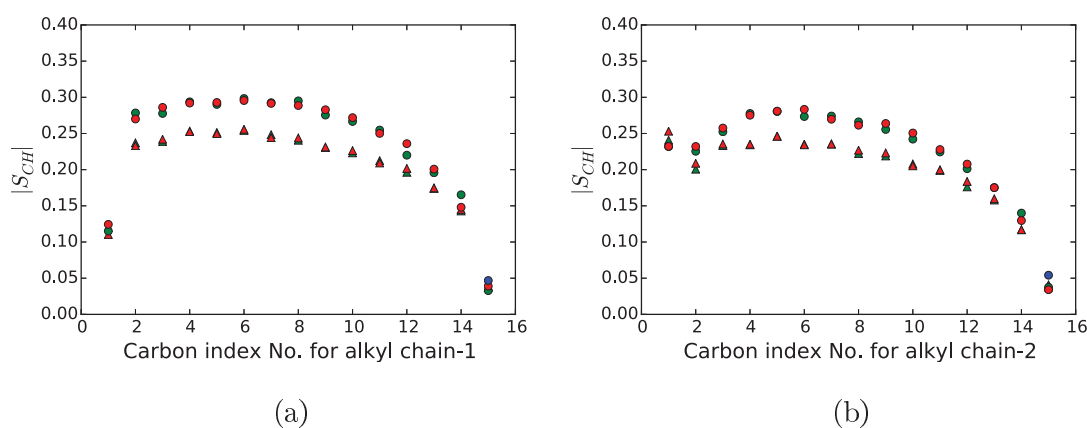


Figure 4.8: Order parameter magnitude $|S_{CH}|$ versus carbon index number for alkyl chains of DPPC bilayer simulated at 333 K in the presence of FTOH molecules (Solid circle), and pure DPPC bilayer (Triangle).

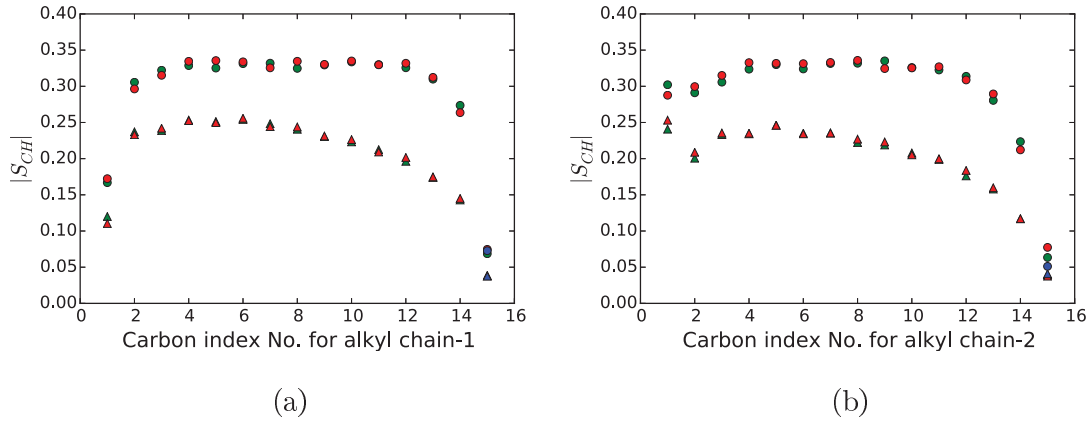


Figure 4.9: Order parameter magnitude $|S_{CH}|$ versus carbon index number for alkyl chains of DPPC bilayer simulated at 323 K in the presence of FTOH molecules (Solid circle), and pure DPPC bilayer (Triangle).

4.9 Fluctuations in the Bilayer Thickness over Time

In this section, variations in the thickness of the DPPC bilayers are described. The simulations here were carried out under constant pressure conditions. The size and the shape of the simulation box were varied in order to adjust the DPPC area and thickness. This will help to compare and validate simulations and reproduce important structural properties such as the Area/Lipid. To investigate the effect of FTOH molecules on bilayer thickness, the same DPPC bilayer compositions were used. Figure 4.10 shows fluctuations in the thickness of bilayers in the presence of FTOH molecules. Initially, a small increase was observed for the thickness of the bilayers. However, at 35 ns, the thickness for the two concentrations (4:1 and 6:1) at 323 K was higher than the thickness at 333 K. The bilayer thickness achieves a maximum value of 46 Å in the presence of FTOH molecules for the two different concentrations. It can be stated that the thickness of the bilayer attains an equilibrium position at 50 ns, accompanied by microscopic fluctuations.

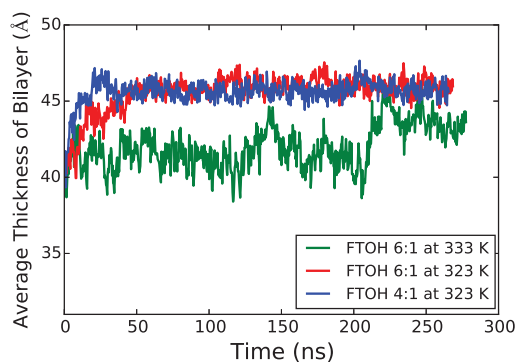


Figure 4.10: Fluctuations in the DPPC bilayer thickness over time in the presence of FTOH molecules during the total simulations time.

4.10 Final Configuration of FTOH Molecules and DPPC Molecules

Figure 4.11 shows the combined system of fluorinated alcohol (FTOH) molecules and the hydrated DPPC bilayer at the end of the simulation. This figure also shows the FTOH molecules that have penetrated into this bilayer. It also explains the tilted nature of the bilayer system. It was tilted by approximately 20° , which correlates with the value already explained by various properties, i.e., the tilt angle of the alkyl chain of DPPC molecules with the normal of bilayer plane and the tilt angle of the FTOH molecules in the membrane environment.

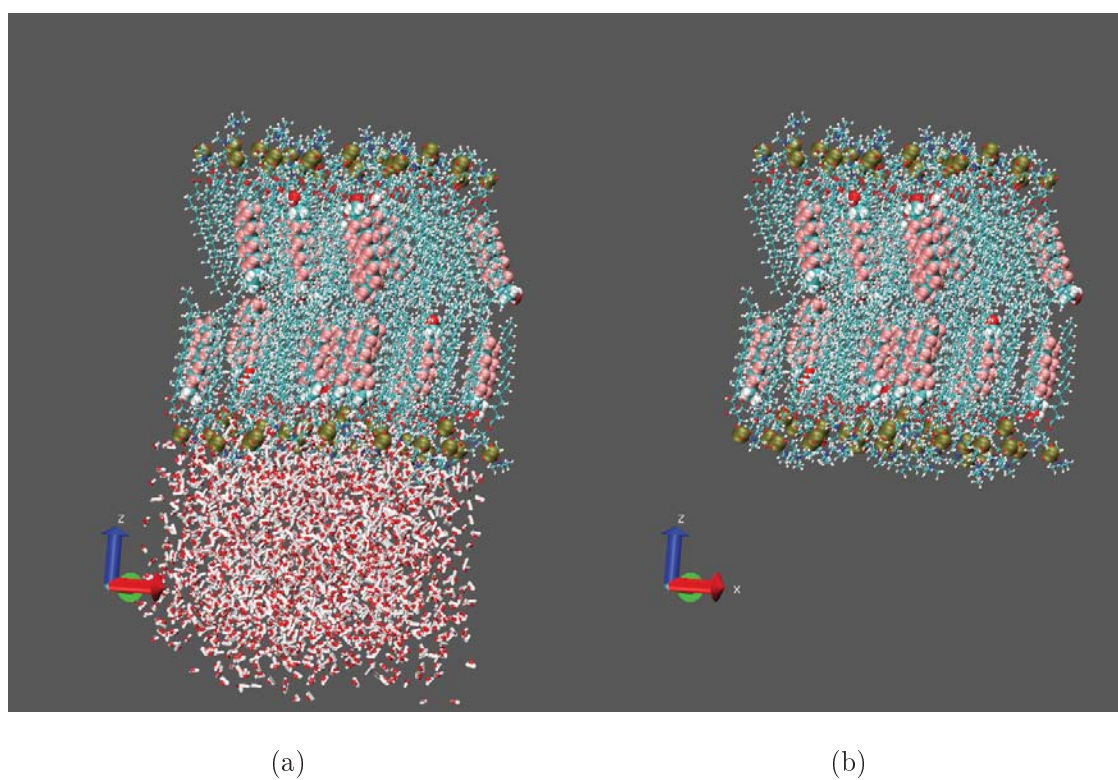


Figure 4.11: Final configuration of the system presenting the DPPC bilayer with penetrated FTOH molecules, at the end of the total simulation time.

Chapter 5

Perfluorinated Acids with a Membrane Bilayer

In this chapter, the interaction of additive molecules i.e., perfluoro octadecanoic acid (PFODA) with a DPPC bilayer is evaluated. The same computational approach as that discussed in section 2.3 was taken here. The PFODA molecules were arranged in the x-y plane in the same way as the perfluoro n-alkanes in section 3.1.1. These molecules were embedded in the DPPC bilayer according to the same process as that described in section 3.1.2. DPPC molecules were arranged in the bilayer and surrounded by 2189 water molecules on both sides. Both PFODA molecules and the DPPC bilayer have the same initial configuration as discussed in section 3.1.1.

5.1 Convergence of the Molecular Dynamics Simulation

Generally, a converged simulation of a system corresponds to a stable simulation. Simulation of the PFODA molecules combined with a DPPC bilayer was performed at 323 K. The convergence of the simulation was evaluated on the basis of the Area/Lipid and MSD. At the start of the simulation time, the Area/Lipid was 67 \AA^2 . Over the course of the simulation, this area decreased and had a value of 61 \AA^2 at 38 ns, as shown in Figure 5.1(a). On average, this value was reduced by approximately 10%, accompanied by fluctuations. Followed by the Area/Lipid, the diffusion of PFODA molecules in the DPPC environment was computed for the overall period of the simulation using MSD. The findings from the MSD plot were similar to those for the Area/Lipid that have already been discussed. Initially, the diffusion of the PFODA molecules was fast, however the diffusion process slowed after 50 ns. A peak at 150 ns appeared; after this, a decrease was observed, which indicates a numerical artifact. MSD, i.e., $\langle r^2 \rangle$ was calculated according to the equations 3.1, 3.2, 3.3, as discussed in section 3.2. Figure 5.1(b) shows the diffusion according to equation 3.1 for PFODA molecules. A decrease in the plot was observed at 150 ns, which indicates the statistical problem.

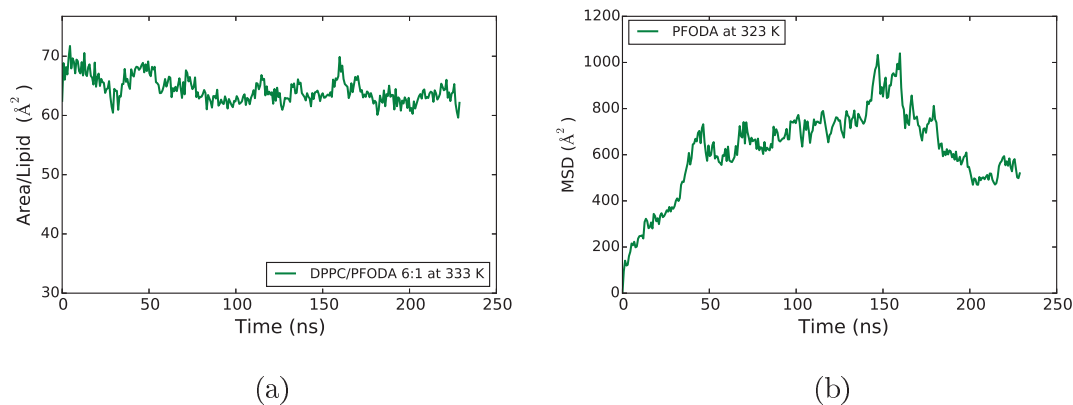


Figure 5.1: (a) Area/Lipid of DPPC bilayer in the presence of PFODA molecules. (b) MSD of the PFODA molecules in the DPPC environment.

5.2 Density Profile

The density profiles of the PFODA molecules were computed in order to evaluate the expected density increase in the region corresponding to the location of these molecules in the DPPC bilayer environment. For the DPPC bilayer and the PFODA molecules, the system was considered as a two-dimensional box. Figure 5.2 shows the center of mass distribution profile of these molecules, which was computed during the last 10 ns of the overall simulation trajectory. This distribution profile also confirms the penetration of these molecules into the bilayer leaflet. There were many peaks visible in the density profile, this probably an artificial noise. These molecules were aligned along the alkyl chains in a slightly scattered form as compared to the F10 and FTOH molecules discussed in the previous two sections, which confirms from its broadened peaks in the plot of density profile. It is possible that these molecules could change their position inside the bilayer with the progress of simulation time for stability reasons.

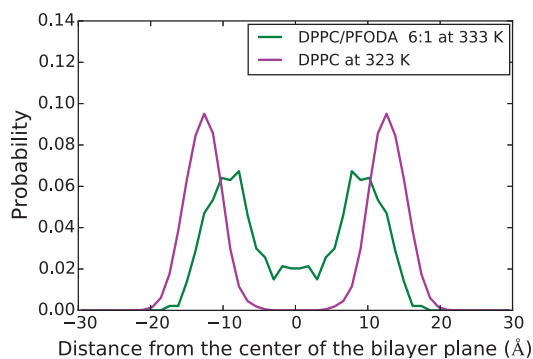


Figure 5.2: Center of mass (CM) distribution profile of a pure DPPC (magenta) and PFODA molecules in the DPPC environment (green) during the last 20 ns out of the total simulation time. Zero represents the center of bilayer plane on x-axis.

5.3 Clustering Phenomena of the Additive Molecules

When studying the behavior of the PFOA molecules in the membrane environment, the radial pair distribution function is the most interesting statistical data that can be calculated. The distribution of these molecules inside the membrane can be analyzed by a radial pair distribution function $g_{XY}(r)$. In Figure 5.3, the first peak in this function represents the presence of PFOA molecules in the first shell. This peak also confirms the phase separation behavior of these molecules and DPPC membrane. After the first peak, the remaining peaks were likely to be of non-uniform amplitude, because the probability of the presence of these molecules in the bilayer environment was also non-uniform. At higher distances r from the reference point, the amplitude of the peaks gradually decreased. From an overall perspective, it was found that these molecules present a weak clustering effect in the DPPC environment and that the peaks were approximately 5 Å from each other.

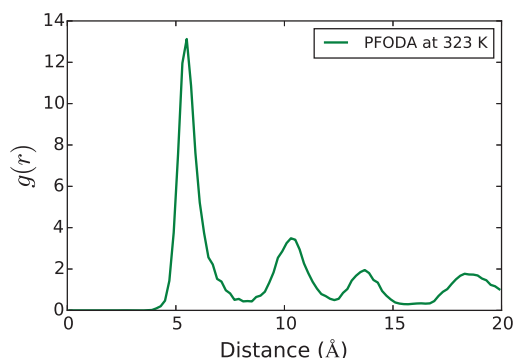


Figure 5.3: Two-dimensional radial pair distribution function explaining the clustering phenomena of PFODA molecules in the DPPC environment.

5.4 Gauche-Trans Conformations of the DPPC Alkyl Chains

In this section, the effect of the PFODA molecules on the alkyl chain structure of the DPPC bilayer was investigated. The dihedral angles were computed during the last 20 ns in order to observe the changes in the overall alkyl chain structure induced by these molecules. In Figure 5.4(a and b) every line shows a dihedral angle, for which the trajectory was listed from the dihedral angle of the first four carbon atoms near the head group region to the carbon atom at the outer end of the alkyl chain. Figure 5.4(a) presents a histogram for the dihedral angles of the alkyl chain of a pure DPPC bilayer, while Figure 5.4(b) shows the dihedral angles in the presence of PFODA molecules. From an overall comparison, it was found that trans conformations were increased by 16% and gauche conformations were reduced by the same percentage. In general, the trans conformations of DPPC bilayer were 70% without PFODA molecules, while these conformations increased to 86% upon

penetration of these molecules into the bilayer.

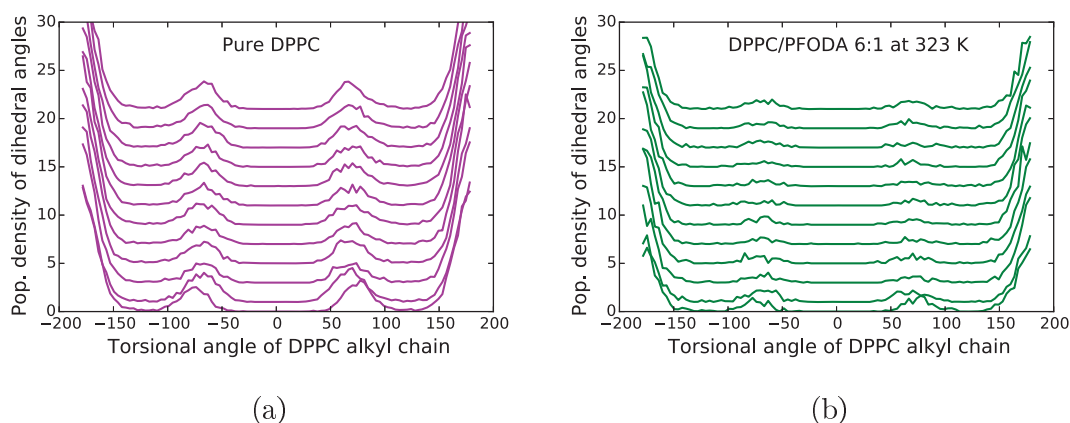


Figure 5.4: Population (Pop) density of dihedral angles illustrating the alkyl chains flexibility of the (a) pure DPPC bilayer and (b) DPPC bilayer in the presence of PFODA molecules. Every line shows the histogram of the dihedral angle population listed from the dihedral angle of the first four carbon atoms near the head group region (bottom) of the DPPC molecules to the outer end's carbon (top) of alkyl chain.

5.5 Fluctuations in the Bilayer Thickness over Time

In this section, the variation in the thickness of the bilayer was monitored during the overall simulation period in the presence of PFODA molecules. Figure 5.5 shows that the DPPC bilayer thickness was initially 40 Å, and it increased to 42 Å at 35 ns followed by an immediate decrease. This is an artificial decrease, which confirms just a fluctuation in bilayer thickness in the presence of PFODA molecules.

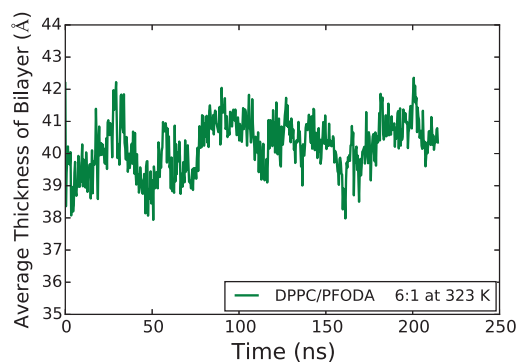


Figure 5.5: Fluctuations in the DPPC bilayer thickness over time in the presence of PFODA molecules during total simulation trajectory.

5.6 Lipid Orientation

The order parameters, which can be calculated experimentally by deuterium Nuclear Magnetic Resonance ($^2\text{H-NMR}$), are important quantities that can be used to explain the order of the lipid bilayers. The investigated lipid bilayer was already in the fluid phase and was highly disordered compared to the gel phase. The same computational approach and mathematical equation as that discussed in section 3.4.3 was used here for calculation order parameters.

Here, C2 represents the carbon atom close to the head group region in each of the fatty acid chain, and C15 is for the carbon atom in a terminal methyl group. Figure 5.6 shows a comparison between the order parameters of alkyl chain-1 and alkyl chain-2 in the presence and absence of PFODA molecules at 323 K. An increase in the order parameters of carbons from C2 to C15 was observed. The penetration of PFODA molecules into the bilayer increased the order of C-H bonds; the order parameters of carbon in the methylene group were strongly affected in particular.

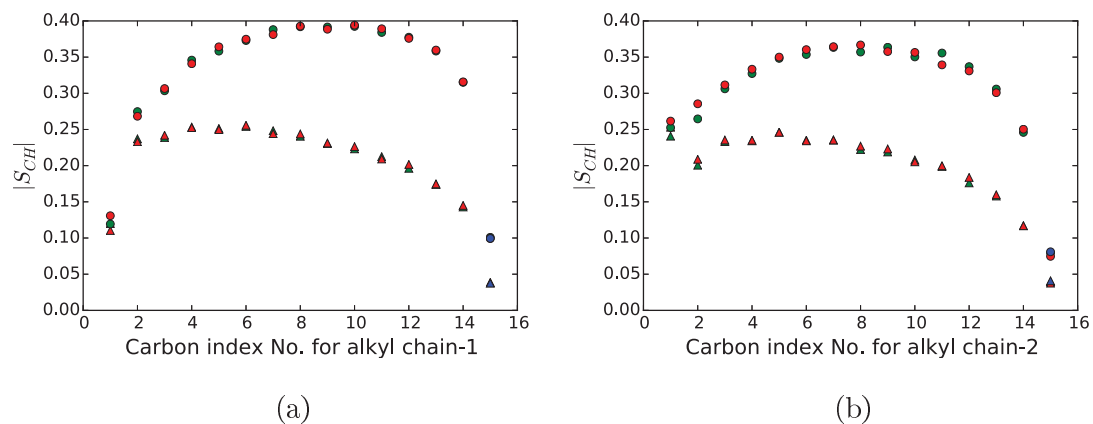


Figure 5.6: Order parameters magnitude $|S_{CH}|$ versus carbon index numbers for alkyl chain-1 and alkyl chain-2 of DPPC bilayer in the presence of PFODA molecules (Solid circle) and pure DPPC bilayer (Triangle).

5.7 Final Configuration of PFODA Molecules and Lipid Molecules

Figure 5.7 shows the final stage of the simulation period for fluorinated acids and a hydrated lipid bilayer. This figure also shows that there is no tilting effect in the DPPC bilayer in the presence of PFODA at this stage of the simulation. The orientational properties were changed significantly, while the effect on the structural properties of lipids was not as evident in the case of penetrated PFODA molecules.

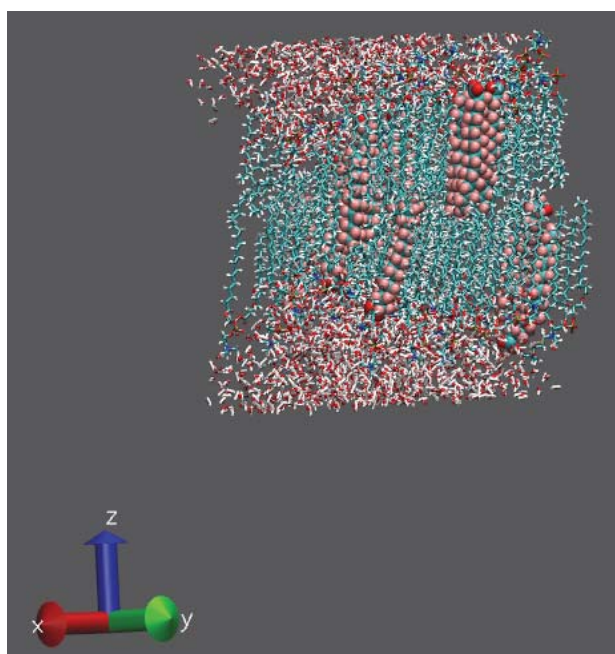


Figure 5.7: Final configuration of bilayer membrane with PFODA molecules at the end of total simulation trajectory.

Chapter 6

Summary

Molecular dynamics (MD) simulations for perfluoro n-hexane (F6), perfluoro n-octane (F8), perfluoro n-decane (F10), partially fluorinated decane [*5 carbons attached with hydrogens, and 5 carbons attached with fluorine*] (H5F5), and normal decane (H10), in a membrane DPPC bilayer in a fluid phase were performed in the isothermal-isobaric (NPT) ensemble. From the amphiphiles family, fluorinated alcohol (FTOH) and perfluorinated octadecanoic acid (PFODA) molecules were used for simulation with a DPPC bilayer. Simulations were performed at 323 K and 333 K and at constant pressure.

After 300 ns of simulation trajectory, the structural and orientational properties of the DPPC membrane such as Area/Lipid, trans-gauche conformations, order parameters, fluidity and phase transitions were significantly affected by perfluorinated, partially fluorinated alkanes, normal alkanes and fluorinated amphiphiles, i.e., (F6, F8, F10), H5F5, H10, and (FTOH, PFODA), respectively. MSD plots revealed a significant reduction in the mobility of longer chain, i.e., F10 molecules due to penetration of

these molecules into the leaflet of the bilayer. The diffusion of the fluorinated alcohol molecules in the lipid bilayer system was faster at the higher temperature as compared to the lower temperature. At the higher temperature, the membrane exhibited a fluidic nature, while at the lower temperature it became frozen. Plots of the rotational dynamics of the additive molecules revealed that the rotational movement of longer chain perfluorinated molecules is markedly hindered, due to its penetration into the leaflet of the lipid bilayer. It is important to note that the additive molecules were found inside the leaflet of the lipid bilayer at this stage of simulation. The penetration of the perfluorinated and fluorinated molecules into the leaflet of the DPPC bilayer leads to a more organized bilayer system, which is reflected in an increase in the compression modulus and a decrease in the Area/Lipid. The longer chain perfluorinated molecules showed better penetration into the leaflet of the lipid bilayer, thus reducing Area/Lipid by 21.0%.

An increase in deuterium order parameters of the lipid alkyl chains was noticed upon incorporation of additive molecules into the bilayer. The increase in the order parameters in case of F10, FTOH, and PFODA molecules is significant. It is concluded that higher the degree of fluorination and longer the carbon chain leads to effective change in the order parameters.

The clustering of F10, FTOH, and PFODA molecules was observed inside the lipid bilayer. The clustering tendency of FTOH and PFODA molecules was sufficiently reduced because of their head group interactions with ionic head group region of lipid molecules. In case of F10 molecules, better clustering was observed because of absence of these additional polar interactions. The clustering phenomenon was not so

evident in all other types (F6, F8, H5F5, and H10) of molecules.

The CM distribution profiles were calculated for the additive molecules and for a pure membrane. Good correlation was observed between the center of mass distributions of additive molecules and membrane molecules. At this stage of the simulation, the perfluorinated molecules penetrated into the leaflet of the DPPC bilayer alkyl chains and stabilized themselves by minimizing their energy. There is also the possibility that these perfluorinated molecules could change their position inside the leaflet of the bilayer for stability reasons after a very long time of simulation. On the basis of our calculations and observations, it was observed that, with the progress of simulation time, perfluorinated molecules that had penetrated into the leaflet of the lipid bilayer might produce pores for water in the head group region. The incorporation of fluorophilic molecules into the DPPC system may provide a new means of controlling the permeability and stability characteristics of DPPC membranes. In our project, we focused on the “complexity of the problem” and “the behavior of relatively small fluorophilic and lipophilic organic molecules in biological systems”. Further in-depth studies are required to address the need for research into these compounds.

Chapter 7

Appendix A

7.1 List of Symbols and Abbreviations

CHARMM	Chemistry at HARvard Macromolecular Mechanics
NAMD	Nanoscale Molecular Dynamics , formerly Not Another Molecular Dynamics
MD	Molecular Dynamics
PFCs	Perfluorinated Compounds
DPPC	Dipalmitoylphosphatidylcholine
RB	Ryckaert-Bellemans
UB	Urey-Bradley
LJ model	Lennard-Jones model
NPT	Number, Pressure and Temperature

NVE	Number, Volume and Energy
NVT	Number, Volume and Temperature
GROMACS	Groningen Machine for Chemical Simulations
PME	Particle Mesh Ewald
TCL	Tool Command Language
TIP3P	Transferable intermolecular potential 3P
FTOH	Fluorotelomer Alcohol
PFODA	Perfluorinated Octa-Decanoic Acid
F6	Perfluoro n-Hexane
F8	Perfluoro n-Octane
F10	Perfluoro n-Decane
H5F5	Partially fluorinated decane [<i>5 carbons attached with hydrogens, and 5 carbons attached with fluorine</i>]
H10	Normal Decane
MSD	Mean Square Displacement
C-F bond	Carbon and Fluorine bond
HFIP	Hexafluoroisopropanol
TFE	Pertrifluoroethanol

PFCAs	Perfluorocarboxylic acids
8:2 FTOH	Fluorotelomer Alcohol with 8 fluorinated carbons and 2 hydrogenated carbons
$g_{XY}(r)$	Radial Pair Distribution Function
C-H bond	Carbon and Hydrogen bond
K	Kinetic energy
V	Potential energy
CM	Center of Mass
ND	Neutron Diffraction
GX	Gravimetric X-ray method
GXC	Gravimetric X-ray Corrected method
FRAP	Fluorescence Recovery After Photobleaching
FCS	Fluorescence Correlation Spectroscopy
AFM	Atomic Force Microscopy
pK_a	An acid dissociation constant, K_a , (also known as acidity constant, or acid-ionization constant) is a quantitative measure of the strength of an acid in solution. The lower the pK_a value, the stronger the acid.

Chapter 8

Appendix B

8.1 Data Related to the Parametrization Process of Fluorocarbons

8.1.1 Total Energy Function of CHARMM Force Field, its Model Interactions and Parameters

The total energy function of CHARMM force field, its model interactions and parameters are provided in the following.

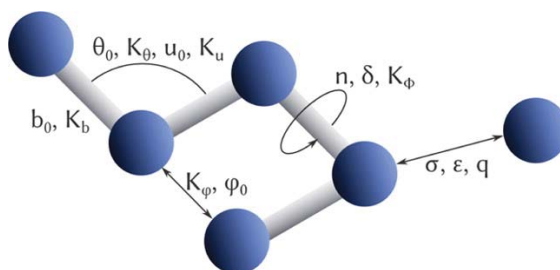


Figure 8.1: Model interactions and parameter usage for the total energy function of the CHARMM force field.

$$\begin{aligned}
E = & \sum_{bonds} K_b(b - b_0)^2 + \sum_{angles} K_\theta(\theta - \theta_0)^2 \\
& + \sum_{dihedrals} K_\phi(1 + \cos(n\phi - \delta)) + \sum_{improper} K_\varphi(\varphi - \varphi_0)^2 \\
& + \sum_{Urey-Bradley} K_u(u - u_0)^2 \\
& + \sum_{i < j} 4\varepsilon \left[\left(\frac{\sigma_{ij}}{r_{ij}} \right)^{12} - \left(\frac{\sigma_{ij}}{r_{ij}} \right)^6 \right] + \sum_{i < j} \frac{q_i q_j}{4\pi \varepsilon_0 r}
\end{aligned} \tag{8.1}$$

8.1.2 Optimization Procedure for Bonded Parameters and Charges

The procedure to derive parameters for new atom types of an optimized structure compatible with the CHARMM force field from both experimental and theoretical quantum chemical data [79] are explained in Figure 8.2. Due to some unclear definitions, issues related to the lipid layers and to bond and angle definitions, as their reference values (b_0 or θ_0 , respectively) do not reproduce the ground state conformation by themselves, both the CGenFF and the CHARMM force field are used for parametrization procedure. The compounds used for the parametrization procedure are, n-alkanes, perfluoro-n-alkanes up to perfluoro-n-octane, and partially fluorinated n-alkanes.

8.1.3 Optimization of van der Waals Parameters

To calculate the optimal parameter values for the van der Waals interaction, both regular aliphatic carbon chains and perfluorinated chains are almost nonpolar but exhibit a highly subtle thermodynamic behavior in terms of mixing/demixing properties. The optimized parameters in question are developed on the basis of liquid densities for both perfluoro-n-alkanes and mixtures of perfluoro-n-alkanes and n-alkanes.

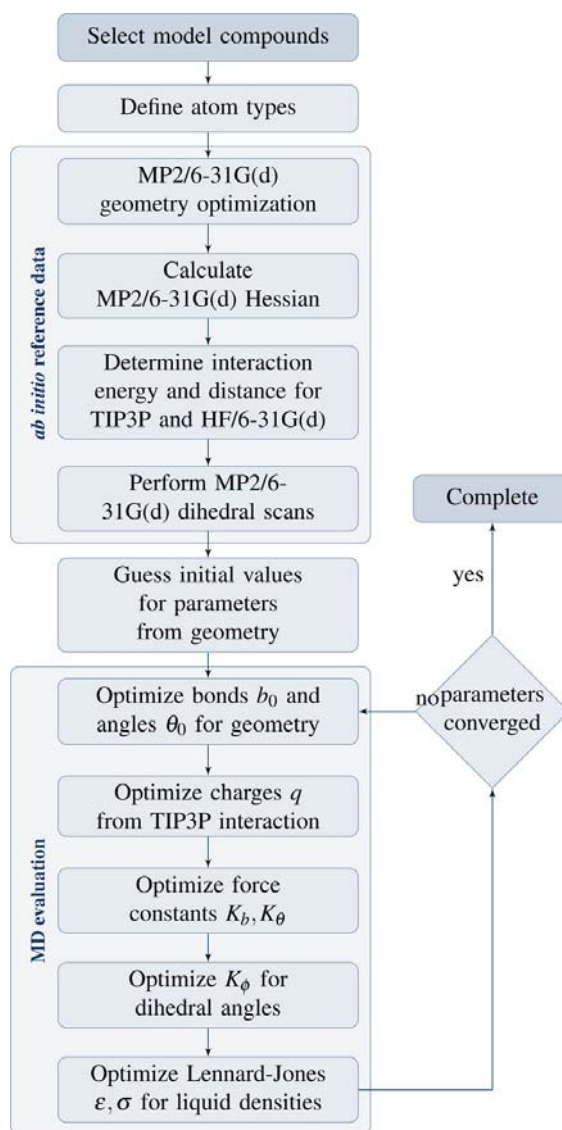


Figure 8.2: Parametrization schema for the CHARMM force field as applied for preparation of fluorocarbons parameters.

8.1.4 Atom Types used for Parametrization

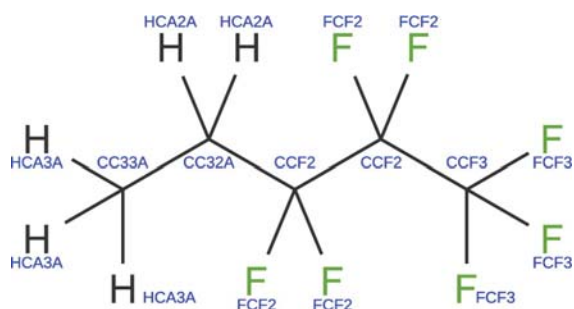


Figure 8.3: Atom types used for parametrization as an notation to one of the sample compounds. FCF₂, FCF₃, CCF₂ and CCF₃ are the newly introduced atom types.

Atom type label	Mass (amu)	Description
CCF ₃	12.01	carbon in CF ₃ group
CCF ₂	12.01	carbon in CF ₂ group
FCF ₃	19.00	fluorine in CF ₃ group
FCF ₂	19.00	fluorine in CF ₂ group

Table 8.1: Introduced atom types with their CHARMM-style label

8.1.5 Bonded Parameters

For bonded parameters, the equilibrium values are computed by using the atom types CC33A, CC32A, HCA3A, and HCA2A for n-alkanes from CHARMM35 [91]. In general, the influence in terms of variation of the values for bonded parameters of the nonfluorinated part of the n-alkanes on the fluorinated part is negligible for n_i and, hence, neither of the conformational parameters varies with increasing chain length i . Together using the most simplified and only four different atom types in two different chemical groups is justified for perfluoro-n-alkanes, and additional atom types at the connection between the fluorinated and nonfluorinated parts are not necessary to simulate in this selection of n-alkane model compounds. This follows the typical approach for alkanes in CHARMM and CGenFF. The resulting parameters

yield good geometries, which have good agreement of the conformations for small as well as for larger compounds, which supports this approach. In the following tables, the final values for the bond parameters and for angles are listed.

Atom types	K_b	b_0
CCF ₃ CC32A	222.5	1.51
FCF ₃ CCF ₃	322	1.34
FCF ₂ CCF ₂	322	1.37
CCF ₂ CC32A	222.5	1.51
CCF ₃ CCF ₂	22.5	1.53
CCF ₂ CCF ₂	270.134	1.5328
CCF ₃ CCF ₃	277.058	1.5308

Table 8.2: Bond lengths b_0 in Angstroms and force constants K_b in kcal/mol/Å²

Atom types	θ_0	K_θ
CC33A CC32A CCF ₃	37.3227	112.397
HCA2A CC32A CCF ₃	34.600	106.820
CC32A CCF ₃ FCF ₃	48.248	111.733
CC33A CC32A CCF ₂	64	111.54
CC32A CCF ₂ FCF ₂	52	110.66
CC32A CCF ₂ CCF ₃	53	114.91
CC32A CCF ₂ CCF ₂	53	114.91
CCF ₂ CC32A HCA2A	52	107.54
FCF ₃ CCF ₃ FCF ₃	35.500	107.100
CCF ₂ CCF ₃ FCF ₃	95	111.05
CCF ₃ CCF ₂ FCF ₂	55	106.36
FCF ₂ CCF ₂ FCF ₂	35	107.53
CCF ₂ CCF ₂ FCF ₃	21.50	107.73
CCF ₂ CCF ₂ CCF ₃	52.08	116.99
CCF ₃ CCF ₃ FCF ₃	47.149	109.724
CCF ₃ CCF ₂ CCF ₃	91.0318	116.620
CCF ₂ CCF ₂ CCF ₂	45.7428	107.626

Table 8.3: Angles θ_0 in degrees and force constants K_θ in kcal/mol/rad². (All Urey-Bradley terms are set to zero).

8.1.6 Charges

Optimization of the charge has been carried out by using classical molecular dynamics. For perfluoro-n-alkanes, it is difficult to fit the optimizations done either for matching interaction distances or for matching interaction energies. It has been solved by defining a mathematical weighting W with physical justification as a single parameter fitting target, and chose the geometric mean of the relative errors. By keeping CF_2 or CF_3 group has to be neutral in total, only the net charges on the fluorines and the partial charge of the carbons is evaluated. The resulting charges, which are given in Table 8.4, are quite similar to values used in different force fields [20, 92].

$$W^2 = \left[\frac{E_i(\text{MD}) - E_i(\text{QM})}{E_i(\text{QM})} \right]^2 + \left[\frac{d_i(\text{MD}) - d_i(\text{QM})}{d_i(\text{QM})} \right]^2 \quad (8.2)$$

Atom types	q	ϵ	R_{min}	ϵ'	R'_{min}
FCF_3	-0.12	-0.0240	1.3400	-	-
FCF_2	-0.185	-0.1050	1.6300	-	-
CCF_3	0.36	-0.0780	2.0400	-0.01	1.9
CCF_2	0,37	-0.0240	2.0500	-	-

Table 8.4: Lennard-Jones parameter ϵ in kcal/mol and R_{min} in Angstroms along with charges in e. For charge in e, a correction (ϵ' and R'_{min}) for 1,4 atoms is suggested by CGenFF.

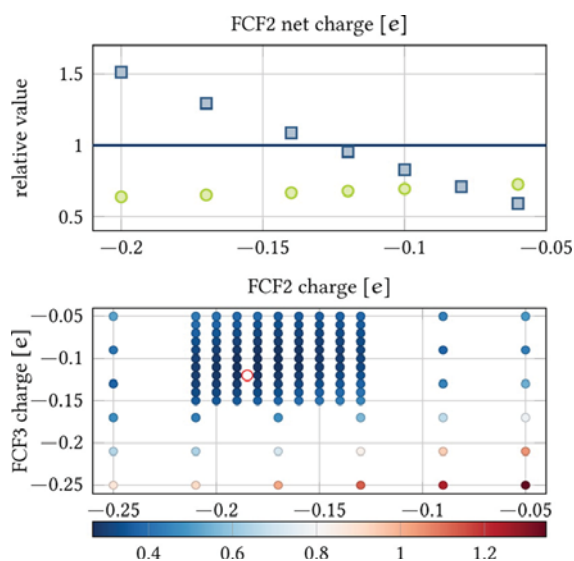


Figure 8.4: Top: Interaction energy (MD) normalized by the MP2/6-31G(d) results (■) and interaction distances normalized the same way (●) over the FCF₂ net charge for f₂ together with the ideal target value (/). The CCF₂ net charge has been set such that the overall CF₂ group is neutral. It is clearly visible that there is no optimum that fits both the interaction energies and the interaction distances. Bottom: Given the weighting in Eq. 8.2, the deviation from the target values depending on the charges of FCF₂ and FCF₃ has been rasterized. The optimal value is highlighted (○).

8.1.7 Dihedral Angles

For perfluoro-*n*-alkanes, the simulations confirm the reported observation about the dihedral for the carbon chain conformations [20, 93]. This effect is modeled accordingly by defining a nonzero phase shift for the appropriate dihedral parameter. For short chains the tilted chain angle is not clearly visible, while for longer chains, it is a bit more clear, therefore different potential has been used. Hence, the overall target is to simulate comparably long perfluorinated chains, this approach is clearly justified. However, the actual conformations of short partially fluorinated compounds have to be used with care.

Atom types				K_χ	η	δ
CCF ₂	CCF ₂	CCF ₃	FCF ₃	0.515	1	180.0
FCF ₂	CCF ₂	CCF ₂	CCF ₃	0.529	1	0.0
FCF ₂	CCF ₂	CCF ₂	FCF ₂	2.505	1	0.0
FCF ₃	CCF ₃	CCF ₂	FCF ₂	0.207	3	0.0
FCF ₃	CCF ₃	CCF ₃	FCF ₃	0.218	3	0.0
CCF ₃	CCF ₂	CCF ₃	FCF ₃	0.082	3	0.0
CCF ₃	CCF ₂	CCF ₂	CCF ₃	1.164	1	180.0
CCF ₃	CCF ₂	CCF ₂	CCF ₂	2.508	1	180.0
CCF ₂	CCF ₂	CCF ₂	FCF ₂	0.040	3	0.0
CCF ₂	CCF ₂	CCF ₂	CCF ₂	3.000	1	180.0
CC33A	CC32A	CCF ₃	FCF ₃	0.164	3	0.0
CCF ₃	CC32A	CC33A	HCA3A	0.121	3	0.0
FCF ₃	CCF ₃	CC32A	HCA2A	0.262	3	0.0
CC33A	CC32A	CCF ₂	CCF ₃	0.16	1	0.0
CC32A	CCF ₂	CCF ₃	FCF ₃	0.16	3	0.0
CCF ₃	CCF ₂	CC32A	HCA2A	0.16	2	0.0
CC32A	CCF ₂	CCF ₂	CCF ₃	1.875	1	0.0
CC32A	CCF ₂	CCF ₂	FCF ₂	0.530	1	0.0
CC33A	CC32A	CCF ₂	CCF ₂	1.481	1	0.0
CC33A	CC32A	CCF ₂	FCF ₂	0.510	3	0.0
CCF ₂	CC32A	CC33A	HCA3A	0.341	3	0.0
HCA2A	CC32A	CCF ₂	CCF ₂	0.316	1	0.0
HCA2A	CC32A	CCF ₂	FCF ₂	0.034	2	0.0

Table 8.5: Dihedrals and their offset δ in degrees, force constants K_χ in kilocalories per mol and multiplicity η

Bibliography

- [1] Nicolson, G. L. The fluid-mosaic model of membrane structure: Still relevant to understanding the structure, function and dynamics of biological membranes after more than 40 years. *Biochim. Biophys. Acta - Biomembr.*, 1838(6, SI):1451–1466, **2014**.
- [2] Singer, S. J.; and Nicolson, G. L. Fluid mosaic model of structure of cell-membranes. *Science*, 175(4023):720, **1972**.
- [3] Xiang, T. X.; and Anderson, B. D. Influence of chain ordering on the selectivity of dipalmitoylphosphatidylcholine bilayer membranes for permeant size and shape. *Biophys. J.*, 75(6):2658–2671, **1998**.
- [4] Winter, R. ; Jeworrek. C. Effect of pressure on membranes. *Soft Matter*, 5:3157–3173, **2009**.
- [5] Xie, W.; Kania-Korwel, I.; Bummer, P. M.; and Lehmler, H. J. Effect of potassium perfluorooctanesulfonate, perfluorooctanoate and octanesulfonate on the phase transition of dipalmitoylphosphatidylcholine (DPPC) bilayers. *Biochim. et Biophys. Acta-Biomembr.*, 1768(5):1299–1308, **2007**.
- [6] Jyoti, A.; Prokop, R. M.; Li, J.; Vollhardt, D.; Kwok, D. Y.; Miller, R.; Mohwald, H.; and Neumann, A. W. An investigation of the compression rate dependence on the surface pressure-surface area isotherm for a dipalmitoyl phosphatidylcholine monolayer at the air/water interface. *Colloids and Surfaces A Physicochemical and Engineering Aspects*, 116(1-2):173–180, **1996**.
- [7] Klopfer, K. J.; and Vanderlick, T. K. Isotherms of dipalmitoylphosphatidylcholine (DPPC) monolayers: Features revealed and features obscured. *J. Colloid and Interface Sci.*, 182(1):220–229, **1996**.
- [8] Carafa, M.; Santucci, E.; Alhaique, F.; Coviello, T.; Murtas, E.; Ricciari, F. M.; Lucania, G.; Torrisi, M. R. Preparation and properties of new unilamellar non-ionic/ionic surfactant vesicles. *Int. J. Pharmaceutics*, 160(1):51–59, **1998**.

- [9] Nakahara, H.; Ohmine, A.; Kai, S.; and Shibata, O. Monolayer compression induces fluidization in binary system of partially fluorinated alcohol ($F_4H_{11}OH$) with DPPC. *J. Oleo Sci.*, 62(5):271–281, **2013**.
- [10] Nagle, J. F. Theory of the main lipid bilayer phase transition. *Annual Rev. Phys. Chem.*, 31:157–195, **1980**.
- [11] Santaella, C.; Vierling, P.; and Riess, J. G. Highly stable Liposomes Derived from Perfluoroalkylated Glycerophosphocholines. *Ang. Chem. Int. Ed. in Eng.*, 30(5):567–568, **1991**.
- [12] Heimburg, T. Handbook of molecular biophysics (ed. Bohr, H. G.). pages 593–616, **2009**.
- [13] Eeman, M.; and Deleu, M. From biological membranes to biomimetic model membranes. *Biotechnologie Agronomie Societe et Environnement*, 14(4):719–736, **2010**.
- [14] Akbarzadeh, A.; Rezaei-Sadabady, R.; Davaran, S.; Joo, S. W.; Zarghami, N.; Hanifehpour, Y.; Samiei, M. Kouhi, M. and Nejati-Koshki, K. Liposome: classification, preparation, and applications. *Nanoscale Research Letters*, 8, **2013**.
- [15] Cullis, P. R.; and Dekruiff, B. Lipid polymorphism and the functional roles of lipids in biological-membranes. *Biochimica et Biophysica Acta*, 559(4):399–420, **1979**.
- [16] Cullis, P. R.; Dekruiff, B.; Verkleij, A. J.; and Hope, M. J. Lipid polymorphism and membrane-fusion. *Biochemical Society Transactions*, 14(2):242–245, **1986**.
- [17] Guido Falk von Rudorff, Tobias Watermann, and Daniel Sebastiani. Perfluoroalkane force field for lipid membrane environments. *J. Phys. Chem.B.*, 118(43):12531–12540, **2014**.
- [18] Simmons, J.H.; and Reed, T.M. *Fluorine Chemistry*, volume 5. Academic Press New York, **1964**.
- [19] Ojogun and A. Vivian. Effect of fluorination on partitioning behavior and bilayer self assembly. Dissertation, **2010**.
- [20] Padua, A. A. H. Torsion energy profiles and force fields derived from ab initio calculations for simulations of hydrocarbon-fluorocarbon diblocks and perfluoroalkylbromides. *J. Phys. Chem. A.*, 106(43):10116–10123, **2002**.
- [21] Riess, J. G. Oxygen carriers ("blood substitutes") raison d'être, chemistry, and some physiology blut ist ein ganz besonderer saft. *Chem. Rev.*, 101(9):2797–2920, **2001**.

- [22] Krafft, M. P.; and Riess, J. G. Chemistry, physical chemistry, and uses of molecular fluorocarbon-hydrocarbon diblocks, triblocks, and related compounds-unique "a polar" components for self-assembled colloid and interface engineering. *Chem. Rev.*, 109(5):1714-1792, **2009**.
- [23] Mukerjee, P.; and Handa, T. Adsorption of fluorocarbon and hydrocarbon surfactants to air-water, hexane-water and perfluorohexane-water interfaces. relative affinities and fluorocarbon-hydrocarbon nonideality effects. *J. Phys. Chem.*, 85(15):2298-2303, **1981**.
- [24] Goss, K.U.; and Bronner, G. What is so special about the sorption behavior of highly fluorinated compounds? *J. Phys. Chem. A.*, 110(30):9518-9522, **2006**.
- [25] Shinoda, K.; Hato, M.; and Hayashi, T. Physicochemical properties of aqueous solutions of fluorinated surfactants. *J. Phys. Chem.*, 76(6):909-914, **1972**.
- [26] Riess, J. G. Fluorous micro and nanophases with a biomedical perspective. *Tetrahedron*, 58(20):4113-4131, **2002**.
- [27] Jimmie, R.; Baran, Jr. Fluorinated surfactants and repellents: a second edition, revised and expanded surfactant science series. volume 97. by erik kissa (consultant, wilmington, de). marcel dekker a new york. 2001. xiv + 616 pp. \$195.00. isbn 0-8247-0472-x. *J. Am. Chem. Soc.*, 123(36):8882-8882, **2001**.
- [28] Dasaradhi, L.; and Ohagan, D. The effect of aryl fluorene in a lipse resolutions. *Bioorg. & Medicinal Chem. Lett.*, 3(8):1655-1658, **1993**.
- [29] Krafft, M. P.; and Riess, J. G. Highly fluorinated amphiphiles and colloidal systems, and their applications in the biomedical field. *A Contribution Biochimie*, 80(5-6):489-514, **1998**.
- [30] Krafft, M. P. Fluorocarbons and fluorinated amphiphiles in drug delivery and biomedical research. *Adv. Drug Deliv. Rev.*, 47(2-3):209-228, **2001**.
- [31] Krafft, M. P.; Rolland, J. P.; Vierling, P.; and Riess, J. G. New perfluoroalkylated phosphocholines effect on particle size and stability of fluorocarbon emulsions. *New J. Chem.*, 14(11):869-875, **1990**.
- [32] Lowe, K. C. Fluorinated blood substitutes and oxygen carriers. *J. Fluorine Chem.*, 109(1, SI):59-65, **2001**.
- [33] Lane, T. A. Perfluorochemical-based artificial oxygen carrying red cell substitutes. *Transfusion Sci.*, 16(1):19-31, **1995**.

- [34] Riess, J. G.; and Krafft, M. P. Fluorinated materials for in vivo oxygen transport (blood substitutes), diagnosis and drug delivery. *Biomaterials*, 19(16):1529–1539, **1998**.
- [35] Gerber, F.; Krafft, M. P.; Vandamme, T. F.; Goldmann, M.; and Fontaine, P. Fluidization of a dipalmitoyl phosphatidylcholine monolayer by fluorocarbon gases, Potential use in lung surfactant therapy. *Biophys. J.*, 90(9):3184–3192, **2006**.
- [36] Gerber, F.; Krafft, M. P.; and Vandamme, T. F. The detrimental effect of serum albumin on the re-spreading of a dipalmitoylphosphatidylcholine Langmuir monolayer is counteracted by a fluorocarbon gas. *Biochim. et Biophys. Acta-Biomembr.*, 1768(3):490–494, **2007**.
- [37] Gerber, F.; Krafft, M. P.; Vandamme, T. F.; Goldmann, M.; and Fontaine, P. Preventing crystallization of phospholipids in monolayers: A new approach to lung-surfactant therapy. *Ang. Chem. Int. Ed.*, 44(18):2749–2752, **2005**.
- [38] Nakahara, H.; Lee, S.; Krafft, M. P.; and Shibata, O. Fluorocarbon-hybrid pulmonary surfactants for replacement therapy - a langmuir monolayer study. *Langmuir*, 26(23):18256–18265, **2010**.
- [39] Cuntze, J.; Owens, L.; Alcazar, V.; Seiler, P.; and Diederich, F. Molecular clefts derived from 9,9'-Spirobi[9H-fluorene] for enantioselective complexation of pyranosides and dicarboxylic-acids. *Helvetica Chimica Acta*, 78(2):367–390, **1995**.
- [40] Pozzi, G.; Colombani, I.; Miglioli, M.; Montanari, F.; and Quici, S. Epoxidation of alkenes under liquid-liquid biphasic conditions: Synthesis and catalytic activity of Mn(III)-tetraarylporphyrins bearing perfluoroalkyl tails. *Tetrahedron*, 53(17):6145–6162, **1997**.
- [41] Tian, Y.; Yang, Q. C.; Mak, T. C. W.; and Chan, K. S. Asymmetric catalytic carbon-carbon bond formations in a fluorous biphasic system based on perfluoroalkyl-binols. *Tetrahedron*, 58(20):3951–3961, **2002**.
- [42] Bartle, P. D.; Knox, L. H.; and Roberts, J. D. *Org. synth.* 5:196, **1973**.
- [43] Curran, D. P. Fluorous reverse phase silica gel. a new tool for preparative separations in synthetic organic and organofluorine chemistry. pages 1488–1496, **2001**.
- [44] Bosanac, T.; Yang, J. M.; and Wilcox, C. S. Precipitons-functional protecting groups to facilitate product separation, Applications in isoxazoline synthesis. *Angewandte Chemie International Edition.*, 40(10):1875–1879, **2001**.

- [45] Ishihara, K.; Hasegawa, A.; and Yamamoto, H. A fluorous super Bronsted acid catalyst, Application to fluorous catalysis without fluorous solvents. *Synlett*, (8):1299–1301, **2002**.
- [46] Martin, J. W.; Derek C. G.; Moody, A. C.; Ellis, D. A.; Kwan, W. C.; Solomon, K. R.; and Mabury, S. A. Collection of airborne fluorinated organics and analysis by gas chromatography/chemical ionization mass spectrometry. *Analytical Chem.*, 74(3):584 – 590, **2002**.
- [47] Stock, N. L.; Lau, F. K.; Ellis, D. A.; Martin, J. W.; Derek C. G.; and Mabury, S. A. Polyfluorinated telomer alcohols and sulfonamides in the north american troposphere. *Environ. Sci. & Tech.*, 38(4):991–996, **2004**.
- [48] Martin, J. W.; Whittle, D. M.; Muir, D. C. G.; and Mabury, S. A. Perfluoroalkyl contaminants in a food web from lake ontario. *Environ. Sci. & Tech.*, 38(20):5379–5385, **2004**.
- [49] Christopher, P. H.; and Luthy, R. G. Sorption of perfluorinated surfactants on sediments. *Environ. Sci. & Tech.*, 40(23):7251–7256, **2006**.
- [50] Darcy, C. B.; Ellis, D. A.; Hongxia, Li.; McMurdo, J. C.; and Webster, E. Experimental pka determination for perfluorooctanoic acid (pfoa) and the potential impact of pka concentration dependence on laboratory-measured partitioning phenomena and environmental modeling. *Environ. Sci. & Tech.*, 42(24):9283–9288, **2008**.
- [51] Goss, K. U. The pka values of pfoa and other highly fluorinated carboxylic acids. *Environ. Sci. & Tech.*, 42(2):456–458, **2008**.
- [52] Riess, J. G. Highly fluorinated amphiphilic molecules and self-assemblies with biomedical potential. *Current Opinion in Colloid & Interface Sci.*, 14(5):294–304, **2009**.
- [53] Tuckerman, M. E. *Statistical Mechanics: Theory and Molecular Simulation*. **2010**.
- [54] Verlet, L. Computer experiments on classical fluids.I. Thermodynamical properties of lennard-jones molecules. *Phys. Rev.*, 159(1):98, **1967**.
- [55] Haile, J. M. *Molecular Dynamics Simulation*. John Wiley and Sons., **1997**.
- [56] Swope, W. C.; Andersen, H. C.; Berens, P. H.; and Wilson, K. R. A computer simulation method for the calculation of equilibrium constants for formation of physical molecules application to small water clusters. *J. Chem. Phys.*, 76(1):637–649, **1982**.

- [57] Allen, M. P.; and Tildesley, D. J. *Computer Simulation of Liquids*. Oxford university press, **1987**.
- [58] Ryckaert, J. P.; Ciccotti, G.; and Berendsen, H. J. C. numerical integration of cartesian equations of motion of a system with constraints molecular dynamics of n-alkanes. *J. Computat. Phys.*, 23(3):327–341, **1977**.
- [59] Andersen, H. C. Rattle - A velocity version of the shake algorithm for molecular dynamics calculations. *J. Computat. Phys.*, 52(1):24–34, **1983**.
- [60] Celine, A.; Alex, H. V.; Hans-Dieter, H.; Peter T. D.; and Siewert-Jan, M. Methodological issues in lipid bilayer simulations. *J. Phys. Chem. B.*, 107(35):9424–9433, **2003**.
- [61] Jorgensen, W. L.; Chandrasekhar, J.; Madura, J. D.; Impey, R. W.; and Klein, M. L. Comparison of simple potential functions for simulating liquid Water. *J. Chem. Phys.*, 79(2):926–935, **1983**.
- [62] Neria, E.; Fischer, S.; and Karplus, M. Simulation of activation free energies in molecular systems. *J. Chem. Phys.*, 105(5):1902–1921, **1996**.
- [63] Pullman, B. In intermolecular forces. 14:331, **1981**.
- [64] Berweger, C. D.; Vangunsteren, W. F.; and Mullerplathe, F. Force field parameterization by weak coupling reengineering SPS water force-field. *Chem. Phys. Lett.*, 232(5-6):429–436, **1995**.
- [65] Berendsen, H. J. C.; Grigera, J. R.; and Straatsma, T. P. The missing term in effective pair potentials. *J. Phys. Chem.*, 91(24):6269–6271, **1987**.
- [66] Matsuoka, O.; Clementi, E.; and Yoshimine, M. CL study of water dimer potential surface. *J. Chem. Phys.*, 64(4):1351–1361, **1976**.
- [67] Watanabe, K.; and Klein, M. L. Effective pair potentials and the properties of water. *Chem. Phys.*, 131(2-3):157–167, **1989**.
- [68] Liu, Y.; and Ichiye, T. Soft sticky dipole potential for liquid water: A new model. *J. Phys. Chem.*, 100(7):2723–2730, **1996**.
- [69] Buch, V.; Sandler, P.; and Sadlej, J. Simulations of H_2O solid, liquid, and clusters, with an emphasis on ferroelectric ordering transition in hexagonal ice. *J. Phys. Chem. B.*, 102(44):8641–8653, **1998**.
- [70] Levitt, M.; Hirshberg, M.; Sharon, R.; Laidig, K. E.; and Daggett, V. Calibration and testing of a water model for simulation of the molecular dynamics of proteins and nucleic acids in solution. *J. Phys. Chem. B.*, 101(25):5051–5061, **1997**.

- [71] Jorgensen, W. L.; and Jenson, C. Temperature dependence of TIP3P, SPC, and TIP4P water from NPT monte carlo simulations: seeking temperatures of maximum density. *J. Computat. Chem.*, 19(10):1179–1186, **1998**.
- [72] Chialvo, A. A.; and Cummings, P. T. Engineering a simple polarizable model for the molecular simulation of water applicable over wide ranges of state conditions. *J. Chem. Phys.*, 105(18):8274–8281, **1996**.
- [73] Dang, L. X. Importance of polarization effects in modeling the hydrogen bond in water using classical molecular dynamics techniques. *J. Phys. Chem. B.*, 102(3):620–624, **1998**.
- [74] Phillips, J. C.; Braun, R.; Wang, W.; Gumbart, J.; Tajkhorshid, E.; Villa, E.; Chipot, C.; Skeel, R. D.; Kale, L.; and Schulten, K. Scalable molecular dynamics with NAMD. *J. Computat. Chem.*, 26(16):1781–1802, **2005**.
- [75] Humphrey, W.; Dalke, A.; and Schulten, K. VMD: Visual molecular dynamics. *Journal of Molecular Graphics & Modelling*, 14(1):33–38, **1996**.
- [76] Mayne, C. G.; Saam, J.; Schulten, K.; Tajkhorshid, E.; and Gumbart, J. C. Rapid parameterization of small molecules using the force field toolkit. *J. Computat. Chem.*, 34(32):2757–2770, **2013**.
- [77] Michaud-Agrawal, N.; Denning, E. J.; Woolf, T. B. and Beckstein, O. Software news and updates MDAnalysis: A toolkit for the analysis of molecular dynamics simulations. *J. Computat. Chem.*, 32(10):2319–2327, **2011**.
- [78] Theobald, D. L. Rapid calculation of RMSDs using a quaternion-based characteristic polynomial. *Acta Crystallographica Section A*, 61(4):478–480, **2005**.
- [79] MacKerell, A. D.; et al. All-atom empirical potential for molecular modeling and dynamics studies of proteins. *J. Phys. Chem. B.*, 102(18):3586–3616, **1998**.
- [80] Mackerell, A. D.; Feig, M.; Brooks, C. L. Extending the treatment of backbone energetics in protein force fields: limitations of gas-phase quantum mechanics in reproducing protein conformational distributions in molecular dynamics simulations. *J. Comput. Chem.*, 25(11):1400 – 15, **2004**.
- [81] Jianhan, C.; Wonpil, I.; Brooks, C. L. Balancing solvation and intramolecular interactions: toward a consistent generalized born force field. *J. Am. Chem. Soc.*, 128(11):3728 – 3736, **2006**.
- [82] Vanommeslaeghe, K.; Hatcher, E.; Acharya, C.; Kundu, S.; Zhong, S.; Shim, J.; Darian, E.; Guvench, O.; Lopes, P.; Vorobyov, I.; and MacKerell, Jr. A. D. CHARMM General force field: a force field for drug like molecules compatible

- with the charmm all-atom additive biological force fields. *J. Computat. Chem.*, 31(4):671–690, **2010**.
- [83] Jones, J. E. On the determination of molecular fields. ii. from the equation of state of a gas. *proc. R. Soc. Lond. A*, 106:463 – 477, **1924**.
- [84] Derocco, A. G.; and Halford, J. O. Intermolecular potential of ARGON, METHANE, and ETHANE. *J. Chem. Phys.*, 28(6):1152 – 1154, **1958**.
- [85] Patra, M.; Karttunen, M.; Hyvönen, M. T.; Falck, E.; Lindqvist, P.; Vattulainen, I. Molecular dynamics simulations of lipid bilayers: major artifacts due to truncating electrostatic interactions. *Biophys. J.*, 84(6):3636, **2003**.
- [86] Darden, T.; York, D.; Pedersen, L. Particle mesh ewald: an $N \cdot \log(N)$ method for ewald sums in large systems. *J. Chem. Phys.*, 98(12):10089, **1993**.
- [87] K. Esselink. A comparison of algorithms for long-range interactions. *Comput. Phys. Commun.*, 87(3):375 – 395, **1995**.
- [88] Lomize, A. L.; Pogozheva, I. D.; Lomize, M. A.; and Mosberg, H I. Positioning of proteins in membranes: A computational approach. *Protein Sci.*, 15(6):1318–1333, **2006**.
- [89] Wolf, M. G.; Hoefling, M.; Aponte-Santamaria, C.; Grubmueller, H.; and Groenhof, G. g_membed: Efficient insertion of a membrane protein into an equilibrated lipid bilayer with minimal perturbation. *J. Computat. Chem.*, 31(11):2169–2174, **2010**.
- [90] Golub, G. H.; and Reinsch, C. Singular Value decomposition and least squares solutions. *Numerische Mathematik*, 14(5):403, **1970**.
- [91] Vorobyov, I.; Anisimov, V. M.; Greene, S.; Venable, R. M.; Moser, A.; Pastor, R. W.; MacKerell, A. D. Additive and classical drude polarizable force fields for linear and cyclic ethers. *J. Chem. Theory Comput.*, 3:1120 – 1133, **2007**.
- [92] Song, W.; Rossky, P. J.; Maroncelli, M. Modeling alkane + perfluoroalkane interactions using all-atom potentials: failure of the usual combining rules. *J. Chem. Phys.*, 119:9145 – 9162, **2003**.
- [93] Morgado, P.; Lewis, J. B.; Laginhas, C. M. C.; Martins, L. F. G.; McCabe, C.; Blas, F. J.; Filipe, E. J. M. Systems involving hydrogenated and fluorinated chains: volumetric properties of perfluoroalkanes and perfluoroalkylalkane surfactants. *J. Phys. Chem. B*, 115:15013 – 15023, **2011**.

Chapter 9

Curriculum Vitae

Ghulam Saddiq

Born: 09.01.1980, Bannu, Pakistan.

Objective

Committed and enthusiastic postdoc with a thorough knowledge of physics, Quantum chemistry and aiming to utilize my talent, experience and qualification in a most effective manner towards building up a career in research

Education

Since 2014 Doctoral study at Faculty of Natural Sciences II - Chemistry, Physics and Mathematics, Martin-Luther University, Halle-Wittenberg under the supervision of Prof. Dr. Wolfgang Paul and Prof. Dr. Daniel Sebastiani. (*Faculty Development Program, Higher Education Commission, Pakistan*).

- 2009–2011 **MS Physics (Computational study of Pervoskites), Islamia College University, Khyber Pakhtoonkhwa (KP), Pakistan.**
The Courses provided me with designing research studies, data collection, validation, management and statistical analysis of data. Comparison of theoretical with experimental data. Successfully completed my research project on *"First Principle study on Structural, Electronic and Optical properties of cubic pervoskites $AgTF_3(T:Mg, Zn)$."*
- 2000–2002 **MSc Physics, Peshawar University, KP, Pakistan.**
The degree course combined theoretical knowledge, and laboratory work experience, and empirical research that provided me with a broad range of abilities required for understanding Physics, classification of material and various physical phenomenons relating to materials.
- 1997–1999 **BSc Physics, Peshawar University, KP, Pakistan.**
The degree course gave basic and comprehensive knowledge about understanding of physical systems and integration and association of Physics to Math-A course and Computer Science.

Work Experience

- 2005–2013 **Lecturer/AP at Govt. Colleges, KP, Pakistan**
- Since June **Lecturer Department of Physics, Islamia College University**
2013 **Peshawar (ICUP), KP, Pakistan.**

Skills Profile:

- Good communication skills gained while working in different roles while studying.
- Experience of working within a team based culture while planning, organizing coordinating, managing and valuing commitment above all.

Publications

- G. Murtaza, **G. Sadique** (Ghulam saddiq), H.A. Rahnamaye Aliabad, M. N. Khalid, S. Naeem, A. Afaq, B. Amin, Iftikhar Ahmad. *First principal study on the structural, electronic and optical properties of cubic perovskites $AgTF_3(T:Mg,Zn)$* . J. Phy. B, Condensed Matter 406(24):4584–4589. 2011

Chapter 10

DECLARATION

This is hereby confirmed that this thesis is entirely my own work and has been written by myself. I only used the mentioned sources and indicated all kind of citations correctly.

Ghulam Saddiq

Nov. 15, 2016

MLU, Halle (Germany).